Università
Ca'Foscari
Venezia

Master's Degree programme – Second Cycle
(*D.M. 270/2004*)
in Environmental Sciences - Joint Master's Degree in Sustainable Development

Final Thesis

Ca' Foscari
Dorsoduro 3246
30123 Venezia

ANALYSIS OF LAND COVER AND LAND COVER CHANGE THROUGH REMOTE SENSING IN THE DOLOMITI BELLUNESI NATIONAL PARK

Supervisor
Carlo Giupponi

Assistant Supervisor
Fabio Cian

Graduand
Simona Zollet
Matriculation Number 842806

Academic Year
2014 / 2015

SUMMARY

INTRODUCTION

This work focuses on the spatial changes in semi-natural grasslands habitats over the past 60 years in the Dolomiti Bellunesi National Park, Italy. Semi-natural grasslands have been created and maintained over the centuries by human activities, resulting in biodiversity-rich landscape mosaics, but the progressive abandonment of traditional grassland management activities such as extensive grazing and haymaking after World War II resulted in a widespread phenomenon of forest expansion, declining biodiversity and shrinking or disappearance of grassland areas.

To understand how the abandonment of traditional mountain activities and the change of grassland management practices has impacted semi-natural grassland ecosystems, and above all for developing measures to mitigate these changes, it is crucial to be able to map and monitor land cover changes efficiently over large geographic areas and long periods of time (K. P. Price, Guo, & Stiles, 2003). Monitoring mountain areas, however, poses considerable difficulties because of the complexity of the terrain, which makes direct access and field monitoring problematic. In this respect, Remote Sensing technologies and Geographic Information Systems (GIS) represent invaluable tools for understanding the dynamics of this phenomenon. Through the integration of remote sensing and GIS techniques, it is possible to classify the land cover pattern and to analyze its changes over a long time period and at the scale of interest (Boyd & Foody, 2011; Fichera, Modica, & Pollino, 2012; Rocchini et al., 2012). Land cover data can be obtained from satellite imagery and aerial photography, and GIS software improves image processing, data organization and quantitative analysis of multi-temporal remote sensing datasets.

This is fundamental for providing support for decision-making and nature conservation management, an aspect of fundamental importance for semi-natural ecosystems because they require active management to sustain their ecosystem services.

In the first part of this work, high-resolution distribution maps of semi-natural grassland habitats within the Dolomiti Bellunesi National Park (Italy) were created based on two aerial imagery datasets: the 1954 GAI flight (the oldest available photographic record of the study area, dating back to before the start of mountain abandonment) and the 2012 TELAER flight. The distribution maps were created through the visual interpretation of aerial photographs

and manual digitization of grassland polygons with the aid of GIS software. The two distribution maps were subsequently combined and compared to assess the spatial distribution and magnitude of changes over the 58-years time period.

The second part of the study explores the potential of mapping the extent of semi-natural grassland habitats and studying their evolution by using Landsat satellite images, employing supervised pixel-based methods for classification and change detection and vegetation indices to increase the separability between different vegetated surfaces. First, a seasonality study was carried out to identify the most suitable period for ensuring maximum land cover separability during the vegetative season; for this purpose, five Landsat 5 TM images from 2005 (May-October) were used for the creation of several different classification scenarios, and the resulting classification accuracies were compared.

Based on the best date identified by the seasonality study, two Landsat images (from the beginning and the end of Landsat TM data availability period) were chosen for NDVI calculation and NDVI differencing change detection. In this type of change detection procedure, the NDVI values of the two images are subtracted pixel-by-pixel, resulting in a change image that can be classified by setting an appropriate threshold to distinguish significant changes (increase or decrease of vegetation cover) from situations where there was no detectable change.

1. THE EVOLUTION OF EUROPEAN MOUNTAIN GRASSLANDS

'Grassland' in its broader sense can be defined as any area where the dominant vegetation is composed by grasses or grass-like plants, with little or no tree cover, despite the differences related to the occurrence of grasslands within a physiognomic continuum between forests and deserts, and the difficulty in characterizing their limits (Dixon, Faber-Langendoen, Josse, Morrison, & Loucks, 2014; FAO, 2005).

Most of Europe's grasslands have been modified to some extent by human activity or have been created and maintained by agricultural practices, so they fall into the category of "semi-natural grasslands", although their plant communities are natural. Grasslands represent some of Europe's most species-rich plant communities, and their biological diversity is high in relation to other taxonomic groups as well, in particular butterflies and other inver-

tebrates such as grasshoppers (European Commission, 2008; Poschlod & WallisDeVries, 2002; WallisDeVries, Poschlod, & Willems, 2002).

In the case of the alpine region, montane grasslands and shrublands located above the tree line, commonly known as alpine tundra, occur naturally due to altitudinal and climatic factors; conversely, nearly all the mountain grasslands below the tree line (subalpine and montane grasslands) are semi-natural (European Commission, 2008). European mountain regions, especially in the subalpine and montane belt, are dominated by semi-natural ecosystems whose evolution has been driven by the coexistence and interaction of natural and anthropogenic disturbance regimes for the past thousands of years (Niedrist, Tasser, Luth, Dalla Via, & Tappeiner, 2009). Traditional low-intensity agricultural practices, such as coppicing, grazing and mowing, have fostered the development of complex and highly biodiverse mosaics of open areas, sparse and dense forests, that are important sources of plant diversity and provide food and habitat for many grassland and ecotone animals, therefore supporting a range of species much wider than the one found in the original natural climax vegetation. As a consequence, land use is considered the most important driving factor for landscape change in the Alps (Garbarino, Sibona, Lingua, & Motta, 2014; Tasser, Walde, Tappeiner, Teutsch, & Noggler, 2007).

Starting from the end of 19th century, but especially following World War II, traditional mountain grassland management across Europe underwent a radical change, driven by deep socio-economic transformations (Mottet, Ladet, Coqué, & Gibon, 2006). Immigration towards urban areas, the intensification of agriculture and the limited possibilities of mechanization offered by mountain areas resulted in extensive depopulation and marginalization of mountain territories (MacDonald et al., 2000). Even just considering the period between 1980 and 2000, 40% of all farm holdings in the European Alps have been abandoned, and among the farms that are still in operation today, almost 70% represent only a secondary source of income (Tasser et al., 2007).

As a consequence, widespread encroachment of woody vegetation onto meadows, pasture patches and other open areas through secondary succession has been observed in the throughout Europe following the abandonment of extensive farming practices, and is leading to the progressive fragmentation and ultimately disappearance of these highly biodiverse areas (European Commission, 2008; Garbarino et al., 2014; MacDonald et al., 2000; Poschlod & WallisDeVries, 2002; Sitzia, Semenzato, & Trentanovi, 2010). The forest expansion process

in many cases can be remarkably swift: for example, a study by Garbarino & Pividori (2006) showed how in a mountain area of the Val Grande National Park, Italy, forests recolonized about 71% of the former open areas in the span of 50 years.

This trend of extensive natural forest recovery has been observed everywhere in the Italian alpine region, both in the Western (Garbarino & Pividori, 2006; Garbarino et al., 2014; Höchtl, Lehringer, & Konold, 2005; Vacchiano, Garbarino, Lingua, & Motta, 2006) and Eastern Alps (Giupponi, Ramanzin, Sturaro, & Fuser, 2006; Sgarbossa, 2010; Tattoni, Ciolli, Ferretti, & Cantiani, 2010; Urbinati, Benetti, Viola, & Ferrari, 2004), as well as in other mountainous or marginal rural areas of the country (Agnoletti, 2007; Mancino, Nolè, Ripullone, & Ferrara, 2014). The same situation has been observed in most parts of the Alpine region as a whole (Tasser et al., 2007), such as in Switzerland (Gellrich & Zimmermann, 2007; Stanga & Zbinden, 2004) and France (Didier, 2001), and in other mountainous regions across Europe, for example Norway (Olsson, Austrheim, & Grenne, 2000), Germany (Poschlod & WallisDeVries, 2002), and the Pyrenees region (Améztegui, Brotons, & Coll, 2010; Mottet et al., 2006; Poyatos, Latron, & Llorens, 2003; Roura-Pascual, Pons, Etienne, & Lambert, 2005).

Only in some regions, most notably western Austria, parts of Switzerland, and South Tyrol, this trend has not prevailed, mostly thanks to governmental intervention and subsidies (Niedrist et al., 2009).

Once forest expansion begins, internal feedbacks (tree-tree or tree-soil interactions) can reinforce the shift to a woodland state (Kremer, Halpern, & Antos, 2014). This secondary succession generally ends in the climax stage of the vegetation adapted to the site, and the pattern of vegetation change is determined by local factors related to elevation, aspect, inclination and water and nutrient regimes and by the land use type existing before abandonment (Tasser & Tappeiner, 2002).

Even though the reforestation process has some positive effects on the environment, such as the increase in the rate of carbon sequestration, soil stabilization and reduced risk of landslides and avalanches (MacDonald et al., 2000), and improved water quality and retention (Tasser et al., 2007), the decrease of landscape heterogeneity and mosaic features deriving from this process also translates not only into fragmentation and loss of biodiversity-rich habitats, but also into the irreversible loss of cultural landscapes that are part of the local history and heritage, and in a decrease of the aesthetic value of the landscape itself (Gellrich, Baur, Koch, & Zimmermann, 2007; MacDonald et al., 2000; Sitzia et al., 2010).

2. REMOTE SENSING AND GIS FOR LAND COVER CHANGE ASSESSMENT

Remote sensing is "the science and art of obtaining information about an object, area, or phenomenon through the analysis of data acquired by a device that is not in contact with the object, area, or phenomenon under investigation" (Lillesand, Kiefer, & Chipman, 2004).

The rapid advancement over the past two decades of remote sensing systems and of the techniques for analyzing remotely sensed data, as well as the large amount of data that has become available from earth observation satellites, have greatly increased the capacity to observe and monitor land cover change at different scales. Global land cover data allows for global change assessments, while more detailed land classifications for change assessment and management have been created at the regional and local scale (Di Gregorio & Jansen, 2005; Turner II, Lambin, & Reenberg, 2008).

The combination of land cover data deriving from different remote sensing technologies (such as aerial photography and satellite images), together with terrain and other ancillary data (historical land cover maps, surveys, etc.), is of fundamental importance for land cover change studies, as it can be used to 1) identify the pattern of land-cover change (the areas where change is taking place); 2) investigate the extent and/or quantity of land cover change and 3) analyze the temporal pattern at which the change occurs (Morgan, Gergel, & Coops, 2010; Pelorosso, Leone, & Boccia, 2009).

2.1 Basic Remote Sensing principles

2.1.1 The electromagnetic spectrum

Electromagnetic energy is the vehicle through which information is transmitted from the feature or phenomenon of interest to the remote sensor. Variations in the quality and quantity of the electromagnetic energy measured by remote sensors allow for the interpretation and the extraction of information regarding various aspects of such feature or phenomenon.

Electromagnetic energy travels in a harmonic, sinusoidal fashion, and electromagnetic waves are generally categorized according to their wavelength λ (the distance from one wave peak to the next), which is located within the electromagnetic spectrum (Figure 1). The

preferred unit to measure wavelength along the spectrum is the micrometer µm (1 x 10^{-6} m). The spectrum ranges from cosmic rays (about 10^{-6} µm) to television and radio waves (about 10^{9} µm). Different remote sensing technologies and sensors (cameras, scanners, radar, LIDAR, etc.) are designed to operate in different regions of the electromagnetic spectrum, so even though there is no clear-cut dividing line between one nominal spectral region and the next, the electromagnetic spectrum is commonly divided into discrete bands or regions (Paine & Kiser, 2012).

The visible portion of the electromagnetic spectrum, that is to say the range of spectral sensitivity of the human eye, extends from about 0,4 µm to 0,7 µm, so it represent a very limited part of the entire spectrum. The most common remote sensing systems operate in one or several of the visible, IR or microwave portions of the spectrum.

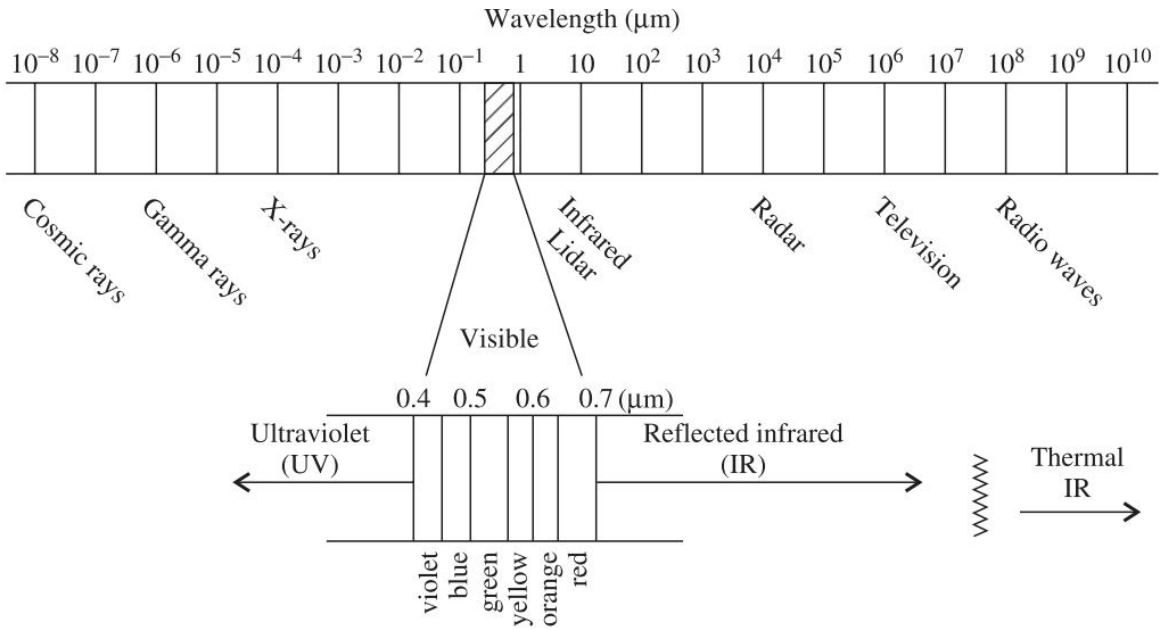

Figure 1: the electromagnetic spectrum (from Paine & Kiser, 2012)

Although the sun is the most obvious source of electromagnetic energy for remote sensors, all matter at temperatures above absolute zero (0 K, or -273°C) continuously emits electromagnetic radiation, which varies in relation to the surface temperature of the object. The maximum of radiative energy from the earth's surface, whose ambient temperature is about 300 K (27°C), occurs at a wavelength of about 9,7 µm. Because this radiation correlates with the heat of surfaces, it is called "thermal infrared" energy, and can be recorded with thermal sensors such as radiometers and scanners. By comparison, the sun's energy

peak occurs at about 0,5 µm, a wavelength to which the human eye and photographic supports are sensitive.

Some sensors, such as radar (RAdio Detection And Ranging) and LiDAR (Light Detection and Ranging) systems, make use of their own source of energy to hit the target, and then the sensor detects and measures the radiation that is reflected or backscattered. These systems are defined *active* systems, in contrast to *passive* systems, such as optical aerial photography and satellite sensors, that sense naturally available energy emitted or reflected by the objects of interest (Lillesand et al., 2004).

2.1.2 Interactions between electromagnetic energy and matter

Electromagnetic energy can only be detected when it interacts with matter. Four fundamental energy interactions are possible: reflectance, absorptance, transmittance and refraction.

Reflectance is the ratio of the energy reflected from an object to the energy incident upon the object. *Absorptance* occurs when electromagnetic energy is absorbed by the surface and converted to another form of energy, such as heat. Absorbed wavelengths that are converted to heat may later be emitted and can be detected by a thermal detector. Within the visible portion of the spectrum, differences in absorptance and reflectance qualities of an object result in in the visual effect called color. For example, an object is seen as "red" when it absorbs all visible wavelengths and reflects in the red spectral region.

Transmittance is the propagation of energy through a medium. When entering and leaving a medium of different density, transmitted wavelengths are refracted. *Refraction* is the bending of transmitted electromagnetic energy caused by its change in velocity as it passes from one medium to another (Paine & Kiser, 2012).

The energy flow between source and sensor begins at the source (typically the sun), is transmitted through space and the atmosphere, is reflected by objects on earth surface, and is finally detected by a sensor. This implies that the characteristics of the energy that eventually reaches the sensor depend both on the interaction with the atmosphere and with the objects.

Regardless of its source, all radiation detected by remote sensors passes through some distance, or path length, of atmosphere. The effects of the atmosphere on the intensity and spectral composition of radiation manifest themselves through the mechanisms of atmospheric scattering and absorption, and are related to the path length, which in turn varies in relation to the position of the sensor: satellite optical imagery, for example, results from sunlight that passes through the earth's atmosphere twice on its journey from source to sensor, so it is strongly affected by atmospheric interference.

Atmospheric scattering is reflectance within the atmosphere caused by small particles of dust and moisture. The most common type of scatter is Rayleigh scatter, which occurs when radiation interacts with atmospheric particles that are much smaller in diameter than the radiation's wavelength. As a consequence, there is a much stronger tendency for short wavelengths to be scattered by this mechanism than long wavelengths. "Haze" effects, which diminishes the contrast of an image, are mainly caused by Rayleigh scatter, and in color photography this results in a bluish-gray cast, especially when the image is taken from high altitude (Lillesand et al., 2004). In addition, not all energy that reaches the sensor is reflected from objects on the earth surface, because some of it derives from atmospheric scattering, which forms the so-called background noise. The total amount of scattered energy increases with an increase in flying altitude (Paine & Kiser, 2012).

Another important type of interaction occurring in the atmosphere is absorption, which results in a loss of energy. Water vapor, carbon dioxide, and ozone are the most efficient absorbers of solar radiation among atmospheric constituents: these gases tend to absorb electromagnetic energy in specific wavelength bands, and as a consequence the majority of energy in these wavelengths does not reach the earth surface. Conversely, the portions of the electromagnetic spectrum where the electromagnetic energy originating from the sun or from an active sensor are transmitted through the atmosphere are referred to as *atmospheric windows*. An example of this is represented by the wavelengths in the visible range (Lillesand et al., 2004).

Remote sensing data acquisition is limited to the atmospheric windows. For example, multispectral scanners sense simultaneously through multiple, narrow wavelength ranges that can be located at various atmospheric windows in the visible and IR spectral region (Figure 2). (Lillesand et al., 2004; Paine & Kiser, 2012).

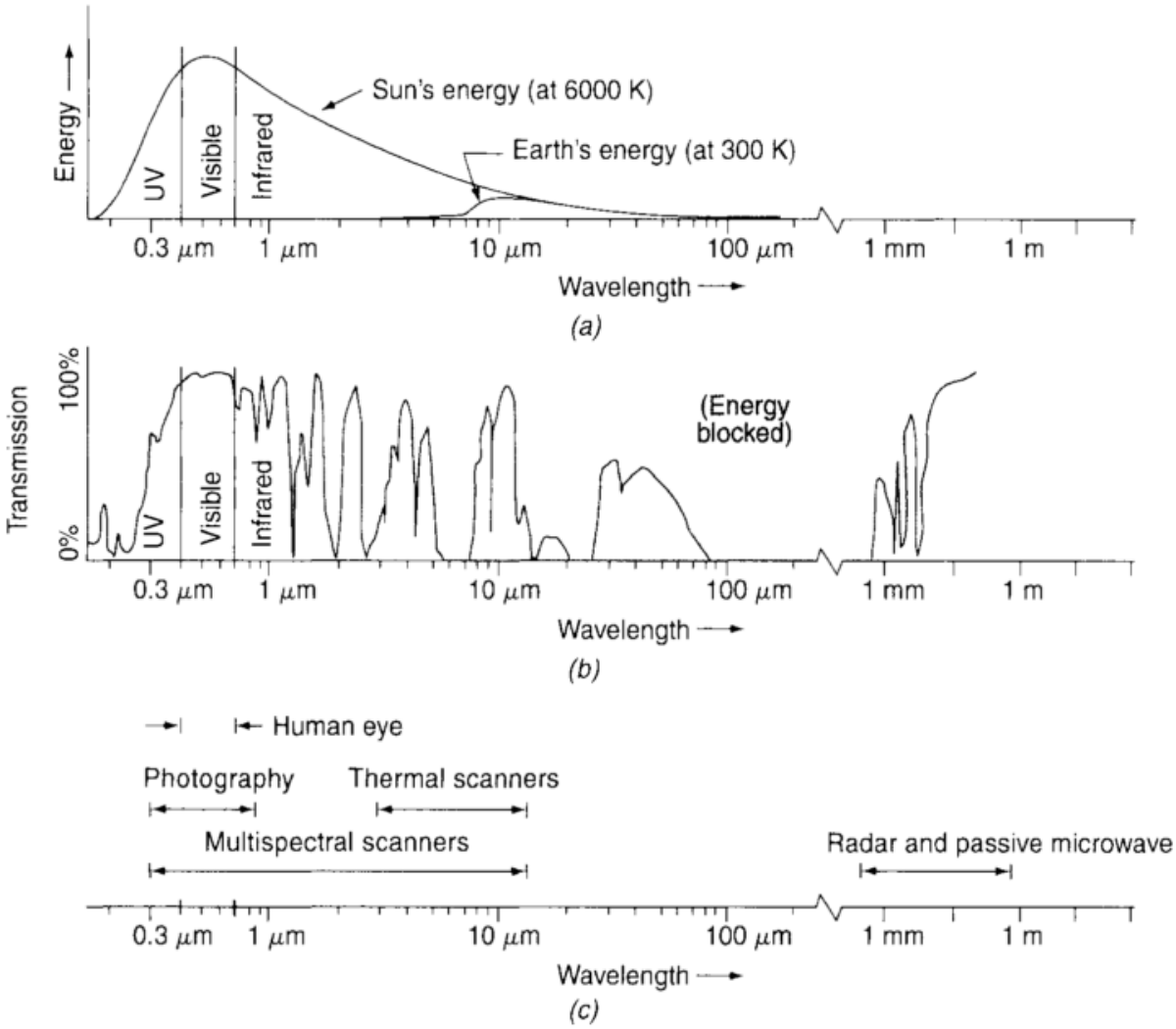

Figure 2: the spectral characteristics of a) the primary sources of electromagnetic energy (the sun and the earth's surface), b) the atmospheric windows through which source energy may be transmitted, and c) the spectral sensitivity of the most common remote sensing systems. The wavelength scale is logarithmic. From (Lillesand et al., 2004)

The selection of the sensor to use for a remote sensing task therefore depends on (1) the presence or absence of atmospheric windows in the spectral range(s) of interest, (2) the spectral sensitivity of the sensors available, and (3) the source, magnitude, and spectral composition of the energy available in these ranges. These choices however are ultimately subordinated to the spectral reflectance properties of the features of interest.

The proportion of energy reflected, absorbed, and transmitted by a surface varies depending on a) the material and condition of the feature of interest, and b) the wavelength of incident energy. In other words, even within a given feature type the proportion of reflected, absorbed, and transmitted energy will vary between different wavelengths, and features

that may result indistinguishable in one spectral range may appear clearly separable in another. The amount of spectral separability between features of interest determines the possibility of successfully identifying, mapping and studying Earth surface features of interest on the basis of their spectral characteristics.

A graph of the spectral reflectance of an object as a function of wavelength is called spectral reflectance curve; its configuration shows the spectral characteristics of an object, and can be used to choose the wavelength region(s) in which remote sensing data should be acquired for the study of that specific feature (Lillesand et al., 2004).

2.2 Optical Remote Sensors

Optical remote sensing employs passive sensors that operate in the part of electromagnetic spectrum spanning from the visible wavelengths to the near infrared (NIR) region, up to thermal infrared (TIR). Sensors belonging to this category can be divided into non-scanning and scanning imaging systems; the former includes film-based photographic camera systems, generally mounted on airborne platforms, while the latter includes digital scanning systems, that can be mounted either on airborne or satellite platforms (Figure 3). The operating principles of scanners mounted on space platforms are essentially identical to those operating from airborne systems (Lillesand et al., 2004). Among the various types of remote sensing data used for the assessment and mapping of landscape change, satellite images and aerial photographs are the most widely used (Kadmon & Harari-Kremer, 1999).

The images resulting from optical sensors can be either analog or digital. Film-based aerial photographs are analog images while aerial and satellite images acquired using electronic sensors are digital images. Digital images offer the advantage of real-time transmission of the remotely sensed data to a ground station for immediate computer-assisted analysis and interpretation. Conversely, analog photography needs to be converted into digital format with a scanning device in order to be used with computer systems.

The quality of remote sensing imagery is largely determined by their resolution. There are four types of resolution that characterize any particular remote sensor: spatial, spectral, radiometric and temporal.

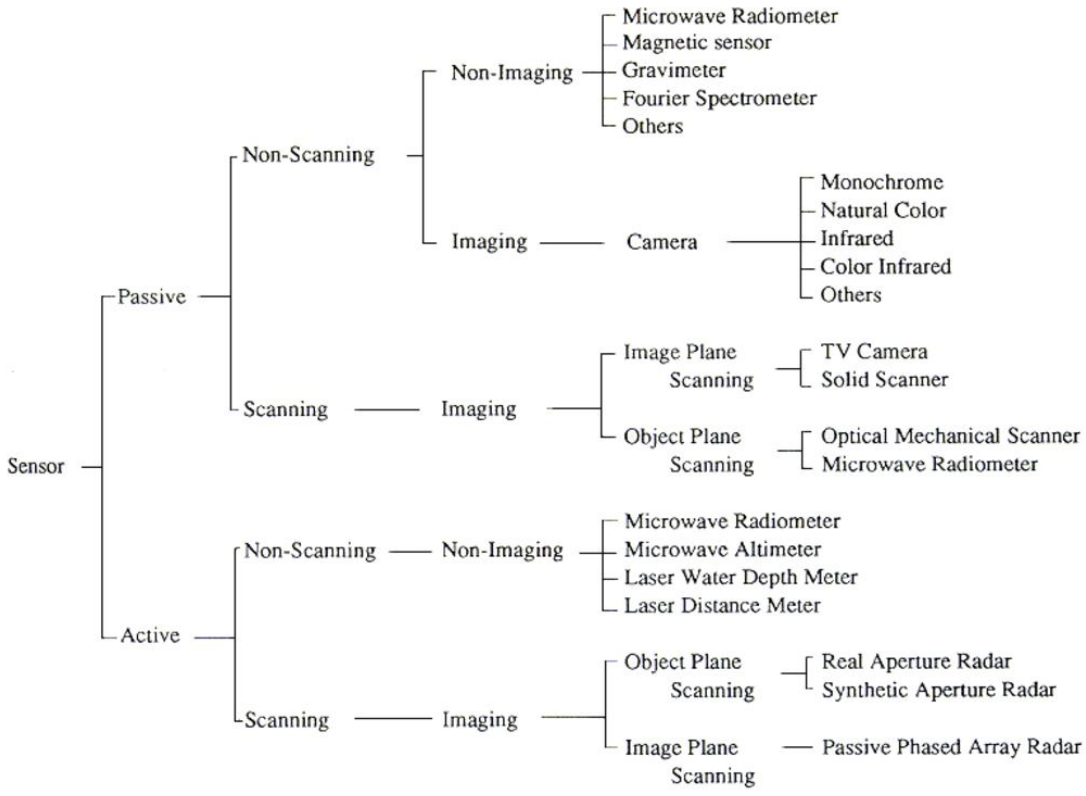

Figure 3: Classification of sensors (Lillesand et al., 2004)

The spatial resolution of an image is can be thought of as the size of the smallest object that can be distinguished on the image itself. In the case of digital sensors the finest unit of resolution is represented by uniform pixels, whose size is determined by the sensors' instantaneous field of view (IFOV). The IFOV is essentially the ground area through which the sensor is receiving the electromagnetic radiation signal and is determined by height and angle of the imaging platform (Lu, Li, & Moran, 2014). For film-based (analog) photographs the spatial resolution depends on the clusters of grains within the emulsion, which tend to be irregularly sized and unevenly distributed (Lillesand et al., 2004; Morgan et al., 2010).

Spectral resolution denotes the ability of the sensor to resolve different bands within the electromagnetic spectrum. The spectral resolution is determined by the number of bands being scanned and their size. In *panchromatic* imaging systems, the sensor is a single channel detector sensitive to radiation within a broad wavelength range. The physical quantity being measured is the apparent brightness of the earth surface, so the spectral information or "color" of the targets is lost. This is the case of black and white aerial photographs, as well as of the panchromatic bands of satellite sensors such as Landsat ETM+ and Landsat OLI/TIRS.

Multispectral imaging systems can sense in more bands (3-10) over a greater range of wavelengths. This results in a multiband image where each layer is sensed simultaneously from the same geometric vantage point but in different bands of the spectrum, and thus retains both the brightness and spectral (color) information of the observed objects. The LANDSAT sensors are examples of such systems (Lillesand et al., 2004). Finally, *hyperspectral* imaging systems acquire images in about a hundred or more very narrow and contiguous spectral bands. The precise spectral information contained in a hyperspectral image enables better characterization and identification of targets (Campbell & Shin, 2011). Since spectral signature is a critical feature for land cover classification, data with high spectral resolution have the potential to better separate different land cover types, especially when the signals recorded in the multiple bands are analyzed in conjunction with each other.

Radiometric resolution refers to the sensitivity of the sensor to variations in brightness and specifically denotes the number of grayscale levels that can be imaged by the sensor. A sensor with an 8-bit resolution for its bands, for example, can record a range of values for each pixel that goes from 0 to 255 (Lu et al., 2014).

Finally, temporal resolution (also called revisit time) is the amount of time between each image collection. This is mainly applicable to satellite system, which have a fixed temporal resolution that is determined by the repeat cycle of the satellite's orbit.

There are some unavoidable trade-offs among the quality of spatial, spectral, and radiometric properties of a sensor. Increases in spatial and spectral resolution, for example, both result in a decrease in the energy available to be sensed. High spatial resolution means that each detector is receiving energy from a smaller area, while high spectral resolution means that each detector is receiving energy in a narrower range of wavelengths.

2.2.1 Aerial photography

Aerial photography is the collection of photographs of the surface of the earth using an airborne camera that can be triggered remotely or automatically. Platforms used in aerial photography include fixed-wing aircrafts, helicopters, drones, balloons, rockets and others (Campbell & Shin, 2011; Paine & Kiser, 2012).

Aerial photography represents the largest and most valuable source of information for long-term assessment of land cover change and vegetation dynamics. Fine-scale (1:40000 and larger) historical aerial photographs are available for many areas, in particular in Europe and North America, and many date back to the early 20th century, long before the advent of satellite-based remote sensing, making them a fundamental historical data archive (Anderson & Cobb, 2004; Strand, Dramstad, & Engan, 2002). They represent the only source of information that can combine high spatial resolution, relatively large spatial extent, and long-term coverage (Kadmon & Harari-Kremer, 1999; Morgan et al., 2010). The detail and coverage of these images makes them suitable for mapping small ecosystems and fine-scale landscape features (Brandt, Bunce, Howard, & Petit, 2002; Hussain, Chen, Cheng, Wei, & Stanley, 2013), for retrieving high-resolution land-cover data in areas not historically sampled using ground-based techniques, and for carrying out quantitative analyses of land cover changes over time (Anderson & Cobb, 2004).

Photographs are a representation of the reflectance characteristics recorded onto photographic film or in digital format. Aerial photographs are captured most commonly as panchromatic (black and white), natural color, or false-color infrared; the range of electromagnetic energy recorded by the film camera and is generally limited to the 0.4 to 0.9 mm region, only slightly wider than the range of human vision (Lillesand et al., 2004; Paine & Kiser, 2012).

The most common type of cameras used in aerial photography are single-lens frame cameras, with lenses designed to provide high geometric quality and minimize distortions. Regardless of the geometric quality of camera lenses, however, they always add a certain amount of curvature to the images, which becomes progressively more pronounced moving away from the center of the photo and is especially pronounced in images acquired with older cameras (Lillesand et al., 2004).

Another source of potential error in an aerial photograph is relief displacement, which derives from the three-dimensionality of terrain features and manifests itself in the form of vertical objects apparently “leaning away” from the center point of an aerial photograph. This error is evident with trees and multistory buildings and is especially problematic when dealing with very steep terrain features, such as in mountain areas.

Digital vertical photographs can be geometrically corrected to remove distortions caused by topographic relief, lens distortion, and camera tilt through a process called orthorectifica-

tion, and are termed ortophotographs or orthoimages (Campbell & Shin, 2011). The scale of an ortophotograph is uniform, and the image has the same lack of distortion as a map, so it can be used to measure true distances, because it is an accurate representation of the Earth's surface. Orthorectification can be conducted on film-based photographs as well, after scanning to convert them into digital format. If the images are needed for photogrammetric work, photogrammetric scanners are generally used, but other types of scanners can still provide digital products suitable for visual interpretation needs. The drawback of these second-generation products, however, is that they may not have the same level of detail found in the original, because scanning photographs can cause the loss of radiometric or tonal detail and of spatial resolution. The spatial and radiometric scanning resolution should therefore be chosen with the aim of creating an accurate representation of the original aerial photograph, but the resulting images are often very demanding in terms of file size and memory requirements. The resolvable scanning resolution (expressed in dots per inch) is mainly limited by the physical characteristics of the film and by the scale of the aerial photograph, but other factors, such as the presence of atmospheric haze and scene contrast, can affect it as well (Morgan et al., 2010).

2.2.2 Satellite images

The modern era of remote sensing began in 1972 with the launch of the first Landsat mission, which provided for the first time a consistent and uniform set of images of nearly the entire Earth surface with frequent revisiting time (Hussain et al., 2013), from which land cover information could be easily extracted and updated. The importance of satellite imagery in mapping vegetation has been increasing over the past two decades and is by now well established; following the Landsat acquisition program, other long term remote sensing programs have been launched, such as SPOT and AVHRR. These programs have been providing repetitive and synoptic observations of the Earth for the past 30–40 years, allowing for time series analysis for long term change studies over large and often inaccessible areas (Hussain et al., 2013; Rogan, Franklin, & Roberts, 2002; Simonetti, Simonetti, & Preatoni, 2014; Vittek, Brink, Donnay, Simonetti, & Desclée, 2013).

Spatial resolution of satellite sensors ranges from high (e.g., QuickBird, Worldview, with sub-meter pixel size), to medium (e.g., 30 m for Landsat images) and coarse (between 250 m to 1000 m, e.g., MODIS, AVHRR) (Lu et al., 2014). The spatial resolution of a sensor influences the thematic information that can be extracted from images, as well as the representation of landscapes: large errors can arise as landscapes are represented at increasingly coarse scale. In most pixel-based classifications, each pixel is classified according to the spectral properties of the dominant land cover type: consequently, with the increase of pixel size the proportion of land cover types which occur in small patches may be underestimated because they will not dominate the reflectance characteristics of the pixel.

This also implies that the appropriate spatial resolution of the sensor also depends on the landscape under analysis (Verburg, Neumann, & Nol, 2011). At a continental or global scale, coarse spatial resolution sensors such as AVHRR, MODIS and SPOT VEGETATION are the most suitable choice because of their large swath width and frequent revisiting time, which give the advantage of frequent coverage and therefore increase the chances to collect a cloud-free multitemporal dataset for the detection of broad scale land cover features (Hostert, Röder, & Hill, 2003; Vittek et al., 2013), but limits their ability of supplying data in spatially complex landscapes (Senf, Leitão, Pflugmacher, van der Linden, & Hostert, 2015),

mainly due to the mixed pixel problem that makes it difficult to extract changed features from coarse spatial resolution data (Lu et al., 2014).

For applications at the regional scale, medium spatial resolution data such as TM and SPOT are generally used. Moreover, the existence of different kinds of sensors providing medium spatial resolution images gives more choices for data collection for a specific study area and thus the opportunity to integrate multi-sensor data to improve classification and/or change detection (Lu et al., 2014). High spatial resolution satellite sensors (QuickBird, IKONOS, OrbView, Worldview), are becoming important data sources at the local scale for monitoring fine-scale landscape features and for use as reference data, partially replacing ground surveys or high resolution aerial photography, also thanks to their decreasing acquisition cost (Coppin, Jonckheere, Nackaerts, Muys, & Lambin, 2004; Hussain et al., 2013; Lu, Mausel, Brondízio, & Moran, 2004). Improvements in radiometric resolution (e.g., from 6 bits in Landsat MSS to 8 bits in Landsat TM to 12 bits in Landsat 8) further increased the potential of satellite data, as they can now provide better separability between different land cover types (Lu et al., 2014).

Other significant features of a satellite sensors include the satellite's coverage area and revisit period (time between successive coverages), that depend on the satellite's orbit. The orbit is defined by altitude, period, inclination, and equatorial crossing time (Figure 4). For most Earth observation satellites, the orbit is approximately circular, with altitudes higher than 400 km above the Earth's surface. The inclination of a satellite's orbit is the angle at which the orbit crosses the equator. Near-polar orbits are those with an inclination close to 90°, so called because the satellite passes near the north and south poles on each orbit. A special case are sun-synchronous orbits, which combine orbital period and inclination in such a way that the extra mass near the equator causes the plane of the orbit to rotate slowly about the Earth's axis. A satellite on that orbit keeps pace with the sun's westward progress as the earth rotates, and consequently it always crosses the equator at the same local sun time.

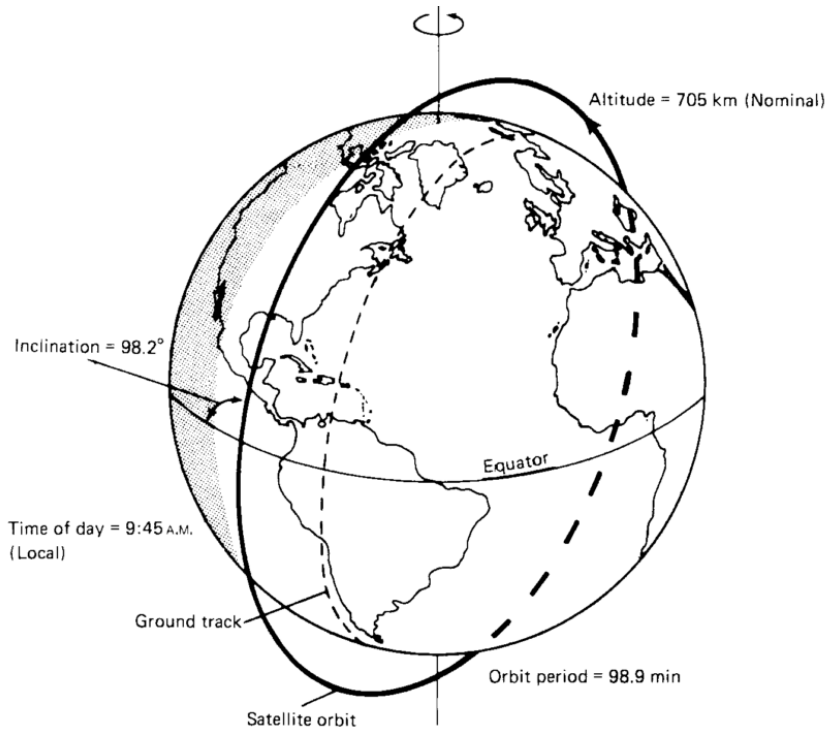

Figure 4: Elements of a circular, near-polar and sun-synchronous orbit (for Landsat 4-7)

A frequent revisit cycle is important especially for certain time-sensitive applications, such as monitoring the effects of flooding, fires, and other natural disasters (Lillesand et al., 2004).

In general, satellite remote sensing data offer the best possibility to monitor changes in land cover through time if compared to survey, census data and even classifications derived from aerial photography, which tend to be infrequent and/or inconsistent in relation to sampling schemes and definitions. Time series based on remote sensing have some drawbacks as well, however, because they can suffer from inconsistencies due to the improved spatial and spectral resolution of new generations of sensors, and sometimes from sensor failure (such as the scan line corrector failure on the Landsat 7 ETM+ sensor, that has been impacting data acquisition since May 2003). Cloud cover may also cause significant problems in the acquisition of usable images, especially when near-anniversary images are needed (Lu et al., 2014; Strahler et al., 2006; Verburg et al., 2011).

Moreover, satellite images are available only for the past four decades, which might not be enough for a complete assessment of land cover variation if the period before the 1970s needs to be considered as well. From the earlier period of the satellite era only coarse to medium resolution images are available, making them unsuitable for change detection at medium-to-high scale (Morgan et al., 2010).

The Landsat satellites

The Landsat program, originally developed by NASA with the cooperation of the U.S. Department of the Interior, is recognized as key milestone in the evolution of remote sensing technology (Rogan & Chen, 2004). As of 2015, a total of 8 Landsat satellites have been launched (although Landsat 6 failed to achieve orbit and was lost), with Landsat 7 and 8 still operational today. The launch of Landsat 9 is planned for 2023 (Figure 5).

Landsat imagery is often preferred for change detection applications because it offers the longest temporal resolution out of all the existing satellite programs, and its medium-high spatial and spectral resolution and fairly frequent revisit time make it applicable to a wide range of situations (Xian, Homer, & Fry, 2009). With their 30 m spatial resolution and 185 km swath, Landsat 4-8 imagery fill an important niche in land cover classification and change detection studies, because the swaths are wide enough for large area coverage, but at the same time the images are detailed enough to allow the identification of human-scale processes (Simonetti et al., 2014). Moreover, after the decision of the US Geological Survey

(USGS) of making all archived Landsat data freely available, the issue of data cost does not longer exist, establishing Landsat data as an irreplaceable resource for long term global change studies.

Landsat 1, the first satellite in this family, was launched in 1972 and carried two sensors: the Return Beam Vidicom (RBV) and the Multi Spectral Scanner (MSS). RBV was a television camera, later replaced by the Thematic Mapper (TM) sensor in Landsats 4 and 5. Landsat 6 failed to achieve orbit, while Landsat 7 (still operational) carries an Enhanced Thematic Mapper Plus (ETM+) sensor as well as a panchromatic one. The most recent satellite in the series, Landsat 8, has been launched on February 11, 2013 and carries two new sensors, the Operational Land Imager (OLI) and the Thermal Infrared Sensor (TIRS) (Simonetti et al., 2014; Ünsalan & Boyer, 2003).

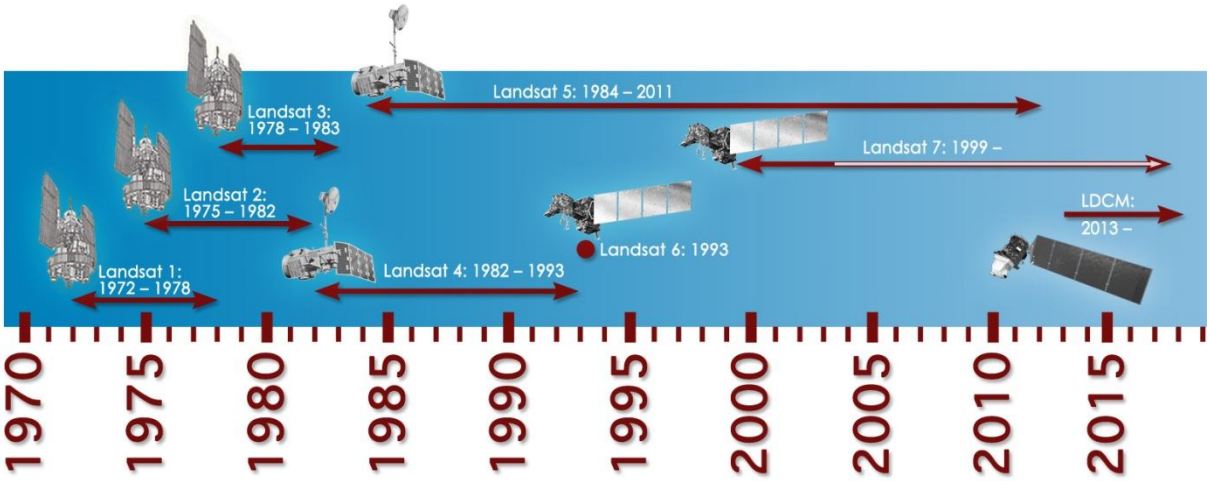

Figure 5: Landsat mission timeline showing satellite lifespans (Source http://www.nasa.gov)

Each Landsat satellite passes over the same area on the Earth's surface during daylight hours about 20 times per year. In reality the number of serviceable images is generally lower, depending on the amount of cloud cover, sun angle, and whether or not the satellite is in operation on any specific pass. Nevertheless, this still provides the opportunity for a given area to have Landsat images available for several dates per year.

Landsat images are catalogued according to their location within the Worldwide Reference System (WRS). In this system each orbit within a cycle is designated as a path. Along these paths, the individual nominal sensor frame centers are designated as rows. Thus, a scene can be uniquely defined by specifying a path, a row and a date. The newer generation Landsat images have a different set of WRS paths from those for Landsat 1, 2, and 3, due to

the differences in coverage pattern. The WRS from Landsat 4 to 8 is composed of 233 paths numbered from 001 to 233, east to west. The same number of rows (60) as the previous WRS system is used (Lillesand et al., 2004). Table 1 summarizes the main characteristics of Landsat satellites and sensors, while Figure 6 and Table 2 show the differences between the bandwidth of Landsat 4-7 (TM/ETM+) and of Landsat 8 (OLI/TIRS). Landsat 8 has a higher number of spectral bands and narrower bandwidths, resulting in differences between the spectral information (for example vegetation indices) that can be obtained from the latest sensor and its previous generations (Hang & Canh, 2014).

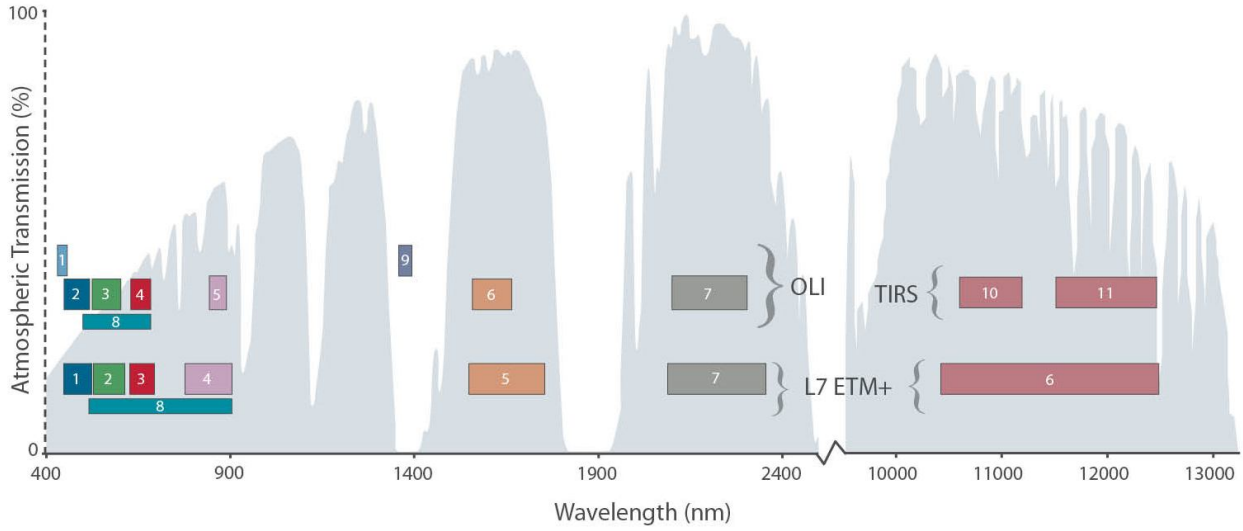

Figure 6: comparison between OLI spectral bands and Landsat 7's ETM+ bands. Source: http://landsat.gsfc.nasa.gov/?p=3186

Satellite	Period of operation	Orbit (revisit time/height)	Sensors	Number of Bands	Spatial resolution (m)
Landsat 1	July 23,1972 - January 6, 1978	18 days/900 km	RBV, MSS	4 (MSS)	RBV 80; MSS 60*
Landsat 2	January 22, 1975 – July 27, 1983	18 days/900 km	RBV, MSS	4 (MSS)	RBV 80; MSS 60*
Landsat 3	March 5, 1978 – September 7, 1983	18 days/900 km	RBV, MSS	5 (MSS)	RBV 80; MSS 60*
Landsat 4	July 16, 1982 – June 15, 2001	16 days/705 km	MSS, TM	7 (TM), 4 (MSS)	TM 30; MSS 60*
Landsat 5	March 1, 1984 – June 5, 2013	16 days/705 km	MSS, TM	7 (TM), 4 (MSS)	TM 30; MSS 60*
Landsat 6	October 5, 1993 (failed to launch)	16 days/705 km	ETM	8 (ETM)	Pan 15; ETM 30
Landsat 7	April 15, 1999 – present	16 days/705 km	ETM+	8 (ETM+)	Pan 15; ETM+ 30
Landsat 8	February 11, 2013 – present	16 days/705 km	OLI, TIRS	9 (OLI), 2 (TIRS)	Pan 15; OLI 30; TIRS 100

Table 1: overview of Landsat missions characteristics. (*) The original MSS pixel size was 79 x 57 meters, but production systems now resample the data to 60 meters. Source: USGS (2015).

LANDSAT 4-7				LANDSAT 8		
Spectral bands	**Spatial resolution (m)**	**Bandwidth (µm)**	**Useful for**	**Bandwidth (µm)**	**Spatial resolution (m)**	**Spectral bands**
-	-	-	Coastal and aerosol studies	0.43 - 0.45	30	Band 1 (Coastal aerosol)
Band 1 (Blue)	30	0.45 - 0.52	Bathymetric mapping, distinguishing soil from vegetation and deciduous from coniferous vegetation	0.45 - 0.51	30	Band 2 (Blue)
Band 2 (Green)	30	0.52 - 0.60	Emphasizing peak vegetation, useful for assessing plant vigor	0.53 - 0.59	30	Band 3 (Green)
Band 3 (Red)	30	0.63 - 0.69	Discriminating vegetation slopes	0.64 - 0.67	30	Band 4 (Red)
Band 4 (NIR)	30	0.76 - 0.90 (TM) 0.77 - 0.90 (ETM+)	Emphasizing biomass content, shorelines and soil moisture	0.85 - 0.88	30	Band 5 (NIR)
Band 5 (SWIR 1)	30	1.55 - 1.75	Discriminating moisture content of soil and vegetation; penetrating thin clouds	1.57 - 1.65	30	Band 6 (SWIR 1)
Band 7 (SWIR 2)	30	2.08 - 2.35 (TM) 2.09 - 2.35 (ETM+)	Discriminating mineral and rock types, sensitive to vegetation mois-ture content	2.11 - 2.29	30	Band 7 (SWIR 2)
Band 8 (Pan)	15	0.52 - 0.90 (ETM+ only)	Sharper image definition	0.50 - 0.68	15	Band 8 (Pan)
-	-	-	Improved detection of cirrus cloud contamination	1.36 - 1.38	30	Band 9 - Cirrus
Band 6 (TIR)	120/60	10.40 - 12.50	Thermal mapping, estimated soil moisture and vegetation stress analysis	10.60 - 11.19	100	Band 10 (TIR 1)
				11.50 - 12.51	100	Band 11 (TIR 2)

Table 2: comparison between Landsat 4-7 (TM/ETM+) and Landsat 8 OLI/TIRS bands.

2.3 Geographic Information Systems (GIS)

Geographic information Systems (GIS) are computer-based systems that can deal with virtually unlimited sources and types of biophysical and socioeconomic data, as long as they can be referenced by geographical location. These systems are capable of handling both locational and attribute (descriptive characteristics) data about the features of interest. This ability to handle and spatially interrelate multiple types of information stemming from a range of sources, easing their synthesis, analysis, and communication, is perhaps the greatest advantage of using a GIS (Lillesand et al., 2004).

Multitemporal and multisource data is becoming increasingly easy to acquire, which makes a GIS a fundamental tool to manage the wealth of information about land units, attribute data, and temporal layers that are generally used for classification or change detection analysis. Through GIS software it is possible, for example, to compare sequences of temporal layers, display the category of change for every land plot and extract areal and positional data automatically in order to describe and quantify land cover changes, analyze patterns of long-term vegetation dynamics and vegetation changes along ecosystem boundaries over time and help in understanding the current situation and predicting future patterns of change (Bender, Boehmer, Jens, & Schumacher, 2005; Ciolli, Serafini, & Tattoni, 2007; Mast, Veblen, & Hodgson, 1997). Many image processing and data analysis software are either integrated or compatible with GIS (Coppin et al., 2004). The incorporation of GIS technology in digital change detection methods also simplifies the development of maps of landscape change, that can be constructed by overlaying different temporal layers (not only remote sensing data, but also other types of data such as historical maps and surveys). This makes it easier to visualize and display changes, their characteristics and dynamics, to present data in map and other graphic formats and to update change maps, in a timely fashion and at scales that are consistent with ecosystem management objectives (Bender et al., 2005; Coppin et al., 2004). Once the spatial and temporal extent of change has been determined, it can be combined with different type of data in order to study various aspects of the issue, thanks to the possibility offered by GIS software to link spatial data with non-spatial but more detailed attribute data (van Lynden & Mantel, 2001).

Over the past decade, the development of well-designed and serviceable Open Source products such as QGis (QGIS Development Team, 2015), is providing researchers and users with valuable and inexpensive resources for landscape analysis (Rocchini et al., 2012; Rocchini, 2004).

3. PRINCIPLES OF LAND COVER AND VEGETATION CLASSIFICATION

Land cover has been defined as ‘‘the observed (bio) physical cover on the earth’s surface’’ (Di Gregorio & Jansen, 2005), and should not be confused with land use, which refers to the way in which people use these biophysical assets and describes human influence.

Image classification is the interpretation of remotely sensed images for the production of thematic maps that show the spatial distribution of the land cover types or features of interest and provide an informative description of a given area (Simonetti et al., 2014). Classification procedures can be implemented either manually (through the visual interpretation of the image and on-screen digitization of the classes of interest), or with automated procedures (supervised or unsupervised), that can either be pixel-based or object-based.

Land cover information is a key dataset for both land use and land cover change (LUCC) studies, for the reason that land cover changes are the most obvious indication of environmental change, which can in many cases be related to land use change as well (Di Gregorio & Jansen, 2005).

3.1 Overview of land cover classification principles

Because of its value as an environmental change indicator, information on land cover and land cover change should ideally be acquired through a common approach across countries and regions, especially considering the growing need for standardized datasets that are compatible with each other and for the necessity to map and monitor change over wide areas in a consistent manner. The reality, however, is that at global, continental and regional level, land cover type products can be very different in terms of their spatial cover, scale and class definition, in relation to the specific purposes for which they were created (Di Gregorio & Jansen, 2005; Gerard et al., 2010).

When trying to harmonize different land cover datasets, or to create new ones based on existing or customized classification systems, it is crucial to take into account the possibility of having to cope with different conceptualizations of the landscape, not only in terms of data structure (e.g., raster vs. polygon vs. point), but also in terms of differences in the objectives of the study and consequently the classification. This is necessary in order to avoid confusion, especially when the

datasets are nominally very similar but are difficult to compare or to integrate because they embody different views of the landscape (Comber, Fisher, & Wadsworth, 2005).

The design or adoption of a classification system is crucial, given that a universally accepted land cover classification system that can possibly satisfy all environmental monitoring needs at different spatial scales doesn't exist (Gerard et al., 2010). Therefore, a prerequisite of any study related to land cover classification and land cover change is the definition, in the least ambiguous way possible, of the land cover types of interest and of their distinguishing features, without forgetting the necessity of producing data that can be compared with pre-existing datasets.

The most successful attempts made so far at creating a standardized but flexible classification system that could be adopted internationally are those by the Food and Agriculture Organization of the United Nations (FAO), most notably the *Land Cover Classification System* (Di Gregorio & Jansen, 2005) and the *Global Forest Resource Assessment* (FRA) (FAO, 2010).

The FRA in particular has become the most widely recognized and used classification system for monitoring forest cover, both at the European and international level (Chirici & Martino, 2009; De Natale, Gasparini, Puzzolo, & Tosi, 2003; Marchetti, Bertani, Corona, & Valentini, 2012). In the past few years, studies have been increasingly conforming to the international FAO standard, rather than employing national or regional definitions, which complies with the increasing need of allowing for an easier comparison of forest cover data between countries for carbon accounting purposes (De Natale et al., 2003). Without a common framework, even just within the European Community substantial differences can be found in the definitions of forest applied in the national forest inventories. For example, threshold values for minimum crown cover range between 10 and 30%, minimum width ranges between 9 m and 50 m, and minimum area between 0.05 ha and 2 ha (Traub, Kohl, Paivinen, & Kugler, 1998). However, in the case of non-forested land cover types such as grassland, a standardized set of classifiers is not equally easy to find.

As for Italy, some attempts have been made at integrating national-based surveys related to land cover and land use change into an international framework, as shown by INFC (Inventario Nazionale delle Foreste e dei serbatoi di Carbonio – National Inventory of Forests and Carbon Sinks) and IUTI (Inventario dell'uso delle Terre d'Italia - Inventory of land uses in Italy). Both of them derive their classification criteria of forest from FAO's guidelines, using a hierarchical classification scheme which can be modified based on different levels of available information and on the detail level of interest (Marchetti et al., 2012). The classification scheme is also compatible with IPCC's Good Practice Guidance for Land Use, Land-Use Change and Forestry (GPG-LULUCF) (IPCC, 2003),

and to some extent with the European Union's CORINE (Coordination of Information on the Environment) Land Cover system; the latter however has been often criticized for its lack of internal consistency, ambiguous class definition and consequent overlap between different classes (Di Gregorio & Jansen, 2005).

To conclude, it seems necessary to discuss briefly terms such as "reforestation", "afforestation", "forest expansion" and "forest recovery", which have all been used somewhat interchangeably in literature to refer to the re-establishment of a forested landscape through the regeneration of woody vegetation (trees and/or shrubs) on disused agricultural lands, meadows and pastures following farm abandonment in regions where the potential natural vegetation is a forest (Hori, Hayashi, Matsubara, Awaya, & Iehara, 2007; Sitzia et al., 2010). In this work, however, a distinction is made between afforestation and reforestation, based on FAO's guidelines. Both terms refer to establishment of trees on unforested land; however, reforestation is defined as the re-growth of forests after a temporary (< 10 years) condition with less than 10% canopy cover due to human-induced or natural perturbations, while afforestation is the conversion from other land uses into forest, or the increase of canopy cover to the 10% threshold that identifies forests (FAO, 2010). In this work only afforestation processes have been taken into consideration.

Another term frequently used in the literature related to the loss of grassland ecosystems due to the natural advancement and/or densification of trees or shrubs (either attributed to climate change or to changes in land-use practices) is forest "encroachment" or "invasion" (Améztegui et al., 2010; Briggs et al., 2005; Coop & Givnish, 2007; Didier, 2001; Halpern, Antos, Rice, Haugo, & Lang, 2010; Laliberte et al., 2004; Price & Morgan, 2008).

3.2 Aerial photographs and visual photointerpretation

Before the introduction of digital remote sensors, the only way to derive land cover information from analog aerial images was visual interpretation, while nowadays digital processing techniques have established themselves as the preferred option (Anderson & Cobb, 2004). Given that the ultimate goal of land cover mapping is to obtain a description of the area of interest that is accurate, suitable for the user's purposes and not cluttered by irrelevant information (Brandtberg, 1999), the replacement of a human interpreter with an automated system is not al-

ways easy, and it can be met with varying degrees of success in relation to the characteristics of the image and to the needs of the end user.

Visual interpretation and classification of aerial images requires the ability to observe and correctly interpret image features in order to define homogeneous areas of cover. This can be made either by tracing the boundaries separating different land cover units (Kadmon & Harari-Kremer, 1999) or by point sampling. Nowadays both the delineation and the class assignation can be executed through GIS software, which to a certain degree simplifies and speeds up the process. The result of a manual classification is typically a vector image where the features of interest are expressed as geometrical shapes: polygons for homogeneous areas of cover and points when a point sampling scheme is used.

Visual interpretation, however, poses two major problems: the first is that the delineation of homogeneous vegetation units is not based on explicit measurement procedures, and as such, the information is not objective and difficult to replicate. Inconsistencies between- and within-interpreters make it difficult to evaluate changes over time and to reconcile multiple maps of the same area. The second is that using large-scale photography or enlargements to extract information at very fine scales over the entire area of interest can be prohibitively time-consuming and labor intensive, depending on the size of the area itself (Culvenor, 2002). Moreover, the planning and acquisition of aerial images is has substantial costs, especially when acquisition has to be repeated at different moments in time, either for change detection applications or for inventory purposes. Relying on visual interpretation and manual digitization of land cover units also makes it difficult to update existing maps quickly and efficiently (Kadmon & Harari-Kremer, 1999; Lillesand et al., 2004; Lu et al., 2004; Pouliot, King, Bell, & Pitt, 2002).

Prompted by the rapid diffusion of remotely sensed data in digital format starting from the 1980s, much research has been devoted to automating classification and data analysis procedures in order to reduce or eliminate the drawbacks associated with manual photointerpretation. Digital computer processing, in addition to offering consistent and repeatable results, can also take advantage of spectral features from the non-visible parts of the electromagnetic spectrum, which are impossible to fully evaluate by a human operator due to the limited ability of the eye to discern tonal values and the difficulty to simultaneously analyze numerous spectral images (Coppin et al., 2004).

The use of automated classification procedures with aerial photographs is not always possible or convenient. While the human eye has a limited ability to interpret spectral patterns and distin-

guish between spectral signatures, computers are limited in their ability to evaluate spatial patterns, making visual and digital techniques complementary in nature. A skilled interpreter analyzing large-scale aerial photography generally produces more accurate results than an automated digital change detection method (Coppin & Bauer, 1996), because they can make full use of their experience and knowledge. There are several non-spectral features of an image that are useful for identification of land cover change through visual interpretation, like shape, size, pattern, tone, texture, shadows, site, association, and resolution (Lillesand et al., 2004). These elements can be used as a support in the decision-making process, but are not common in the digital change detection analysis yet because of the difficulty of extracting and interpreting them (Lu et al., 2004).

For these reasons, careful consideration must be given to which approach (or combination of approaches) fits a specific application best (Lillesand et al., 2004), and manual interpretation is still an effective and widely adopted approach for classification and change detection, especially when dealing with historical material (Brandt et al., 2002). This is demonstrated by its use in several recent studies (Coop & Givnish, 2007; Corona, Pompei, & Scarascia Mugnozza, 2005; Frate et al., 2014; Gerard et al., 2010; Hori et al., 2007; Lega & Vincini, 2003; Sgarbossa, 2010; Urbinati et al., 2004; Walton, Nowak, & Greenfield, 2008). The reasons behind the choice of this approach are varied; for instance, insufficient spatial or radiometric resolution (especially when using historical aerial photographs), tonal differences between areas with the same type of land cover at different elevations or aspects within the same photoset, or similarities between different types of land cover that could, without prior knowledge of the study area, be mistaken for each other (Coop & Givnish, 2007). Another factor that may significantly influence the classification process is the presence of shadows, typical when images are taken when solar elevation is not as close to directly overhead as possible, or in the presence of certain topographic features (for example narrow valleys), as in Sgarbossa (2010) and Ciolli, Serafini, & Tattoni (2007). In most cases the necessity of working with pre-existing and historical material gives no choice but to use images taken at suboptimal times (Whiteman & Brown, 1998). When using automated classification methods, shadows are very likely to cause thematic errors; conversely, when using manual interpretation, the presence of shadows can offer to the photo-interpreter important clues, such as the height of trees (Bitelli et al., 2005).

3.3 Vegetation mapping through multispectral images and Vegetation Indices

The first automated and semi-automated land cover classification techniques were pixel-based methods, developed in the 1970s for analyzing Landsat MSS data. Pixel-based approaches take the image pixel as fundamental unit of analysis, using its spectral signature as the numerical basis for categorization to assign a land cover class to each individual pixel (Aplin & Smith, 2008). Pixel-based classification methods are the most commonly used, especially when coarse and medium spatial resolution images are used (Lu et al., 2014).

Multispectral remote sensing data can be effectively used to map vegetation and differentiate it from other land cover types on the basis of its spectral characteristics. Photosinthetically active vegetation is generally characterized by conspicuous absorption in the red and blue bands of the visible spectrum (up to 70 to 90% of the incident radiation) in relation to its chlorophyll content, and by high reflectance in the green and especially in the NIR bands (Jackson & Huete, 1991). In the NIR part of the spectrum, differences in reflective properties of plant species are more pronounced than in the visible region. There is however a distinctive variability between different vegetation types, determined by parameters such as leaf shape, size and biochemical constituents, overall plant shape, leaf water content, background soil type and density of vegetative cover (Figure 7).

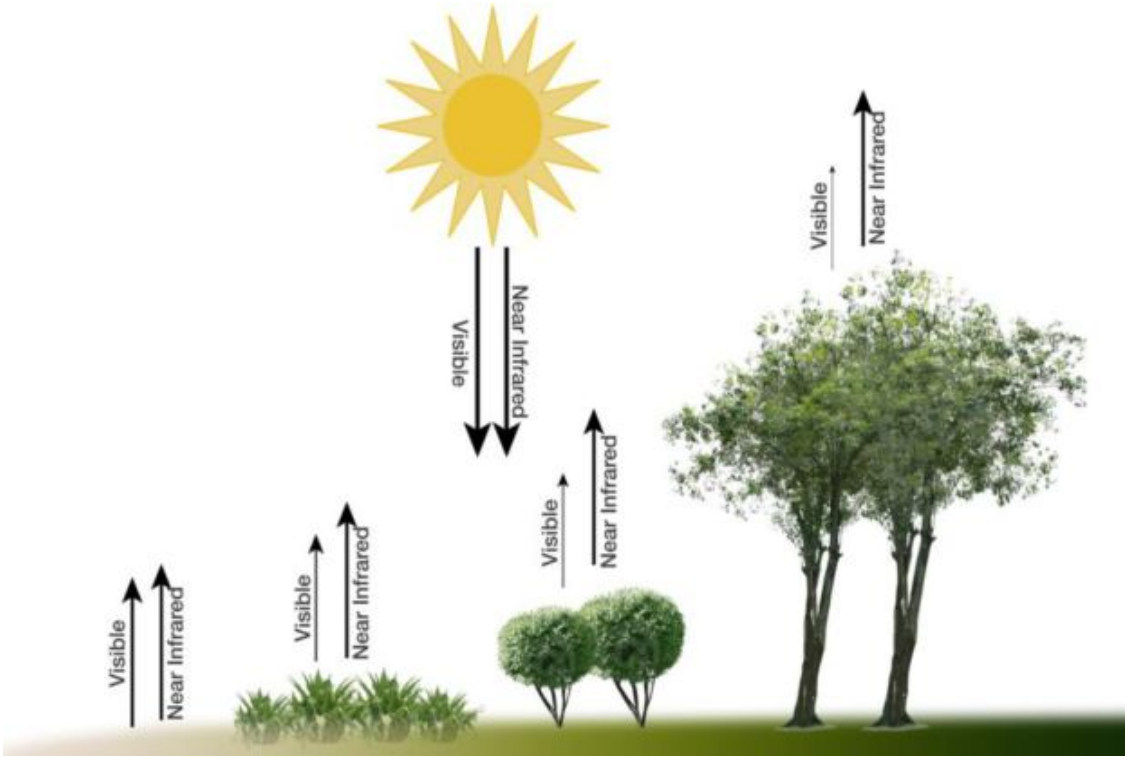

Figure 7: Depending on the vegetation type and density, vegetated areas can absorb different amounts of visible light and reflect different amounts of NIR light.

The differentiation between different vegetation types can rarely be based only on the interpretation of spectral properties alone, however, because their spectral characteristics change significantly within the vegetative period and can be very similar to each other in some parts of the growing season and very different in others (Esch, Metz, Marconcini, & Keil, 2014). For this reason, spectral data from multispectral remote sensors is often aggregated to create vegetation indices (Simonetti et al., 2014).

Vegetation indices (VI) are mathematical transformations (usually ratios or linear combinations) of reflectance values measured in different spectral bands (especially the visible and NIR ones), based on the differences in the reflectance patterns between green vegetation and other surfaces (Payero, Neale, & Wright, 2004). Over the years several vegetation indices have been proposed, ranging from very simple to very complex band combinations.

The main advantages in using vegetation indices instead of single-band radiometric responses lies in their ability to synthesize the information contained in the spectral bands, reducing the data volume for processing and analysis but also providing information that is not available in any single band. The ideal vegetation index should be highly sensitive to vegetation dynamics and not sensitive to soil background and atmospheric variations (Lyon, Yuan, Lunetta, & Elvidge, 1998; Singh, 1989), but no single vegetation index can completely summarize the information contained in a multidimensional spectral data space, and a certain amount of information loss may be expected (Simonetti et al., 2014). In addition, indices considered suitable for a specific analysis may not be appropriate in another context (Coppin et al., 2004).

One of the most widely used vegetation indices is the Normalized Difference Vegetation Index (NDVI)(Turner, Cohen, Kennedy, Fassnacht, & Briggs, 1999). NDVI is a ratio-based index, and is calculated dividing the NIR band by the red band of the image according to this equation:

NDVI= (NIR-RED) / (NIR+RED)

NDVI values range from -1 to +1. Higher values indicate a larger difference between the red and NIR radiation recorded by the sensor, which is associated with highly photosynthetically-active vegetation. For growing green vegetation, the reflectance in the NIR is greater than in the visible, while dead or stressed vegetation reflects more in the red and less in NIR part of the spectrum. Values between +0,6 and +0,9 typically represent dense forest stands or crops at their peak growth stage, while sparse vegetation such as shrubs and grasslands may show intermediate NDVI values, for example between +0,2 to +0,5 (Simonetti et al., 2014). Low NDVI values mean there is little difference between the red and NIR signals; this happens when there is little or no photosyn-

thetic activity, like on non-vegetated surfaces such as bare soils and rocks, that have NDVI values close to 0. Clouds, water and snow have higher visible reflectance than NIR reflectance, thus they are characterized by negative index values (Jelinski & Wu, 1996; Lillesand et al., 2004). NDVI has been found to be highly correlated with crown closure, leaf area index (LAI), and other vegetation parameters (Hayes & Sader, 2001).

Using ratio-based indices such as NDVI can emphasize differences in brightness values of the spectral response curves of different features and help suppressing differential solar illumination affects due to topography and aspect, as well as normalizing differences in brightness values when using multiple date images. The popularity of NDVI in vegetation mapping studies is mainly due to its ability to compensate for changing illumination conditions, surface slope, and viewing angle (Campos, Lawrence, McGlynn, & Gardner, 2011; Nordberg & Evertson, 2005; Simonetti et al., 2014).

There are however some limitations in the use of NDVI; the first is that when the index is used for environments with a high percentage of bare ground and exposed rock, the characteristics of the soil surface can influence its values by a large degree: the presence of dry, light colored soils lowers NDVI values, while when wet or darker soils are present this effect is less detectable (Huete & Jackson, 1988).

The second limitation in using NDVI is that, beyond a certain biomass density it asymptotically approaches a saturation level, at which point the index becomes insensitive to different densities. This saturation effect is typical of multilayer vegetation such as forests or agricultural crops (Gu, Wylie, Howard, Phuyal, & Ji, 2013; Mašková, Zemek, & Květ, 2008; D. P. Turner et al., 1999). In addition to this drawback, NDVI does not eliminate atmospheric effects. In order to avoid these problems, indices such as the Enhanced Vegetation Index (EVI) have been proposed. EVI allows for improved sensitivity in high biomass regions and improved vegetation monitoring capability through the de-coupling of the canopy background signal and the reduction in atmospheric influences. EVI is calculated according to this equation:

$$\mathbf{EVI = G * (NIR - RED) / (NIR + C1 * RED - C2 * BLUE + L)}$$

where NIR/RED/BLUE are atmospherically-corrected or partially atmospherically corrected (for Rayleigh effect and ozone absorption) surface reflectances, L is the canopy background adjustment coefficient, and C1, C2 are the coefficients of the aerosol resistance term, which uses the blue band to correct for aerosol influences in the red band.

A significant drawback of vegetation indices like EVI, that include terms not expressed as a band ratio (like the constant term L), is their sensitivity to topographic effects. In these instances, topographic correction should be carried out before calculating the indices, unlike NDVI which doesn't strictly require topographic correction because the topographic effect is eliminated or weakened (Matsushita, Yang, Chen, Onda, & Qiu, 2007).

The values of a vegetation index collected over a long period of time can be averaged to obtain the "normal" growing conditions in a region for a given time of year, while plotting time-series vegetation index data produces a temporal curve that summarizes the various stages that green vegetation undergoes during a complete growing season. This curve can be used to extract key phenological variables such as the start, the peak and end of the growing season (Simonetti et al., 2014).

4. LAND COVER CHANGE DETECTION

Change detection, defined by Singh (1989) as "the process of identifying differences in the state of an object or phenomenon by observing it at different times'' is based on the use of multitemporal datasets of the same area to distinguish changes between different dates of imaging in order to qualitatively and quantitatively analyze the temporal effects of phenomena. Change detection is one of the main applications of remotely sensed data in fields such as bio-physics, environmental monitoring and land use/land cover change analysis (Hussain et al., 2013; Lillesand et al., 2004).

The purpose of land cover change detection studies is to identify the spatial and temporal patterns of land cover change in respect to their extent, quantity and characteristics (Morgan et al., 2010) by analyzing remote sensing images of the same geographical area taken at different times (Radke, Andra, Al-Kofahi, & Roysam, 2005). It can be applied to a wide variety of problems, such as urbanization, monitoring of shifting cultivation, deforestation assessment, changes in vegetation phenology, crop stress detection, and other environmental changes, and the results are useful to assess environmental impacts and risks (Singh, 1989). Change detection assessments provide a fundamental input for environmental studies, planning and management, because they can improve the knowledge of the magnitude of the problem in terms of its areal extent and intensity (Serra, Pons, & Saurì, 2003; Whiteman & Brown, 1998). In particular, studying long-term vegeta-

tion changes is necessary to understand the ecology of plant successions, the effects of climate change on vegetation, the impacts deriving from land use, and as a predictive tool in ecosystem science and management (Anderson & Cobb, 2004).

A complete change detection assessment should provide the following information: a) whether a change has occurred or not, b) the nature of the change (the change trajectories of land-cover types), c) the areal extent and the rate of the change, and d) the spatial pattern of the change. In addition, it is fundamental to provide an accuracy assessment of change detection results (Lu et al., 2004).

The major data sources for land cover change detection applications during the past decades have been optical airborne- and satellite-based sensors (Lu et al., 2004; Morgan et al., 2010). Remote sensing data are used for digital change detection based on two assumptions (Coppin & Bauer, 1996; Hussain et al., 2013; Singh, 1989): the first is that different land cover types have their own spectral signatures, so changes in land cover must result in variation of spectral signatures. Any radiance variation over time for a particular area can be associated with an alteration in its reflective/emissive characteristics, which in turn can be related to changes in the biophysical properties of the surface. Land cover change can therefore be detected through the comparison of the spectral signatures of two moments in time using a suitable algorithm (Lu et al., 2004). The second assumption is that changes in the object of interest alter the spectral behavior (reflectance value or local texture) of the object itself in a way that that is distinguishable from changes caused by other factors such as differences in atmospheric conditions, illumination (sun angle), background conditions (for example the differences in soil moisture), and sensor calibration. This means that variations in radiance caused by land cover change between the time periods considered must be large compared to radiance variations arising from external factors.

The successful design and implementation of a digital change detection procedure depend on many factors related to the specific conditions of the study. A general scheme is comprised of the following steps: 1) definition of the change detection research problem; 2) selection of remotely sensed data; 3) application of preprocessing procedures to the images; 4) extraction of variables suitable for the assessment of the specific type of change detection problem; 5) selection of appropriate change detection algorithms; and 6) evaluation of the results (Hussain et al., 2013; Lu et al., 2014, 2004).

4.1 Data selection

The selection of the most appropriate satellite data for a change detection procedure is influenced by three major factors, namely: a) the characteristics of the sensor, b) the temporal characteristics of the remotely sensed imagery, and c) the characteristics of the study area. The ideal conditions (usually never met in practice) would be to have access to multitemporal images from the same sensor, with the same radiometric and spatial resolution, with no cloud cover and taken at anniversary or near anniversary acquisition dates (when considering changes occurring between different years) in order to minimize the effects of external sources such as sun angle, seasonal and phenological differences (Coppin & Bauer, 1996; Lu et al., 2004).

4.1.1 Sensor characteristics

The spectral, spatial, temporal, and radiometric resolutions of the sensor have a significant impact on the success of a change detection project, so the selection of suitable data sets and image acquisition dates for a specific study is conditioned by the understanding of the strengths and weaknesses of different types of sensor in relation to the user's needs, complexity of landscape, areal extent of the study area, and so on (Lu et al., 2014). This aspect has already been discussed in section 2.2.2 Satellite images. Even using imagery from the same sensor doesn't guarantee that the sensor characteristics will be perfectly equal. Sensors degrade over time, causing a change in radiometric qualities and, in some cases, a partial loss of data.

4.1.2 Temporal characteristics

There are several temporal requirements to take into consideration when choosing dates for multitemporal satellite images for change detection. This problem has two dimensions: the temporal resolution (the length of the interval between one image and the next) and the calendar acquisition dates.

The use of anniversary dates or anniversary windows (annual cycles or multiples thereof) minimizes differences in reflectance caused by different sun angles and seasonal vegetation changes

(Aldrich, 1979; Coppin et al., 2004). Plants undergo intra-annual variations or cycles (phenology) mediated by physical drivers such as temperature, solar radiation, and water availability. In higher latitudes, for example, plant cycles are principally driven by temperature and photoperiod, and during different stages of growth the same vegetation type can appear significantly different (Lunetta, Ediriwickrema, Johnson, Lyon, & McKerrow, 2002). Images acquired during the same time of the year and at the same time of the day belong to the same phenological stage of growth, but have also similar solar illumination angles, which ensures that shadowed ground areas, as well as brightly illuminated areas, will be similar in appearance for both early and late dates. This is of particular importance when the study area has an irregular topography. It is possible to normalize the effect of different illumination angles by using a DEM, but this approach has some limitations. Acquiring near-anniversary images from the same sensor can be difficult, however, especially in areas where it is extremely hard to find cloud-free images (Hussain et al., 2013). In this case, the use of multi-sensor images or non-anniversary dates is the only viable choice (Lu et al., 2014).

The calendar acquisition date of the images is important because it is necessary to select a time of the year when the features of interest can be accurately differentiated from other features.

The ideal season for change detection is still a controversial topic in literature, and varies according to the geographical area and the type of land cover change to be detected. For forest change, for example, several authors recommend summer as the most suitable season because of their phenological stability. Imagery from the autumn, spring and winter periods is not suited for forest classifications due to the lower sun angles which cast shadows (Meyer, Itten, Kellenberger, Sandmeier, & Sandmeier, 1993). Choosing the driest period of the year (depending on local conditions), also enhances spectral separability while minimizing spectral similarity, because surface wetness has a strong influence (Coppin & Bauer, 1996). For a semi-arid grassland environment, Langley et al. (2001) found that September was the best month, because of more distinct spectral responses for the target vegetation classes and fewer shadows in that geographic region at that time of year. In most cases herbaceous species, shrubs, and forests show contrasting seasonal variations in vegetation activity. In temperate climates, the peak activity for herbaceous species and shrubs usually occurs in spring, while for forests in summer (Vicente-Serrano, Pérez-Cabello, & Lasanta, 2008).

The use of inter-annual multi-seasonal imagery for classification of land cover has also been proved to be useful. For example, Yuan et al. (2005) found that by combining late spring and summer images, fields planted with annual crops could be distinguished more easily from forests,

because they respond as bare soil. When only a summer image is used, forests and some crops appear spectrally similar. However, the late summer image is needed to separate those same crop fields from urban areas with significant amounts impervious surfaces that are spectrally similar to bare soil in a spring image. Compared to the single dates, both the average and the minimum separability were increased by the combination of spring and summer images.

It is also important to consider the dependency of the type of change sought on the temporal interval between dates of imagery: data collected within a short time interval might not show the change process, while data collected between temporal moments too far from each other might be prone to excessive omission error (Hussain et al., 2013).

In many studies, however, the most important factor that influences the choice of periodicity of the data acquisition remains the availability of data of acceptable quality (Coppin & Bauer, 1996), especially when the interest is on monitoring changes over a relatively short period of time. In the case of optical satellite images, data availability is heavily influenced by cloud cover, that needs to be minimal in order to avoid loss of information and no-data clusters in the final change map (Mihai, Savulescu, & Sandric, 2007).

4.1.3 Environmental characteristics

Different landscapes have different land cover composition features and spatial patterns, and this aspect has to be considered in the selection of remote sensing data and change detection techniques (Lu et al., 2014). Landscape heterogeneity and the size of homogeneous land cover classes affect change detection error because they determine the mixed pixels present in the dataset, meaning those pixels whose reflectances arise from more than one land-cover class. (Smith, Stehman, Wickham, & Yang, 2003). Less dominant land cover types tend to disappear as grain becomes coarser, but their pattern of spatial distribution influences the rate at which this information loss occurs. Cover types that are dispersed in the landscape are lost more rapidly than clumped cover types (M. G. Turner, 1990).

Classification and change detection are also especially challenging in mountain environments because of the highly fragmented landscape, steep terrain features and related shadows, orographically increased cloud cover and snow cover with rapid changes in its spatial extent (Gartzia, Alados, Pérez-cabello, & Bueno, 2013; Waser & Schwarz, 2006). Moreover, changes in mountain vegetation tend to be slow and can go undetected in the short term; for example, the speed of

shrub encroachment on subalpine grassland has been estimated at 2 m/year. As a consequence even small improvements in classification accuracy can be vital in detecting changes in this kind of environment (Gartzia et al., 2013).

A further element of variability in phenological characteristics may be introduced by local precipitation and temperature variations, soil moisture, site characteristics, atmospheric conditions and plant species, even when the images are acquired at anniversary dates.

Ensuring similar atmospheric conditions between two dates of imagery is complex because they tend to change on an hourly or daily basis and are not always homogeneous across an image. For this reason, the application of an atmospheric normalization procedure is in most cases considered necessary (Song, Woodcock, Seto, Lenney, & Macomber, 2001). Moreover, differences in soil moisture between images can affect the detected changes if soil represents a significant portion of the signal. This is especially noticeable when using image bands that are sensitive to water, such as Landsat TM band 5. Soil moisture can also indirectly affect plant stress, thus altering the appearance of similar vegetation so that it may appear as if the vegetation composition has changed. Choosing anniversary dates can help to minimize the effects of different soil moisture conditions, however, precipitation records should be compared to further asses their similarity.

4.2 Pre-processing procedures

The goal of pre-processing procedures is to minimize the impact of sensor and external differences to make all images appear as if they were acquired with the same sensor, at the same time and under the same atmospheric conditions (Coppin & Bauer, 1996; Lillesand et al., 2004; Song et al., 2001). Moreover, considering that the aim of a change detection procedure is to detect significant changes while rejecting non-significant ones, it is important to eliminate or filter out common types of non-significant changes (image noise) before undertaking the change detection process itself. Image pre-processing procedures include geometrical rectification and image registration, radiometric and atmospheric correction, and topographic correction if the study area is in mountainous regions (Hussain et al., 2013; Lu et al., 2004; Radke et al., 2005). In some cases, it is also necessary to remove or mask irrelevant features (e.g. clouds) or land cover types not of interest (Coppin et al., 2004).

4.2.1 Geometric correction

If individual digital or digitized images are acquired with no spatial reference, it must be added, and it is also necessary to correct their vertical and horizontal geometric displacement and remove geometric distortions (Lillesand et al., 2004). Geometric (positional) errors may alter the perceived location of features over a landscape, their size, or both. As a consequence, geometric distortions in the images must be removed before quantitative measurements can be made, especially when conducting a multitemporal study.

The spatial distribution of positional error over the region of interest is rarely random or uniform. In many cases a distinct pattern can be recognized, arising from either the sensor's properties and/or the topography of the ground. Relief heterogeneity is one of the most important causes of distortion, especially for aerial photography, because it makes features at higher elevations appear larger than features of similar size located at lower elevations (Kadmon & Harari-Kremer, 1999; Rocchini & Di Rita, 2005). For this reason, mountainous environments are very challenging for achieving geographically accurate data (Rocchini et al., 2012). Rocchini (2004) demonstrated that if geometric distortions are corrected using an improper rectification method, changes in some land cover classes can be overestimated by up to double the occupied area.

When using multitemporal datasets for change detection, both the geometric accuracy of each single image and the accuracy of the spatial registration of multidate imagery to a common spatial framework have to be considered (Foody, 2002; Townshend, Justice, Gurney, & McManus, 1992). The positional error in the individual layers and the imperfect co-registration among each dataset has the effect of either masking or exaggerating change (Boyd & Foody, 2011; Verbyla & Boles, 2000), because land cover is evaluated at the wrong location between one time and another, changing measurements and the ecological change estimates derived from them (Carmel, Dean, & Flather, 2001; Dai & Khorram, 1998; Rocchini & Di Rita, 2005; Serra et al., 2003; Townshend et al., 1992; Verbyla & Boles, 2000; Wang & Ellis, 2005).

This is of particularly significance in the case of highly heterogeneous or fragmented landscapes (Foody, 2002; Morgan et al., 2010; Roy, 2000; Wang & Ellis, 2005), as demonstrated by Townshend et al. (1992) and Serra et al. (2003), who showed how in this type of landscape the effect of misregistration error is greater than in homogeneous areas. In addition, this affects steeper areas more than flatter areas (Lu et al., 2004; Van Niel, McVicar, Li, Gallant, & Yang, 2008). Dai & Khorram (1998) observed that the false changes added by misregistration are mainly distributed

spatially along the edges of the images, while the true changes removed by misregistration are spatially distributed away from edges.

Geometric correction techniques can be divided between procedures that just assign horizontal map (x, y) coordinates to digitized or digital images (georeferencing and rectification procedures), and procedures that also add vertical map (x, y, and z) coordinates to images in order to accurately represent distances, angles, and areas (orthorectification) (Lillesand et al., 2004; Morgan et al., 2010; Rocchini et al., 2012).

Despite the fact that rectification can correct several kinds of image distortion through the process of shifting (translating, transforming, warping/rubbersheeting, etc.) the pixel locations of a target image through the use of Ground Control Points (GCPs), it cannot correct relief displacement, because no information regarding the elevation of GCPs is provided. In this case an *orthorectification* procedure is more suitable, because it can correct for image displacements due to sensor (camera) and platform (aircraft or satellite) characteristics and to terrain elevations. Local elevation is obtained from a digital elevation model (DEM) or from the elevation at each GCP measured by a GPS (Rocchini et al., 2012; Willneff & Poon, 2006). Rocchini & Di Rita (2005) demonstrated that given the same GCPs, in landscapes with high geomorphological complexity orthorectification is superior to simple rectification because it guarantees lower geometric displacement, leading to the possibility of computing distances and areas more accurately, while on flat areas displacement error is similar for all transformations (Rocchini et al., 2012; Willneff & Poon, 2006).

When using two or more spatial layers together, a frequently used term is *co-registration*, which indicates the process of accurately overlaying the layers onto each other (Rocchini et al., 2012). When using two or more independently georeferenced or orthorectified datasets in change detection studies, it is commonly assumed that the images are co-registered with no error, so they can be compared directly (Coppin & Bauer, 1996; Foody, 2002). However, perfect co-registration of multi-temporal images is not possible, as there is always residual error in orthorectification models, and even residual misregistration at the sub-pixel level can lead to inaccuracies in the areal assessment of change at the change/no-change boundaries (Coppin & Bauer, 1996; Coppin et al., 2004; Verbyla & Boles, 2000). Accurate geometric registration of multi-temporal imagery is one of the most important requirements in digital change detection methods, especially if change analysis is performed on a pixel-by-pixel basis, as demonstrated by several studies such as (Dai & Khorram, 1998; Stow & Chen, 2002; Stow, 1999; Townshend et al., 1992; Verbyla & Boles, 2000).

To be able to compare separate layers pixel by pixel, the pixel grids of each layer must conform to the other layers in the database. Sub-pixel level geometrical registration accuracy is generally required, and becomes even more important when data is from different sensors and at different resolutions (Hussain et al., 2013; Jianya, Haigang, Guorui, & Qiming, 2008; Lu et al., 2004). If co-registration of two or more images is considered not to be sufficiently accurate, the one believed to be the most accurate should be used as standard of location, and the others re-registered to fit it (Hori et al., 2007). It is also necessary to test the geometric accuracy of the images before extracting quantitative information from them, in order not to risk obtaining misleading results (Rocchini & Di Rita, 2005; Verbyla & Boles, 2000).

Assessment of registration accuracy is usually calculated as the root mean square error (RMSE), which represents a measure of deviation of corrected GCP coordinate values from the original reference GCPs used to develop the correction, and that in turn depends on the transformation used to register the images (Brovelli & Minghini, 2012; Rocchini et al., 2012). RMSE values of 0,5 to 1,0 pixels are normally considered adequate to minimize artificial change caused by positional error, and visually the results of overlaying two images with this level of misregistration are acceptable (Townshend et al., 1992; Verbyla & Boles, 2000). In some cases, however, even sub-pixel co-registration error can lead to significant error in the quantification of land cover change, especially across the boundaries between different land cover classes (Coppin & Bauer, 1996; Townshend et al., 1992; Wang & Ellis, 2005) and in highly fragmented landscapes (Serra et al., 2003). Townshend et al. (1992) followed by Dai & Khorram (1998) demonstrated that to achieve errors of 10% in vegetation index values obtained from Landsat MSS images, a registration accuracy of 0,2 pixels or less is required, but this level of accuracy is hardly achievable in practice.

4.2.2 Atmospheric correction

The second critical requirement for successful change detection is to obtain a comparable spectral response from images acquired at different dates. Digital sensors record the intensity of electromagnetic radiation from the Earth's surface in the form of a pixel digital number (DN), which is a linearly transformed representation of at-sensor radiance for a discrete resolved area of the Earth's surface. The DN range of a sensor depends on its radiometric resolution, and DN values do not depend only on the properties of the observed objects, because they are influenced both

by sensor-induced and scene-related radiometric effects. Sensor-induced effects are caused by technical issues such as detector calibration, filtering, platform and system stability, while scene-related effects include the influence of topography, atmosphere, viewing angle, adjacency effect, position of the sun and the reflectance properties of the objects of interest (Meyer et al., 1993).

As a consequence, the spectral signature of a specific land cover is not comparable between different images if expressed as DN, so it is important to eliminate differences between image acquisitions that are not related to the remotely sensed objects themselves (Coppin et al., 2004; Hussain et al., 2013; Morgan et al., 2010; Song et al., 2001; Xie, Sha, & Yu, 2008; D. Yuan & Elvidge, 1996). The impact of some of these factors, such as those related to sun angle and phenology effects, may be partially reduced by selecting near-anniversary images from the same sensor (Serra et al., 2003). The most important factor, however, is the influence of the atmosphere, for which a variety of atmospheric correction techniques have been developed.

These techniques can be broadly divided into *absolute* and *relative* atmospheric correction (normalization). Absolute correction aims at removing all atmospheric interference due to absorption and scattering in order to extract the reflectance values at the Earth's surface from the original DN values (Hussain et al., 2013; Xie et al., 2008). These procedures require knowledge of both the sensor spectral profile and the atmospheric properties at the acquisition time, which are difficult and time-consuming to acquire (Du, Teillet, & Cihlar, 2002; Xie et al., 2008). Examples are Dark Object Subtraction (DOS) and atmospheric modelling (e.g. Second simulation of the satellite signal in the solar spectrum, 6S) (Hussain et al., 2013; Lu et al., 2004; Song et al., 2001).

Relative radiometric correction on the contrary is based on the assumption of a linear relationship between image bands across time, implying that the spectral reflectance properties of the sampled pixels do not change during the considered time interval (Du et al., 2002). This requires the radiometric measurements of pseudo-invariant features (PIF) in the images, which are objects spatially defined and radiometrically stable (e.g. mature forest stands, clear deep lakes, etc.). This method allows the normalization of the image (the same DN values across all the normalized images represent the same reflectance, independently of what the actual surface reflectance value is), and is often preferred because it is easier to achieve compared to absolute radiometric correction (Hussain et al., 2013; Song et al., 2001; Xie et al., 2008). However, this type of radiometric normalization can lead to low levels of accuracy, because the result is dependent on the subjective selection of PIFs (Du et al., 2002; Singh, 1989).

Song et al. (2001) and Schroeder et al. (2006) compared the effectiveness of different absolute and relative radiometric correction procedures, and both concluded that all corrections improved change detection accuracy, regardless of their absolute or relative nature, and that more complex atmospheric correction methods did not necessarily lead to consistent improvements in classification change detection and classification accuracies.

In some cases atmospheric correction is not strictly necessary, for example when independent classifications are performed prior to the change detection analysis. However, when using band ratios rather that simple spectral bands, as in the case of NDVI, atmospheric correction has to be done, because atmospheric effects contaminate the NDVI signal in a non-linear way. Contributions from the atmosphere to NDVI can amount to 50% or more over thin or fragmented vegetation cover (MacDonald et al., 2000).

4.2.3 Topographic correction

Topographic effect is the variation in radiance that accompanies a change in orientation from a horizontal to an inclined surface of the same cover type, in response to a change in light source and sensor position (Matsushita et al., 2007). In terrains with high relief, topography effects may cause pixels belonging to the same land cover class to have different spectral values, and pixels belonging to different cover types to have similar ones. This can introduce significant errors, especially when change detection is performed by using methods based on spectral analysis of individual pixels (Fahsi, Tsegaye, Tadesse, & Coleman, 2000). For example, it has been demonstrated that terrain-induced illumination variations have made it difficult to distinguish between forests and non-forest background (Meyer et al., 1993). In mountainous or rugged study areas, topographic correction may be necessary to reduce the impact of topography on reflectance.

The most common type of topographic corrections are slope-aspect ones, which should ideally remove all topographically induced illumination variation to ensure that two pixels with the same reflectance properties but different orientations have the same value; as a visible consequence of the correction, the three-dimensional relief impression of a scene gets lost and the image looks flat (Allen, 2000).

The basic requirement of any topographic correction method is illumination, which is the proportion of direct solar radiation that hits a pixel and varies with the cosine of the incidence angle. Due to atmospheric scattering, sun elevation is also important, because a surface perpendicular to

the sun at a low sun elevation will receive less radiation than a surface perpendicular to the sun at a high solar elevation (Ekstrand, 1996).

Topographic correction methods can be further grouped in those that assume Lambertian conditions (the surface reflects incident solar energy uniformly in all directions, therefore reflectance is independent on the observation angle) and those that consider directional reflectance. The simplest and most used approach belonging to the first category is the cosine correction, because it does not require external parameters. This method however tends to overcorrect the areas under low illumination conditions and to actually increase variance (Fahsi et al., 2000; Hantson & Chuvieco, 2011; Shepherd & Dymond, 2003). The cosine method is wavelength independent, meaning that it doesn't take into account the difference between bands in diffuse irradiation. For this reason, algorithms including band dependent parameters have been proposed, the most used of which is the C-correction. In this method the diffuse irradiance is considered through a semi-empirical estimation of the factor C, which should be determined for every band and land-cover separately for optimal results (Hantson & Chuvieco, 2011; Meyer et al., 1993).

Among the non-lambertian methods, the most used is the Minnaert correction, which models the non-lambertian behavior for every band and land cover separately. it makes use of a Minnaert constant *k* that depends on the nature of land-cover, topographic factor and wavelength, and helps avoiding overcorrection effects. The value of the Minnaert constant can vary between 0 and 1, where a value of 1 means that the surface is considered as a perfect lambertian reflector. A drawback of this approach is that it is difficult to establish model parameters. The easiest way to perform a Minnaert correction is to use a single global k value for an entire image, even though this does not reflect reality because land cover variations and differences in topographic impacts on surface reflectance generate spatial variations in k values. Another type of approach uses multiple k values based on land cover, assuming that different types of land cover have different influences on reflectance (Allen, 2000; Hantson & Chuvieco, 2011; Lu et al., 2008), but even in that case different topographic slopes have different impacts on land-cover reflectance. Lu et al. (2008), developed a pixel-based Minnaert coefficient image for topographic correction of Landsat ETM+ images in mountainous regions based on the relationships between k values and slopes. This approach has shown more advantages in improving the topographic correction performance than a single k value or multiple k values, as it considers the interactions of k, land cover, and topographic conditions.

Hantson & Chuvieco (2011), after evaluating different topographic correction methods for a large number of images acquired at different periods of the year and under different terrain conditions for the generation of radiometrically stable time series of Landsat imagery, found that the C-correction method gave the best results, but only after the necessary parameters were estimated separately for different land cover classes. This was obtained by dividing the study area in two land-cover classes by a threshold in the NDVI to separate areas with a high portion of bare soil from vegetated areas.

Richter et al. (2009) achieved the best results with the modified Minnaert method, closely followed by C-correction. Vanonckelen et al. (2013) evaluated the effect of different atmospheric and topographic correction methods on land cover classification accuracy, which showed that the best overall classification results were achieved after combination of an atmospheric correction based on transmittance functions with pixel-based Minnaert or pixel-based C-correction. Another finding was that some land cover classes (coniferous and mixed forest classes) achieved much better classification accuracies after correction, while others (broadleaved forest, bare soil, grass and water) showed only a minor improvement.

Although many different approaches have been used for topographic correction (see Vanonckelen et al. (2013) for an exhaustive list), an effective and universal approach to reduce topographic effects has not been developed yet (Balthazar, Vanacker, & Lambin, 2012; Lu et al., 2008), because the simple topographic correction algorithms do not give satisfying result, while the more advanced ones are hard to generalize and not automatically applicable (Hantson & Chuvieco, 2011). However, since many studies suggest that the topographic component has a higher influence on classification accuracy than the atmospheric component, topographic correction is a fundamental step in a multi-temporal study (Vanonckelen et al., 2013).

4.3 Change detection variables

The variables that can be chosen for detecting changes between multi-temporal remote sensing images range from simple spectral bands to band combinations and other variables such as vegetation indices, transformed images, textures, segments, sub-pixel features and classification results. They can be grouped in five types: 1) spectral features; 2) spatial information; 3) sub-pixel information; 4) thematic information; 5) biophysical attributes (Lu et al., 2014). Here only the

types relevant to this work will be discussed in more detail, specifically spectral features and thematic information.

a. Use of remote sensing spectral features

Spectral response is the most common variable used for detecting change, especially when the analysis is conducted on medium and coarse spatial resolution images. It is critical to identify the variables that can best represent the spectral difference between the features of interests and the others (Lu et al., 2014). The transformation of spectral data to vegetation indices may further improve change detection performance by enhancing some specific vegetation information and establishing a more direct connection between data and biophysical phenomena (Coppin et al., 2004; Sant, Simonds, Ramsey, & Larsen, 2014).

Lyon et al. (1998) compared the performance of seven vegetation indices based on (1) whether they produced similar results, (2) their statistical characteristics, and (3) whether they were feasible for detection of change in the examined study area (State of Chiapas, Mexico). They found that among all the indices, only NDVI showed image histograms with normal distributions, and that the NDVI group was least affected by topographic factors in this study. Therefore the NDVI difference technique was considered the best vegetation change detection for the study area. Matsushita et al. (2007) also demonstrated that NDVI is not affected by topographic effects, even on non-Lambertian surfaces. Nordberg & Evertson (2003) compared NDVI and SAVI for the assessment of change vs. no-change through image differencing in the low alpine region of Swedish mountains, and found that NDVI performed significantly better despite the presence of large patches of bare soil, even though that may be related to the specific reflectance properties of the soil in that area (Nordberg & Evertson, 2005).

b. Use of thematic information

One solution to avoid the impact of the variability found in spectral response due to external factors, is to conduct separate image classification for each date of imagery, and then to use the classified images to examine land cover change trajectories. In this sense, classification results become the variable used to assess change. This type of change detection approach commonly defined post-classification comparison. (Lu et al., 2014).

4.4 Change detection techniques

There is no single approach of change detection from remotely sensed data that can be considered optimal and applicable to all cases, since different change detection algorithms have their own merits. The selection of the most appropriate change detection method for a given application is still an active research topic, because it is influenced by several variables and can affect the qualitative and quantitative estimates of the change process in a significant way (Coppin & Bauer, 1996; Lu et al., 2014, 2004). Each change detection method is affected differently by spatial, spectral, temporal, and thematic constraints. Because of the impact of complex factors, different authors often arrived at different and sometimes contrasting conclusions about the effectiveness of the same change detection technique. Even in the same environment different approaches may result in different change maps. This explains the large number of change detection techniques that have been developed in relation to specific requirements and conditions, and that continue to appear due to new thematic and accuracy needs and to the increasing availability of high-resolution data (Hussain et al., 2013; Lu et al., 2014).

Most digital change detection methodologies combine both the procedures for change extraction (the change detection algorithm itself) and a decision function (the operation to produce a decision, i.e. change vs. no-change) for change separation/labeling (Coppin & Bauer, 1996; Hussain et al., 2013).

Based on the unit of image analysis, change detection techniques can be grouped into pixel-based and object-based approaches (Hussain et al., 2013; Lu et al., 2004) (see Section 3.3 Vegetation mapping through multispectral images and Vegetation Indices). Another common way of broadly classifying change detection techniques is into pre-classification and post-classification techniques. Pre-classification methods apply change detection algorithms (for example image differencing or image ratioing), directly to single or multiple spectral bands, vegetation indices or principal components of multiple dates of stacked satellite imagery. Post-classification methods, on the contrary, perform a comparative analysis of independently produced classifications of images from different dates (Coppin et al., 2004; Lu et al., 2004).

The changes detected through a change detection procedure can belong to either of these two categories: change between classes (conversion of a land cover from one category to a differ-

ent one, for example in the case of deforestation) and change within classes (modification of the condition of a land cover within the same category, like degradation, reforestation, shrub encroachment, etc.). Detection of vegetation conversion is relatively easy due to the significant differences in spectral signatures between vegetation and non-vegetation types, while detection of vegetation modification is more complex (Lu et al., 2014).

4.4.1 Overview of digital change detection methods

Several reviews of digital change detection techniques for remote sensing data have been published in the literature (Coppin & Bauer, 1996; Coppin et al., 2004; Hussain et al., 2013; Lu et al., 2014, 2004; Singh, 1989), which thoroughly describe the main types of change detection techniques. Most of these reviews cover pixel-based change detection techniques for coarse and medium spatial resolution data such as MODIS, Landsat and SPOT, even if some recent works have focused on object-based approaches applied to high resolution data as well (Hussain et al., 2013; Im, Jensen, & Tullis, 2008; Willhauck, Schneider, De Kok, & Ammer, 2000).

An analysis of change detection literature shows that, despite the many factors affecting the selection of suitable change detection methods, in practice image differencing and post-classification comparison are the most commonly used, even if in recent years more advanced techniques such as Spectral Mixture Analysis (SMA), Artificial Neural Networks (ANN) and object-based methods have been emerging as promising techniques for change detection applications as well (Lu et al., 2004).

a*. Image differencing*

This methods belongs to the pixel-based thresholding category, which includes all those techniques that distinguish change from no-change using thresholding methods based on variables related to the spectral responses of the images (either spectral bands directly or, more commonly, derived images created by using vegetation indices and transform algorithms).

In the case of image differencing, images from different dates are co-registered and mathematically combined on a pixel-by pixel basis through a subtraction operation. The resulting pixel values usually follow a normal distribution, where the pixel that have not changed are centered around the mean (values equal or close to zero) and those that have changed are located at the tails of the distribution (positive and negative) (Singh, 1989).

This method is relatively simple, straightforward and easy to implement, but it cannot provide detailed information about land cover change trajectories; it can only show the spatial distribution and the magnitude of the change (Hussain et al., 2013; Singh, 1989; F. Yuan et al., 2005). For this reason they are often coupled with other techniques, or alternatively to create a mask to highlight areas that have undergone a change in order to apply more advanced change detection methods only to the changed areas.

This category of techniques is very sensitive to scene-dependent effects, such as atmospheric effects, phenology and soil moisture, so it is necessary to carry out a radiometric normalization procedure in the pre-processing stage (Coppin & Bauer, 1996; Coppin et al., 2004). Two other aspects are also critical for the quality of the change detection results: the selection of variables (image bands or derived images) that can effectively identify the changes of interest and the selection of a suitable decision function to distinguish between change and no-change areas (Lu et al., 2004).

The most common type of decision function is a threshold. Deciding where to place the threshold boundaries between change and no-change pixels is not an easy task, because a low threshold will exclude areas of change and a high one will include external influences caused by atmospheric conditions, Sun angle, soil moisture and phenological differences in addition to the real land-cover changes. This is true especially for unsupervised algorithms, when ground truth is not available to supply prior knowledge. The most common method used for the selection of thresholds is a statistical measure, where the threshold is obtained through the selection of a suitable standard deviation from the mean through interactive or manual trial-and-error procedure (Lu et al., 2004; Mancino et al., 2014; Singh, 1989).

Despite the relative subjectivity in selecting suitable thresholds, this type of decision function is still the most extensively applied in detecting binary change and no-change information because of its simplicity and intuitiveness (Lu et al., 2004).

In those cases where the identification of binary change/no-change dynamics is considered sufficient to fulfill the study's requirements, image differencing has been widely used, and in a variety of geographical environments (Coppin et al., 2004). Several change detection studies have also shown that data enhancement using vegetation indices or data transforms prior to image differencing considerably improves the identification of changes in vegetation properties compared to single band analysis, because it reduces data volume and captures information not available in any single band (Coppin & Bauer, 1996; Mas, 1999).

b. Post-classification change detection

Classification-based change detection methods are perhaps the most commonly used in practice, because they can provide detailed from-to change information, instead of only indicating binary change/non-change (Hussain et al., 2013; Im et al., 2008). The most intuitive form of classification-based change detection is the comparison of different images of the same areas classified independently, followed by comparison of classification results. This method is called post-classification comparison or sometimes "delta classification" (Serra et al., 2003; Singh, 1989). The separate classification of the two dates of imagery has the great advantage of minimizing the need for radiometric calibration to correct atmospheric and sensor differences between images, making it very useful when multi-sensor images are employed for change detection (Mas, 1999). It also provides a complete matrix of change direction information, and the possibility of selectively grouping or filtering out classes to analyze any subset of changes of interest, and can be used starting from either pixel-based or object-based classifications. (Hussain et al., 2013; Lu et al., 2004; Singh, 1989).

The classification process however is time consuming (especially if manual or supervised methods are used), and the quality of change detection results is fundamentally dependent on the classification accuracy of each date of imagery being considered, so the classification errors from the individual-date images will affect the final change detection accuracy (Lu et al., 2014), which can be further decreased by misregistration between the multidate images. Image transformation, vegetation indices, advanced classification methods, modelling, and integration of different data sources are often used to improve classification results, especially when dealing with historical images (Lu et al., 2004).

This method is also not optimal for a) situations characterized by mixed pixel problems in coarse spatial resolution images or by high spectral variation in high spatial resolution images, and b) for detecting modifications and subtle changes within the same land cover class (Lu et al., 2014; Rogan et al., 2002). On the other hand, creating an independent classification of each date of imagery can be used to build a historical series that can be more easily updated and used for applications other than change detection (Yuan et al., 2005).

4.5 Accuracy assessment

The accuracy assessment of remote-sensing-based classification and change detection procedures is necessary to be able to express the level of confidence in the results and to ensure that the changes detected are not confused with errors. Many factors, already discussed in the previous sections, contribute to the error present in land cover change results, encompassing all the phases of data acquisition, pre-processing and analysis (Boyd & Foody, 2011). In brief, they include (1) the precision of geometric registration of and between multitemporal images, (2) the radiometric and atmospheric calibration (3) the complexity and fragmentation of the study area, (4) the change detection methods and algorithms used, (5) the chosen classification and change detection scheme, and (6) the analyst's skills, experience and familiarity with the study area (Lu et al., 2004). When talking about accuracy assessment, the focus is mainly on thematic (or "classification") accuracy, which is the correspondence between the class label assigned through the classification process and the land cover observed in reality (Kadmon & Harari-Kremer, 1999; Rocchini, 2004). However, the other aspects should be taken into consideration as well as part of the accuracy assessment process.

The biggest challenge in the implementation of an accuracy assessment scheme for change detection results lies in the difficulty of collecting ground truth data for each date of the multitemporal series, in particular past ones for which it is not always possible to find reference data for comparison.

Moreover, different change detection methods have different sources of uncertainty. Post-classification approaches require very good accuracy in all the individual classifications because the classification accuracy of the change map is the product of the accuracies of the individual classifications and is subject to error propagation. All the errors that affect the classification of each individual image included in the multitemporal change analysis have a cumulative effect on change detection accuracy (Dai & Khorram, 1998; Hussain et al., 2013; Rocchini & Di Rita, 2005; Simonetti et al., 2014; Wang & Ellis, 2005). As a result, the final accuracy is very close to that resulting from the multiplication of the accuracies of each individual classification. For example, the change map obtained from two images classified with 80 per cent accuracy might have only a 0.80 x 0.80 x 100 = 64 per cent overall accuracy. Multiplying the accuracies of each individual classification is not sufficient, however, because misregistration problems further decrease the accuracy

(Coppin & Bauer, 1996; Hussain et al., 2013; Mas, 1999; Serra et al., 2003; Singh, 1989; Townshend et al., 1992).

The magnitude of classification and positional errors can be assessed separately using standard techniques, for example the overall accuracy or the kappa statistic for classification error, and the total RMSE for positional error, but evaluating their combined effect on land cover change estimates is not easy (Brandt et al., 2002).

As for pre-classification approaches, most of these procedures provide little information about the specific nature of land cover changes. The selection of thresholds to differentiate change from no-change is usually a trial-and-error process, and it is not always possible to identify all changes, resulting in a less complete legend. (Smits and Annoni 2000). Finally, misregistration between images remains a problem, and it is often not properly considered (Serra et al., 2003).

5. MATERIALS AND METHODS

5.1 Research objectives and workflow description

The overarching objective of this study is to assess the phenomenon of forest expansion on semi-natural grasslands from a quantitative point of view, and to evaluate the ability of different remote sensing mediums (specifically, aerial photographs and satellite images) and of different analysis techniques (manual and automated classification and change detection) to characterize the land cover dynamics within the study area. The study was therefore divided into two parts, according to the type of remotely sensed data used and the techniques used for data processing and analysis.

The first part of the work is dedicated to the analysis of aerial photography data in digital form, according to a traditional photointerpretive approach conducted with the aid of GIS software for on-screen digitization of land cover features. This choice is based on the type of photographic data available, whose low spectral and radiometric quality makes the use of automated or semi-automated approaches rather difficult in practice, and doesn't guarantee results with sufficient accuracy. The objective is to create two maps of grassland distribution, one for 1954, before the beginning of the abandonment of mountain activities and of the forest expansion process, and one for 2012 to document the current situation, and to compare them to assess the historical change of grassland extension over this 58-years long period of time. This can be obtained through the overlay of the distribution maps obtained and the creation of change maps and other thematic cartography in a GIS environment. From the combination of these layers, new information can be obtained about the quantitative land cover change (amount of areas subjected to reforestation), the spatial distribution of the phenomenon (areas where the most significant variations can be observed) and some qualitative aspects (such as the presence of grassland habitats of outstanding conservation value in relation to the areas where the major changes have been taking place).

The second part of the work focuses on the analysis of Landsat satellite imagery to explore the possibilities of mapping land cover and land cover change through the use of semi-automated pixel-based classification procedures that employ the spectral characteristics of different land cover

types. The purpose is to evaluate the possibility of obtaining complementary information on forest expansion through this type of data, that despite having a coarser spatial resolution may still be used to expand the knowledge about the dynamics of interest thanks to its greater spectral and radiometric resolution. The methodology is based on the assessment of the accuracy of different classification scenarios obtained from the classification of a)single-date Landsat scenes, b) VI combinations (NDVI and EVI) and c) VI and Landsat scene combinations.

The creation of NDVI and EVI time series is used as support to identify the phenological profile of each land cover type over the course of the vegetative season, and evaluate whether this aspect can be helpful for the improvement of classification results.

Workflow of Part 1

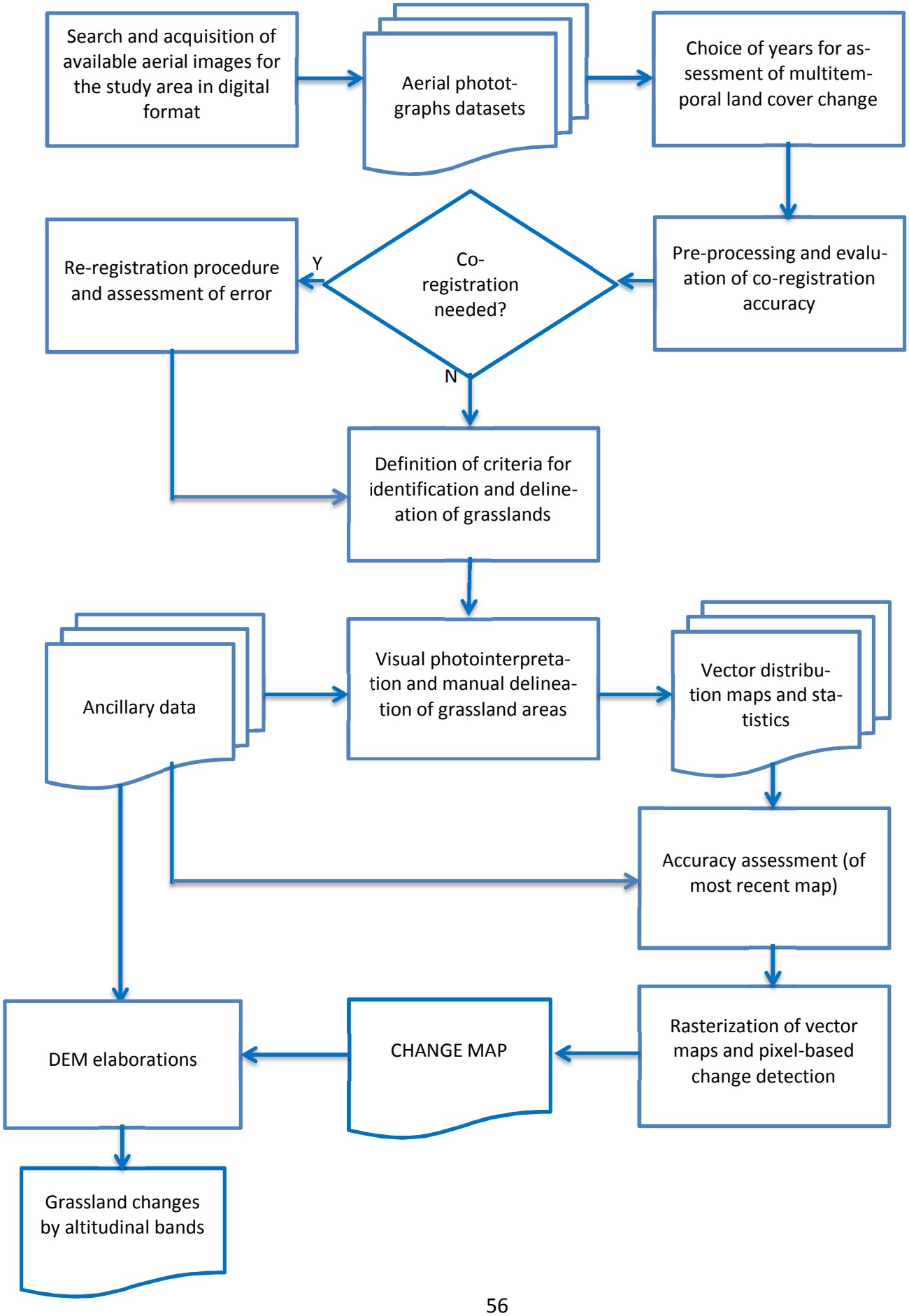

Workflow of Part 2

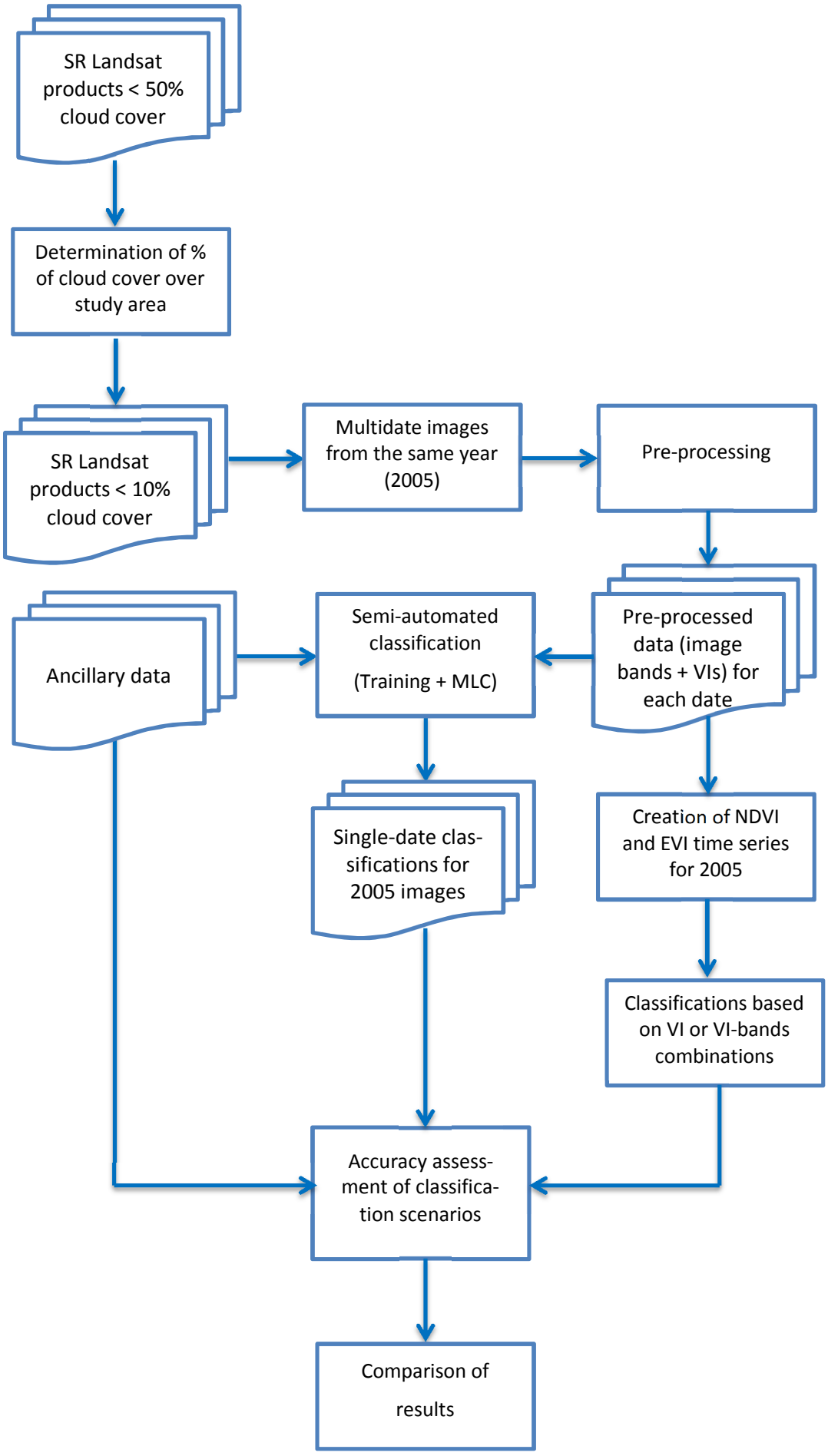

5.2 Study area

The Dolomiti Bellunesi National Park (NW: 46° 19', 11° 46'; SE: 46° 1', 12° 15'), established in 1993, occupies an area of approximately 31000 ha (310 km^2), entirely comprised within the boundaries of the Belluno Province in the Eastern Italian Alps (Figure 8).

Figure 8: Dolomiti Bellunesi National Park and its position in Italy

The territory within the Park's boundary is almost entirely mountainous, with an elevation ranging between 400 and 2565 m a.s.l. The area is constituted mostly of sedimentary rocks (limestone or dolomite), with a limited presence of metamorphic facies that create different subsoil conditions that affect both the landscape forms and the floristic composition (Parco Nazionale Dolomiti Bellunesi, 2015). The hydrographical network is complex, with the Cordevole, Mis, and Caorame rivers representing the main water courses. The two lakes present in the Park, Stua and Mis, are both artificial basins built for hydroelectric energy production.

The climate is continental, with annual average rainfall of 1400 mm and average monthly temperatures ranging between -5°C in January and +23°C in July (Giupponi et al., 2006).

The altitudinal zonation within the Park is not easy to define, because vegetation cover is strongly influenced by the complex topography and microclimate. The belt comprised between the valley floor up to 1000-1200 m a.s.l. (on the southern slopes) and to 700-800 meters m a.s.l (on the northern slopes) is characterized by deciduous forests, dominated by hornbeam (*O. carpinifolia and C. betulus*), ash (*F. ornus, F. excelsior L.)* and maple (*A. pseudoplatanus*). This area was historically the most heavily influenced by human activities, especially in terms of deforestation, coppicing, and creation of semi-natural pastures and hay meadows. Between 600-700 and 1600-1700 m a.s.l., large forest stands are present with prevalence of beech (*F. sylvatica*), sometimes mixed with conifers; The upper belt, from 1500 (1200-1300 in the northern slopes) m a.s.l.

up to the upper forest line is comprised mostly of norway spruce (*P. abies*) and larch (*L. decidua Miller*), with extensive dwarf mountain pine (*Pinus mugo*) stands in the higher altitude zones (Andreatta, 2007).

The most representative grassland habitats within the Park include, among others, some high conservation value Natura 2000 habitats of the Alpine bioregion (Habitat Directive 92/43, Annex I). The most widespread are alpine and subalpine calcareous grasslands (code 6170), typical of shallow calcareous soils, that host many vulnerable animal species ranging from invertebrates to alpine bird communities (European Commission, 2008), followed by siliceous alpine and boreal grasslands (6150), in particular *Nardus*-rich extensive alpine pastures.

Another noteworthy semi-natural grassland type are semi-natural dry grasslands and scrublands on calcareous substrates (Festuco-Brometalia, code 6210), which are of great floristic and conservation value, as they are important habitats for the conservation of orchid species (European Commission, 2008; Ziliotto, Andrich, Lasen, & Ramanzin, 2004). These habitats were formed mainly through extensive grazing or mowing, and as such they are extremely susceptible to woody plant encroachment following the abandonment of land use activities. At lower altitudes, significant semi-natural grassland habitats are the extensively managed hay meadows of the submontane zones (Code: 6510), that include both dry meadows as well as humid to wet meadows, with distinctive species such as *Alopecurus pratensis* and *Sanguisorba officinalis*.

Most of the areas now belonging to the Park have been historically subjected to intense anthropic use. Deforestation of the lower part of many mountain slopes has been documented since the Middle Ages, but the period of highest exploitation of forest resources started under the Venetian rule. In the 18th century, the population growth and the increasing need for firewood and coal for industrial purposes, as well as the need for pastureland, led to the deforestation of mountain slopes at increasing altitudes (Andreatta, 2007). Starting from the 1950s, however, the widespread abandonment of mountain settlements and the consequent decrease in the utilization of forest and grassland resources, which mirrors a pattern of socio-economic dynamics common to most alpine areas all over Europe, has reversed this trend, causing the natural revegetation of previously deforested areas the decline of semi-natural mountain grasslands habitats (Urbinati et al., 2004). Therefore starting from the 1950s-1960s, the evolution of the landscape was determined mostly by natural dynamics of secondary succession (Ciolli et al., 2007). The abandonment of agricultural activities is not only limited to the Dolomiti Bellunesi National Park area, but represents a widespread phenomenon in most of the Belluno Province, due to the high morphological and en-

vironmental variability of the terrain that limits the areas suitable for intensive agriculture (Giupponi et al., 2006).

5.3 MATERIALS

A preliminary phase of this study was devoted to searching and collecting all remotely sensed (aerial and satellite images) and cartographic data available for the study area that could be potentially useful for the analysis of the land cover change process of interest. A preliminary screening of the available material was carried out on the basis of its availability (data cost, format and manner of acquisition), spatial and temporal coverage, pre–processing requirements, and resolution (depending on the level of detail needed for each phase of the grassland cover assessment and change detection).

In land cover change detection studies, the use of data from different sources, especially of remotely sensed data from different sensors, is very frequent, as this choice is in many case unavoidable when assessing changes over a long period of time. For studies that go back in time to before the 1970s, satellite images are not available, and in this case the integration with multi-source data such as aerial photographs, existing thematic maps and other ancillary data for the older dates is the only possibility (Petit & Lambin, 2001; Sankey & Germino, 2008). Differences in data format, structure, quality and resolution make this kind of assessment challenging, but the combination of data from different sources can increase the quality and quantity of information that can be extracted.

5.3.1 Aerial photographs

The first part of this study aimed at obtaining an assessment of the evolution of grassland habitats with the highest possible accuracy and over a long period of time. Consequently, aerial photographs were chosen as the most suitable data source, as they combine high spatial and temporal resolution. Many studies of land cover change and forest expansion in mountain areas have employed aerial photographs for evaluating the phenomena of interest, both through the use of

manual and automated techniques, finding them especially suitable for this purpose (Ciolli et al., 2007; Mognol, 2007; Sgarbossa, 2010; Urbinati et al., 2004).

The screening of all the available aerial photography imagery led to the selection of two main datasets to use for the analysis: the **GAI flight (1954-55)** and the **TELAER flight (2012)**. One additional datasets (**IT2000 flight**) was acquired to support the photointerpretation process. All aerial images were provided in digital format by the Veneto Region and the Dolomiti Bellunesi National Park. Their main characteristics are summarized in Table 3.

The “GAI 1954-55” flight provides the first complete aerial coverage of the Italian territory, and as such it is one the most valuable sources of historical land cover information. The original project was undertaken by a consortium of private companies named GAI (Gruppo Aereo Italiano) and was completed between 1954 and 1955 (Berti, 2008; Lega & Vincini, 2003). In particular, the images covering the Dolomiti Bellunesi National Park area were acquired in July 1954.

The original images are panchromatic black and white analogic photographs of standard size (23 x 23 cm) taken at a height ranging between 5.000 to 10.000 m, which corresponds to an approximate scale of 1:30.000 to 1:62.000. For the photographs of the area of interest the spatial scale is about 1:62.000 (due to the necessity of maintaining a higher flying height because of the mountainous terrain). Thanks to a project carried out by the Veneto Region (Regione del Veneto, 2011), it was possible to acquire the photographs directly as orthorectified digital images (Figure 9) .

The Flight “TELAER 2012”, which was carried out between 2009 and 2012 by the TELAER consortium for the Italian “Agenzia per le Erogazioni in Agricoltura” is composed of digital color ortophotos, acquired directly in raster format. The images for the study area were taken in summer 2012 (Figure 10). With a pixel size of 0.5 m, they represent the resource with the highest spatial resolution available. The "IT2000”™ (TerraITaly™1998/99) flight images by Compagnia generale Ripresearee S.pA. - Parma are color ortophotographs as well, acquired with a digital camera between 1998 and 1999. The spatial scale of the images is 1:10.000 with a pixel size of 1 m.

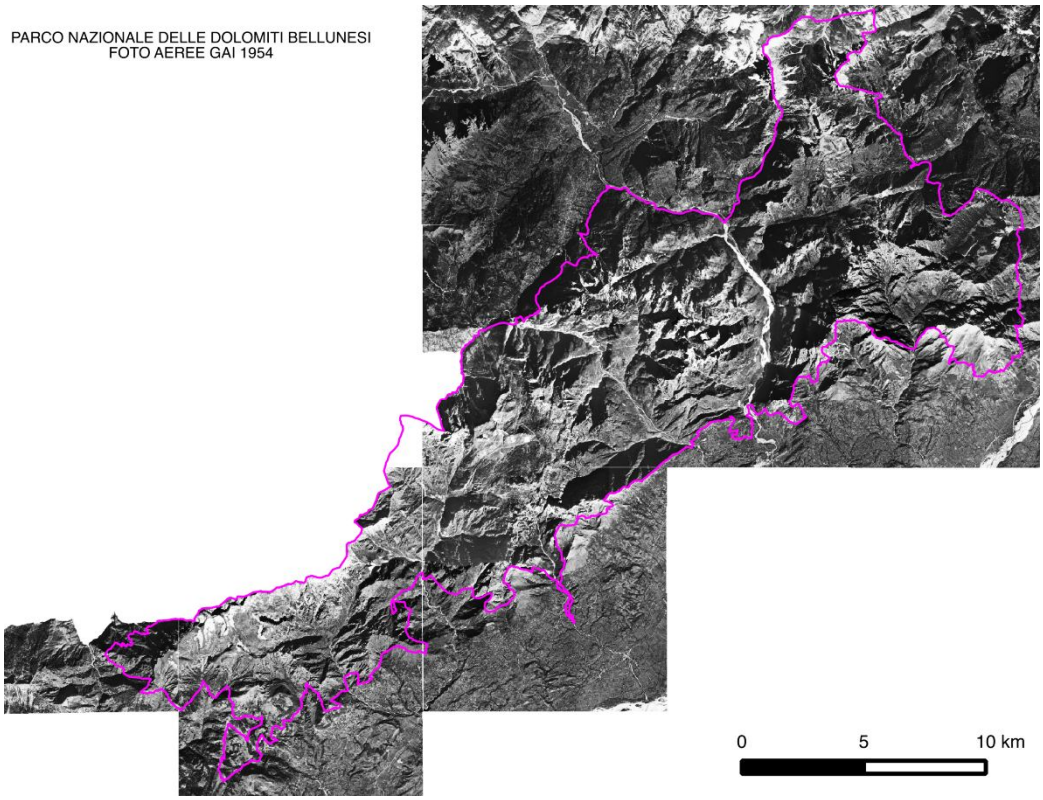

Figure 9: Orthorectified and mosaicked GAI 1954 photographs covering the Dolomiti Bellunesi National Park territory

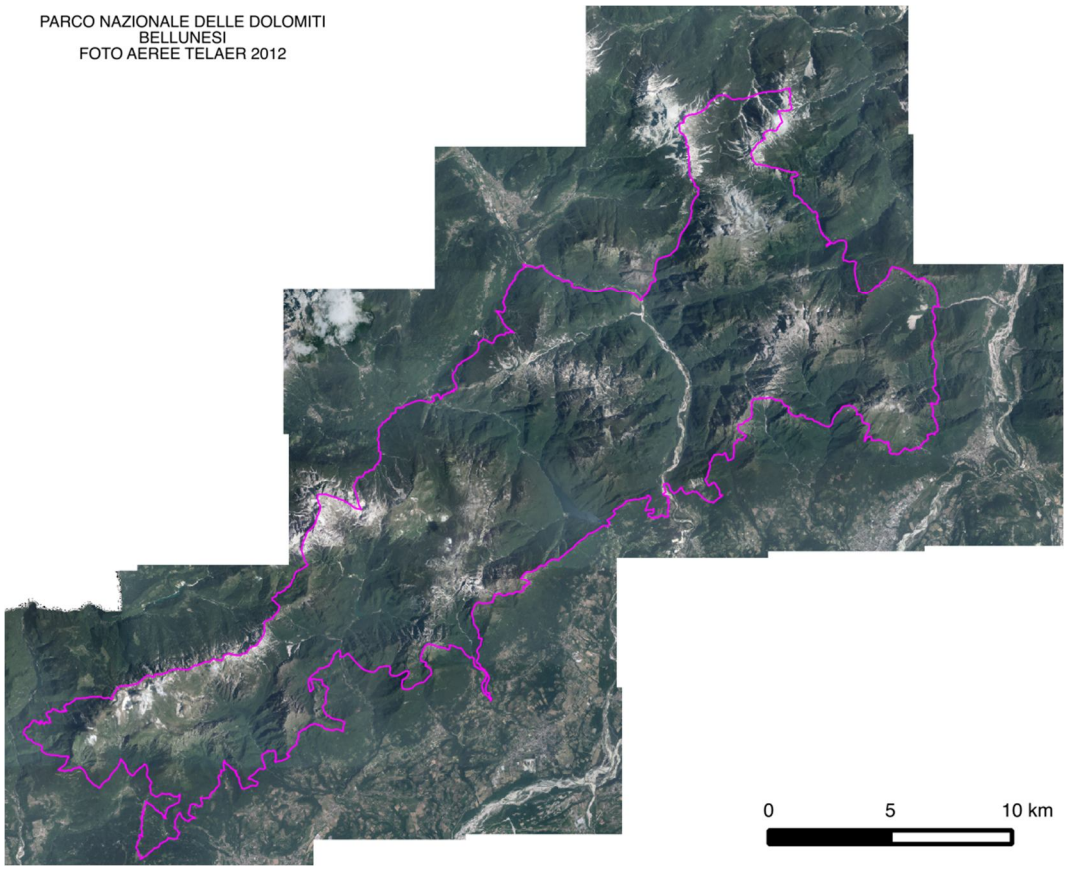

Figure 10: TELAER 2012 digital ortophotographs covering the Dolomiti Bellunesi National Park territory

Resource name	Original format	Year of original acquisition	Scale and flight height	Acquisition format	Spatial resolution
GAI 1954-55 flight	Analogic, panchromatic b&w	1954-1955	1:30.000 – 1:60:000 (5000-10000 m)	Original images scanned at 600 dpi, orthorectified and mosaicked. Cut on the basis of the CTR 25000	2 m
TerralTaly™ "IT2000" flight	Analogic, color	1998-1999	1:10000 (6000 m)	Digital images, orthorectified, mosaicked and cut on the basis of the CTR 10000	1 m
TELAER 2012 flight	Digital, color	2009-2012	1:10000 (6000 m)	Digital images, orthorectified, mosaicked and cut on the basis of the CTR 10000	0.5 m

Table 3: main features of selected aerial image datasets

5.3.2 Satellite data

Among the many existing satellite sensors, Landsat images were chosen for this study on the basis of their long time coverage, medium-high spatial resolution, and a spectral resolution higher than that of most higher-spatial-resolution satellites such as SPOT, IKONOS and Quickbird. Data accessibility is another major factor to consider, and the free availability of all the USGS archived and new Landsat data is of crucial importance for studies that require a high number of images such as multitemporal and multiseasonal studies.

Landsat can provide more than 30 years of systematic Earth observations at a spatial resolution of 30 m or less. Despite Landsat's nominal repeat cycle of 16 days, however, most areas are not imaged with such frequency, because Landsat data acquisition is scheduled based on seasonality, solar zenith angle, cloud cover and other factors (USGS, 2015b). Taking into account the cloud cover present in the imaged scenes, in practice data availability is drastically reduced, especially when two or more images are needed from the same year or consecutive years.

All the Landsat images used in this study were acquired from the USGS Earth Resources Observation and Science (EROS) Centre archive (http://earthexplorer.usgs.gov/). Through the EROS center it is possible to acquire free of charge not only the original images, but also a series of derived products like Surface Reflectance (SR) images (already atmospherically corrected to surface

reflectance), so all images were ordered through the EROS website and downloaded in this form, with a waiting time for processing small batches of images that was on average less than one day.

About two million Landsat images over Europe and North Africa are stored by the European Space Agency (ESA) as well, as the European International Cooperator. Following the USGS, the ESA also adopted a free-of-charge Landsat data acquisition policy, but with limited viewing and product download options and stricter access requirements that include a brief project description and somewhat intricate registration procedures. Considering that the processing level and characteristics of ESA and EROS Landsat images are different and therefore not directly comparable (Northrop, 2015) and that no significant amount of usable images was found for the time period of interest in the ESA archive, in this study only EROS images were utilized.

The study area is entirely included into Path 192, Row 28 of Landsat's WRS-2. The time frame considered was 1984 – present, that is to say from the beginning of Landsat TM acquisitions. The choice of images was limited to the TM and ETM+ sensor of Landsat 4-7. Landsat 7 images acquired after 31/05/2003 were excluded, due to Landsat 7's failed scan-line corrector that limits their applicability for classification purposes. Landsat MSS images were excluded due to the difficulty of integrating lower resolution (60 m) data into the analysis, while Landsat 8 have different band wavelength specifications compared to Landsat 4-7, which may be problematic for the comparison of classification results and vegetation indices.

A preliminary screening of Landsat images was conducted on the basis that a) the acquisition date of the images had to be included between May and October in order to avoid the presence of snow, and b) that the cloud cover over the study area had to be less than 10%. Considering that the study area covers only a small part of a full Landsat scene (0.9%), all images with cloud cover under 50% were examined (87 images), and those that at a first visual assessment didn't appear to have a significant cloud cover over the study area were ordered and acquired from the EROS website as Surface Reflectance (SR) data, that is to say atmospherically corrected to surface reflectance using the Landsat Ecosystem Disturbance Adaptive Processing System (LEDAPS) algorithm (Masek et al., 2006).

Landsat Surface Reflectance data are generated at 30-meter spatial resolution on a Universal Transverse Mercator (UTM) mapping grid. SR products from Landsat 4-7 TM and ETM+ contain, in addition to the atmospherically corrected images, some quality assessment files that help in the evaluation of image quality. In particular, the Quality Assessment band for clouds (sr_*cloud_qa*)

was clipped to the study area and used to calculate the percentage of the study area covered by clouds. The complete list of images with cloud cover < 10% (22 images) is shown in Appendix B.

The availability of Landsat scenes over the area of interest and for the specified years and dates is on average very low, with only one image per year in most cases, and some years with no images of acceptable quality. The images chosen for the study were selected on the basis of this second screening, and also on the availability of higher resolution reference data for accuracy assessment, which in this case are represented by aerial images and ancillary data such as the IUTI inventory. Five Landsat images from 2005 were employed for the seasonality assessment, due to the unusually high amount of images with acceptable cloud cover available for this year. For land cover change detection, two Landsat 5 images, one from 27/07/1987 and one from 18/07/2007 were chosen. The 20-years gap between the two images should ensure the possibility of detecting land cover changes, and the choice of near-anniversary dates should help achieving similar environmental and illumination conditions.

5.3.3 Ancillary data

The term ancillary data indicates all data from sources other than remote sensing, used in digital image processing to assist in the analysis and classification of the images, or to populate metadata and attributes. The ancillary data used in this study were obtained from the Veneto Region – Forest and Agriculture sector's database, the Veneto Regional Geoportal and the Dolomiti Bellunesi National Park, and are listed in Table 4.

Resource name	Format	Reference period	Derived from	Main features	Source
Forest area map GAI 1954-55	raster	1954-55	object based semi-automated classification of GAI 1954 images	3 classes: Forest, Non Forest, Not classifiable	Veneto Region
Regional forest map 2006	vector (polygon)	1998-1999	Manual photointerpretation of IT2000 aerial images for forest unit delineation, ancillary data and field surveys for thematic classification	Scale 1:10000 Forest areas mapped according to regional criteria but compatible with FRA's definitions	Veneto Region
Map of "Natura 2000" habitats	vector (polygon)	2006-2008 (field survey)	Field surveys with the support of IT2000 aerial images, CLC2000, and thematic cartography	1:10000, Habitat classification according to the "Interpretation manual	Dolomiti Bellunesi National Park

				of European union habitats"	
DEM 5m/25 m	ASCII (txt)	2006	IGM 1:25.000 map, CTR 10000 map, field survey	Contour lines and spot elevations obtained from IGM 1:25.000 map, from CTR 10000 and ARPAV relief survey, and then used to generate a TIN. ASCII files divided based on the CTR sections	Veneto Region
IUTI inventory	vector (point)	1990 – 2000 – 2008	TerraItaly 1988/89 TerraItaly IT2000 TerraItaly 2008 aerial images	Manual photointerpretation of aerial images from each date	Ministero dell'ambiente e della tutela del territorio e del mare (MATTM)

Table 4: List of ancillary data

The IUTI Inventory

IUTI (Inventario dell'Uso delle Terre d'Italia) is an Italian inventory created to support the National Carbon Sink Accounting Register, and documents land use (or, more appropriately, land cover) for the years 1990, 2000 e 2008 by using a sampling scheme of geographically located points. Point-based sampling schemes cannot give a complete assessment of the land cover distribution and land cover change dynamics, but at the same time do not suffer from the uncertainties related to the use of polygons and the consistency of their delineation over time, strongly reducing commission and omission errors. Therefore they are an alternative to wall-to-wall mapping, and allow to carry out fast land cover surveys that can be easily updated, compared and integrated with a variety of different land cover information sources and datasets. As such, the IUTI inventory an important informative layer for the cross-validation and accuracy assessment of the land cover products created in this study. The IUTI points distribution is based on a systematic unaligned sampling, and the points have been manually classified through photointerpretation of aerial orthophotographs, respectively: TerraItaly 1988/89 images for the 1990 points, IT2000 for the 2000 points and TerraItaly 2008 for the 2008 points (Marchetti et al., 2012).

The IUTI inventory classifies the Italian territory according to a hierarchical system composed of six main land cover types: 1) forest land, 2) cropland, 3) grassland, 4) wetland, 5) settlements, 6) other lands. This level of the classification responds to the need of adhering to international

standards, in particular those set by FAO and IPCC (GPG-LULUCF). Some of the Level I classes are further divided into II and III level sub-classes defined by IUTI, which relate to the specific needs of mapping the Italian territory. Table 5 shows classification levels I and II. The categories 1.1, 3.1, 3.2 and 6 are the most relevant for this work, and the ones that were considered in the accuracy assessment.

LEVEL I – IPCC CATEGORY	LEVEL II – IUTI CATEGORY
1. Forest Land	1.1 Forest land (corresponds to "*forest land*" in the FRA classification)
	1.2 Temporarily unstocked forest areas
2. Cropland	2.1 Arable land (herbaceous crops)
	2.1 Permanent crops (trees)
3. Grassland	3.1 Grasslands and pasturelands
	3.2 Other wooded lands: shrublands or sparse (5-10% cover) woodland (corresponds to "*other forest land*" in the FRA classification)
4. Wetland	4. Water and wetlands
5. Settlement	5. Urban areas
6. Other Land	6. Bare or sparsely vegetated areas

Table 5: IUTI classification levels

5.3.4 Software

The software used for all the data processing and analysis operations is QGis 2.10 “Pisa” (Figure 11). QGIS is an official project of the Open Source Geospatial Foundation (OSGeo), and as such it is an Open Source GIS licensed under the GNU General Public License.

Other than being available at no cost, QGIS is also cross platform and runs on Linux, Unix, Mac OSX, Windows and Android, making it available to a wider range of potential users than many other commercial GIS software. It also supports many different vector, raster, and database formats and functionalities.

Among the reasons of QGIS’ growing popularity are its user-friendly interface that makes it easier to use compared to other open source GIS software, and the possibility to enormously expand its functionality through the integration with other open source GIS packages, including PostGIS, GRASS, and MapServer and the access to a constantly growing database of plugins from which users can download the ones best suited to their specific needs.

Moreover, QGIS has an active volunteer developer group that provides help with the software's functionalities, bug-fixing, and the solution of problems, as well as a thriving user-based community that ensures peer support for any issue related to QGIS and many web-based sources for tutorials and tips.

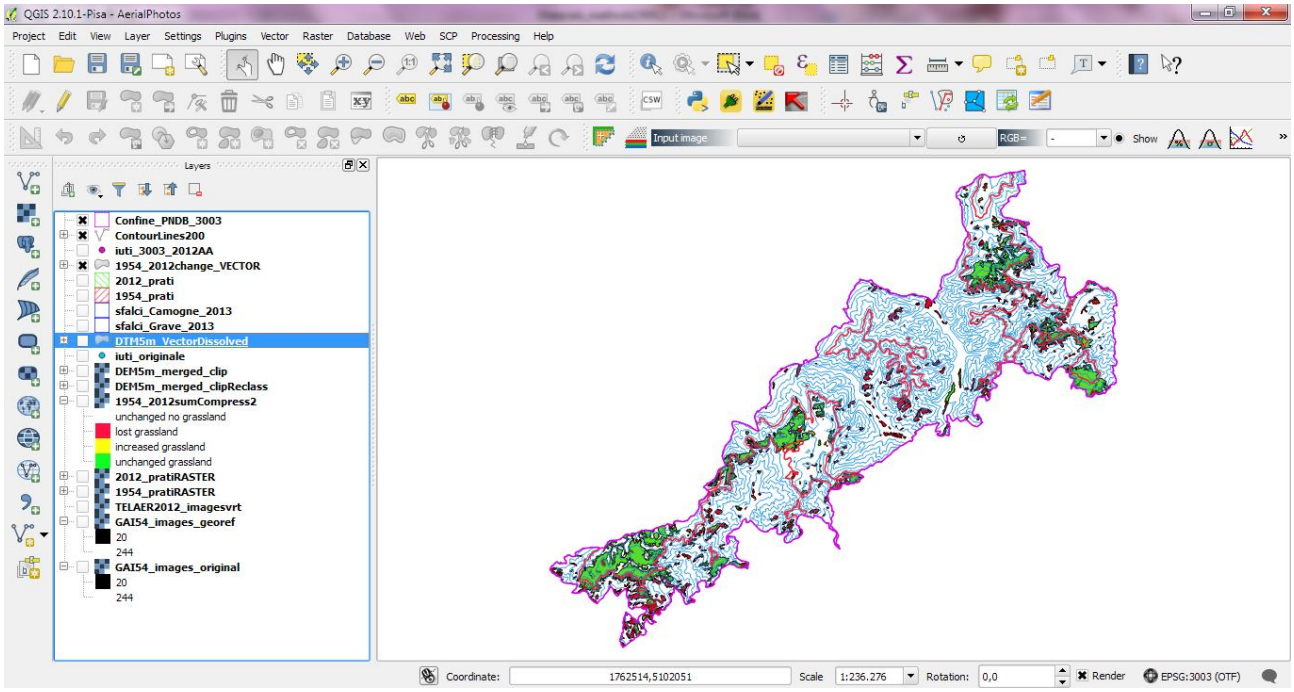

Figure 11: an example of QGIS 2.10's interface

5.4 METHODS

5.4.1 PART 1: Aerial images

Obtaining an accurate classification from historical aerial photography with semi-automated classification methods is a daunting task, because of the limited spectral and radiometric depth produces poor results from pixel-based approaches (generally dependent on spectral characteristics for the separation of land cover types) and is problematic with object-based approaches as well due to the low textural contrast and separability between image objects. This is further worsened by the lack, in most cases, of ground truth data to validate the classification (Morgan et al., 2010).

In this case, since the focus of the study was only on a specific land cover and land cover change type, the change detection procedure is simpler because it is only necessary to develop a method to extract the land-cover type of interest without a complete land cover classification scheme. For this reason, it was decided to employ visual interpretation for the extraction of grassland polygons. The use of manual digitization of polygons when working with historical black and white photography is a common occurrence in literature; other studies conducted in the Italian territory, in particular, faced similar issues in the treatment of the GAI 1954-55 images for the classification of land cover features (Ciolli et al., 2007; Garbarino & Pividori, 2006; Lega & Vincini, 2003; Salvadori, Pilli, & Anfodillo, 2006; Urbinati et al., 2004). Until the 1950s, aerial photography was generally collected used a non-metric camera with only black and white panchromatic film, so photogrammetric or digital image processing methods have limited applicability (Coop & Givnish, 2007; Mast et al., 1997). After evaluating the different classification options, manual classification through visual photointerpretation and on-screen digitization of polygons was chosen for this part of the study, considering the greater ability of a human photointerpreter to make choices under so many constraints.

Each temporal layer was photointerpreted separately, to obtain two maps representing the grassland distribution as it was at the time of the photos.

In the case of the TELAER 2012 images, photointerpretation was generally easier due to their higher spatial and radiometric resolution and limited distortions. Even if in this case an automatic classifier would have been easier to apply, it was decided to use manual delineation of classes to ensure uniformity with the other temporal layer. When faced with situations of uncertain classifi-

cation, the Natura 2000 Habitat Map was used as thematic support, as well as the IT2000 images (with caution, due to the gap between the two acquisitions), because the phenological differences between vegetation types here appear more evident due to the flight date (late summer/autumn).

Pre-processing

a. Image-to-image co-registration

The accurate overlay of source rasters is fundamental to ensure the best possible accuracy in each classification and consequently, in the change map obtained by overlaying the two multitemporal classifications.

The first aspect to verify when using geographic data obtained from different sources, is that the coordinate reference system (CRS) is the same for all layers. The data acquired for this part of this study employ the former the Italian national system Roma40/Gauss-Boaga zone 1, also called Monte Mario zone 1 (EPSG:3003), of which several variants exist, so it is important to make sure that the projection's parameters are correctly defined (see Appendix A). Despite the fact that in 2012 ETRF2000 was adopted as the official CRS for Italy (D.L. 10 novembre 2011, "Adozione del Sistema di riferimento geodetico nazionale") the geographic data acquired from the Veneto Region still adopt the old system.

In the case of the data acquired for this study, however, the whole range of projection variations was present, including deprecated ones, so it was necessary to convert them into EPSG:3003, which is the official definition and also the only one that allows to correctly reproject to WGS84/UTM32N coordinate systems (needed in the second part, when working with Landsat data) without any shift. If the images are needed for visualization purposes only, different variations of the same CRS can be handled by QGIS' "On-the-fly" reprojection feature (provided that the CRS definition is correct), but the use of geoprocessing tools requires all the input layers to be in the same CRS.

After this preliminary check, co-registration accuracy was evaluated as well. Both the 1954 and 2012 aerial image datasets were acquired in orthorectified form. The complexity of the orthorectification procedure of the GAI 1954 images, caused by the lack of the camera's calibration certifi-

cate, has been discussed in detail in the publication "*L'evoluzione dei boschi veneti – Analisi delle dinamiche spaziali dei popolamenti forestali regionali*" (Regione del Veneto, 2011). Despite the fairly accurate results obtained in that work (with a RMSE of about 5 m), when overlaying the 1954 and 2012 images a noticeable shift could be detected in some areas, even if it didn't appear to be the same throughout the image, most likely due to the differential distortions present in the 1954 images. Considering the necessity of creating a high spatial detail classification, it was decided to attempt a re-registration procedure between the images to try and improve their spatial alignment.

A related issue was that the 1954 dataset is composed 10 non-overlapping images. One option was to mosaic the images first to obtain a single image and then carry out the co-registration procedure, while the other was to proceed to the registration of each image individually. Using a single image is easier to manage than a set of images, and individually georeferencing each image separately implies that, after the registration procedure, the corresponding features located at the borders of adjacent images may not match perfectly, or there may be spaces between one image and the other. On the other hand, individually registering smaller subsets of a dataset can give more accurate results than registering the whole dataset as a single image (Brovelli & Minghini, 2012), especially considering the nature of the distortions present. This is the main reason why it was decided to work on the individual images, even at the price of sacrificing some metric and semantic continuity. This can be considered acceptable, however, because the images are used as visual reference and not for quantitative assessment, and the main purpose was to ensure the maximum local positional accuracy.

The procedure used for image-to-image registration comprises the following steps: a) identification of ground control points (GCPs) on the 1954 images (input image) and their corresponding locations on the 2012 images; b) application of a transformation function and resampling of DN values of the pixels of the output image based on the values of the pixels of the input image; c) assessment of residual positional error (Lillesand et al., 2004; Rocchini et al., 2012)

Choice of GCPs and transformation function

GCPs can be obtained from any type of reference layer (topographic maps, satellite imagery or orthophotographs), as long as its spatial resolution is higher or at least equal to the resolution of the layer to register. The 2012 orthoimages, with their recent acquisition date, higher resolution,

and digital acquisition (that allows to avoid the scanning process and therefore the related distortion problems) were chosen as the reference layer.

GCPs are features easily identifiable on both the reference data and the uncorrected image, and should be distributed evenly over the entire image (or the area of interest within an image) to ensure optimal coverage and to registration errors due to the points being clustered (Morgan et al., 2010).

Considering the lower spatial resolution of the GAI 1954 images and extremely poor radiometric contrast, it was not possible to identify GCPs with the same accuracy as on the 2012 images. Given that the time difference between the two datasets is almost of 60 years, it was also necessary to find features that remained recognizable and mostly unchanged throughout this time frame, a challenging task in a sparsely urbanized and densely forested landscape which contains very few distinctive features to begin with. In most cases the chosen features were the center of road intersections, road bends with distinctive shapes that were retained through the years, corners of buildings or isolated rocks with unique shapes. Care was also taken to select points as more uniformly distributed as possible within the image, including edges, but also to choose additional ones close to grassland areas in order to ensure the best possible accuracy in the areas of main interest (this is especially important when using a local and exact transformation algorithm such as Thin Plate Spline, that warps the image locally around the GCP location).

Transformation function

Transformation functions define, for a given GCP, the transformation from the original coordinates of the point to its rectified coordinates; transformation algorithms can be classified into global versus local, and exact versus non exact. Global algorithms are based on transformations that are applied to the whole image in the same way and whose parameters are calculated based on the coordinates of all GCPs. Local algorithms work on finite portions of the image, using each time a different set of GCPs, so that the parameters of the transformation have a local validity. Exact algorithms force the points on the input image to coincide exactly to the corresponding GCPs in the reference image, while non exact algorithms don't require the exact fitting of GCPs locations (Balletti, 2006; Brovelli & Minghini, 2012).

The Georeferencer plugin offers several choices of transformation algorithms ("QGis 2.0 User Manual," 2014):

- **Helmert transformation**

- **Projective transformation**.
- **Polynomial algorithms (first, second and third order)**
- **Thin Plate Spline (TPS) algorithm**

Helmert, polynomial and projective transformations are examples of global, non-exact algorithms, while Thin Plate Spline is a local, exact algorithm. Choosing a type of transformation algorithm depends on both the nature of the data and the desired final result. For example, if the aim is to obtain an image in which errors are globally distributed and no local effect is present, a global, non-exact algorithm represents the best choice. The most used among these is the family of polynomial models (Brovelli & Minghini, 2012; Rocchini & Di Rita, 2005). The first order polynomial (also called affine transformation) allows only scaling, translation and rotation, while higher order polynomial models can correct for more complex and non-linear distortions.

Thin Plate Spline can introduce local deformations in the data to match GCPs exactly, by providing a smooth interpolation between the set of GCPs. This algorithm is useful when low quality originals are being georeferenced, but can introduce significant distortions in the areas not close to any GCP, similarly to what happens when using higher order polynomial transformations (Brovelli & Minghini, 2012; Eberly, 2011).

In this case, co-registration was initially attempted both with polynomial transformations of second and third order, which didn't give a satisfactory result in all areas, especially those affected by the strongest distortions. Finally, TPS was chosen, with an improvement of registration accuracy.

The minimum required number of GCPs is a function of the transformation algorithm used, but also of the roughness of the terrain and the entity of distortions present in the image (Neteler & Mitasova, 2008; Rocchini et al., 2012), and the GCP selection and repositioning is an iterative process, repeated several times until an acceptable result can be reached.

In this case, given that each image was referenced separately, the number of GCP varied based on the position of the image: for some "corner" images, where only a small part of the image itself lay within the Park's boundaries, GCPs were chosen only in the area inside the park and in nearby locations, with as few as 6 points. For images lying entirely or almost entirely inside the Park, up to 16 GCPs were defined. The total number of all chosen GCPs was 119.

Since it was not necessary to preserve the original radiometry of the pixel because no quantitative analysis was going to be carried out on the images themselves, the resampling method used

was cubic convolution. Compared to other methods it provides sharper and less blurry images that are more suitable for visual photointerpretation, without the spatial offset of image features typical of simpler resampling methods like nearest neighbor.

Evaluation of error

The simplest way to evaluate of the quality of the chosen geometric transformation is a visual comparison between the output image and the reference data, for example through a semi-transparent overlay of the layers.

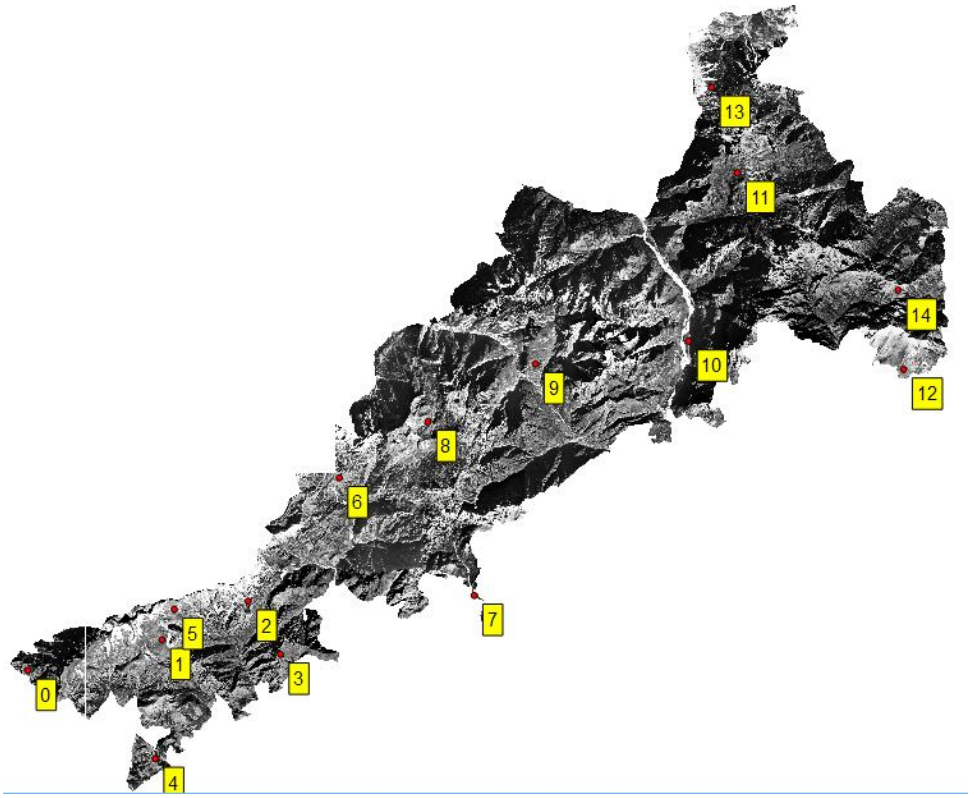

GCP table

ID	Source X	Source Y	Dest. X	Dest. Y	dX (pixels)	dY (pixels)	Residual (pixels)
0	1,71458e+06	5,10772e+06	1,71458e+06	5,10772e+06	-0,131987	0,993925	1,00265
1	1,71998e+06	5,10896e+06	1,71998e+06	5,10896e+06	0,367884	-0,575495	0,683032
2	1,72345e+06	5,1105e+06	1,72345e+06	5,1105e+06	-0,894026	-0,302328	0,943761
3	1,72475e+06	5,10837e+06	1,72474e+06	5,10837e+06	-0,213842	-0,42781	0,478278
4	1,71971e+06	5,10418e+06	1,71971e+06	5,10418e+06	0,0154782	0,0135939	0,0206002
5	1,72048e+06	5,11018e+06	1,72047e+06	5,11018e+06	-0,532901	-0,098521	0,541932
6	1,72711e+06	5,11546e+06	1,72711e+06	5,11547e+06	0,344692	-0,422098	0,544959
7	1,73254e+06	5,11074e+06	1,73254e+06	5,11074e+06	0,892551	-0,50095	1,02352
8	1,73068e+06	5,11773e+06	1,73068e+06	5,11772e+06	0,596716	0,270944	0,655348
9	1,73501e+06	5,12005e+06	1,73501e+06	5,12005e+06	0,137933	1,32397	1,33113
10	1,74117e+06	5,12096e+06	1,74117e+06	5,12096e+06	0,42026	0,594094	0,727713
11	1,74313e+06	5,12773e+06	1,74314e+06	5,12774e+06	-0,070139	-0,780053	0,7832
12	1,74982e+06	5,11983e+06	1,74982e+06	5,11983e+06	-0,901148	-0,136502	0,911428
13	1,74209e+06	5,13117e+06	1,74209e+06	5,13117e+06	-0,277219	-0,422169	0,505052
14	1,7496e+06	5,12301e+06	1,7496e+06	5,12301e+06	0,245748	0,469403	0,52984

Figure 12: CP table and location

For quantitative assessment of registration accuracy, the most common parameter is the root mean square error (RMSE), which represents a measure of the deviation of corrected GCP coordinate values from the original reference GCPs. In turn, this depends on the transformation used to register the images, so in order to obtain unbiased estimates of RMSE, the calculation should be made by using independent GCPs (also called Check Points, CP) not used for the transformation (Rogan & Chen, 2004). This is especially recommended when implementing exact algorithms such as TPS, for which GCPs residuals are all equal to zero (Brovelli & Minghini, 2012; Serra et al., 2003).

In order to give a measure of the geometric accuracy of the re-registered GAI 1954 dataset, 15 new points that had not been used for implementing the transformation algorithm were chosen as CPs to test the performance of the georeferencing transformation (Figure 12).

b. Radiometric correction/image enhancement

Applying any radiometric correction procedure was not considered necessary, as the 1954 images have already been provided with corrections after the scanning phase, and in the 2012 the presence of atmospheric interference, especially of clouds, was not significant. A simple image enhancement operation of contrast stretching was applied to increase contrast between the image features and facilitate their visual interpretation. A serious issue with the 1954 images, however, was the widespread presence of shadowed areas due the rugged mountain topography, that appeared uniformly dark and usually impossible to

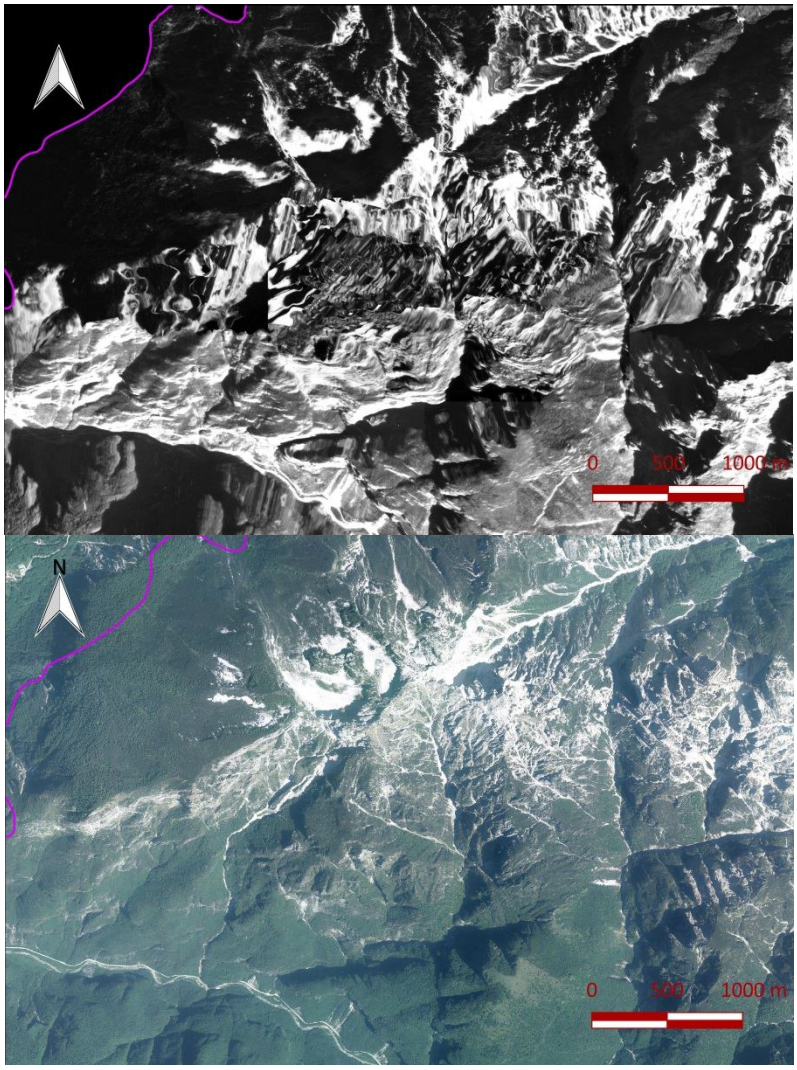

Figure 13: comparison between GAI 1954 orthorectified images showing shadows and distortions, and the corresponding location in the 2012 images.

interpret; in addition, the existence of severe distortions due to orthorectification, further increased the areas for which it was impossible to identify the land cover type (Figure 13).

This made it necessary to create a mask of these areas by manually digitizing each one of them and assigning the classes “shadows” and “distortions” according to their type.

This mask was later applied to the 2012 classification in order to take into account, during the change detection phase, only of those areas that could be seen and interpreted clearly in the 1954 images. The purpose of this step is to ensure the consistency between classifications, and avoid considering as “new” grassland areas those grasslands that were already present in 1954 but couldn’t be mapped due to the constraints discussed above.

Definition of classification criteria and creation of grassland distribution maps for 1954 and 2012

The choice of creating a land cover map through manual photointerpretation implies a certain level of subjectivity in the delineation of land cover units. For this reason it is necessary to ensure that this process is carried out in the most repeatable and unambiguous way possible, by establishing clear criteria for distinguishing land cover classes and defining a rigorous methodology to conform to.

Given that the objective of this part of the study was the assessment of the temporal evolution of mountain grasslands in relation to woody plant encroachment, it was fundamental to decide how to identify the forest-grassland boundary. Since the classification systems most widely used (see Section 3.1) for these land cover types employ classifications criteria based mainly on vegetation cover percentage and areal extension, it was decided to adopt such criteria as well for the definition of grassland areas and their boundaries in relation to forest and other land cover types.

In the FRA guidelines, the term “*forest*” defines a land cover type with area wider than 0.5 ha (5000 m^2), tree canopy cover higher than 10%, and trees higher than 5 m at maturity. Another class used in the FRA is “*other wooded lands*”, which includes areas of shrubs and bushes (height of less than 5 meters) where no trees are present and with a canopy cover of 10% or more. The latter is especially important in the context of this work, because it comprises some alpine tree vegetation types like *Pinus mugo* stands, very common in the study area.

It can be noted how these definitions are optimized for ground surveys, as it is not generally possible to easily identify tree height from digital remote sensing images (Chirici & Martino, 2009; De Natale et al., 2003). For the purpose of this study, however, no difference has been made between forests and shrublands, and both are considered as "not grassland" as long as wooded plant cover is higher than 10%.

Considering that the FRA focuses on forested areas, grassland is not given an official definition, but rather falls into the general category of "*Other land*" which includes agricultural land, meadows and pastures, built-on areas, barren land, etc. (FAO, 2010) and is therefore not suitable for this study. For the purpose of defining classification criteria that can be harmonized with international standards, it is necessary to derive them "by difference" from other land covers' classification criteria.

It was decided to use the IUTI definition, that, despite following the international FAO guidelines, also includes a separate grassland class (IUTI code 3.1, "grassland and pastureland") identified by a minimum extension of 5000 m^2 and defined as "any land occupied by natural pastureland, high altitude grassland, grassland-pastureland, areas deriving from the abandonment of agricultural practices and in general any formation composed of spontaneous non-woody vegetation with cover higher than 40% and dominated by grasses (Marchetti et al., 2012).

In conclusion, the definition of grassland employed for this phase of the study includes these criteria:

- Minimum extension: 5000 m^2,
- Minimum cover of herbaceous vegetation: 40%
- Maximum woody plant cover: 10%

As a consequence, areas with bare rock/soil mixed with grassland were excluded if percentage of bare rock was higher than 60%. In the same way, areas with sparse trees/shrubs were excluded if their cover was higher than 10%. A vector grid with cell area of 5000 m^2 was created and overlaid to the images to help estimating tree density and facilitating the photointerpretation procedure and the delineation of forest-grassland boundaries.

After the delineation of polygons, a thorough topology check was conducted, and all the geometries that presented any problem were corrected. This is especially important because manual

digitization can create involuntary topology errors that are likely to cause errors when combining vector layers.

Classification accuracy assessment

Classification accuracy assessment is usually performed by creating an error (also called confusion) matrix to observe the differences between the classified map and the reference data. The error matrix-based accuracy assessment technique is the most common method for assessing classification accuracy, and it is based on the selection of a sample of locations (the ground truth) that are used to determine the "real" land cover type using field observations and/or high resolution images. Error matrices will be discussed in more detail in section 5.4.2.

The choice of reference data should be done considering several aspects, such as: a) data independence, meaning that the reference data cannot have been used for the creation of the classification or change map being assessed; b) source of reference data, that should be more accurate than the predicted accuracy of the data being tested; c) number of sample points. Many standards require a minimum of 20 samples per ground cover class, with more (at least 30) being recommended; d) distribution of samples across the study area, that must represent the full variety of topography and land cover types present (Congalton & Green, 2009).

For the 1954 images, it has not been possible to find any reference data against which to check the classification accuracy.

In the case of the TELAER images, the IUTI inventory was chosen for the accuracy assessment, specifically the 2008 classification that is the closest in time to the date of acquisition of the TELAER images. No other available reference data with a higher accuracy than the classification performed in this study could be found. In this case, it was not possible to create a full error matrix because the TELAER images were classified only according to the presence/absence of grassland areas, so prior to the accuracy assessment procedure only the IUTI points falling within the mapped grassland areas were chosen. In order to have as much data as possible to work with, the full 2012 grassland distribution map was used, not only the areas not covered by the 1954 shadows/distortions.

The IUTI points overlapping the mapped areas were extracted by running a Spatial Query on QGIS. This yielded 119 points (out of 1237) (Figure 14), whose class code for 2008 was extracted and compared with the grassland classification.

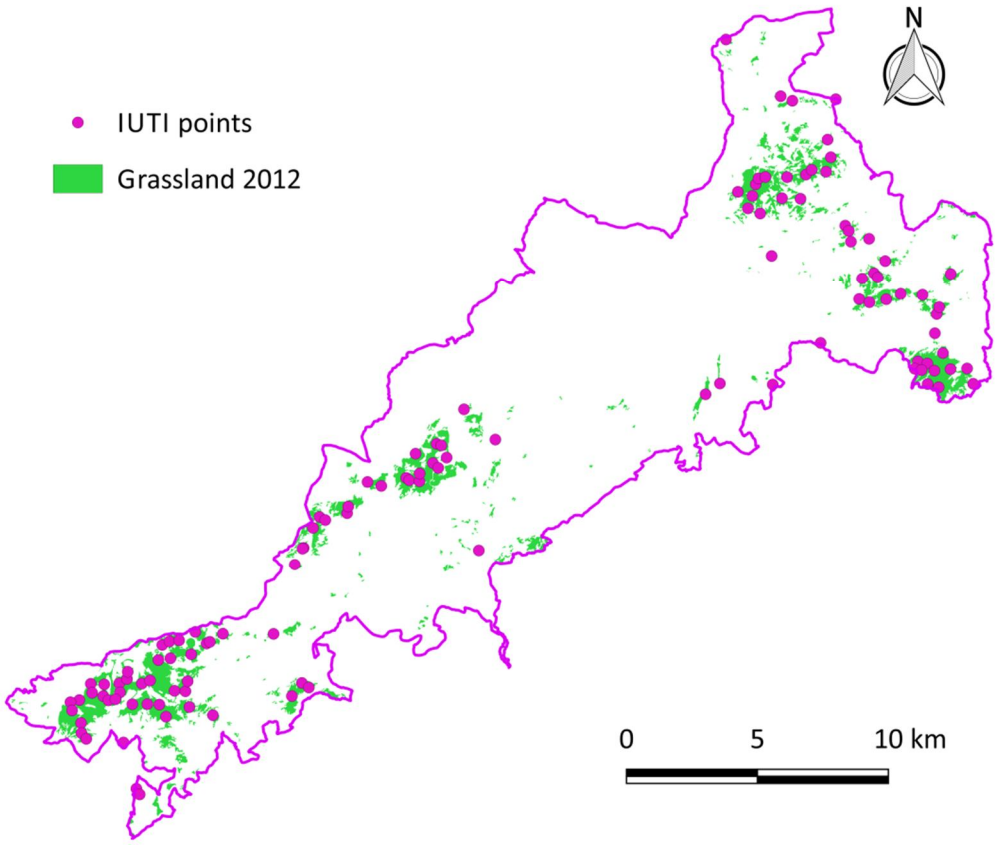

Figure 14: IUTI points overlapping 2012 grassland areas

Post-classification change detection

A preliminary step was the rasterization of the two vector layers, assigning to both rasters the same spatial resolution of 2 m, equal to the coarser resolution of the 1954 images, and the same grid origin, in order to ensure their perfect overlay (Appendix A, A3. Rasterization of vector files). Considering how different pixel sizes and/or grid origins make the process of stacking layers for change analysis more complicated, as it introduces further positional error to the error already existing due to the imperfect alignment between the images, it is important to take care of these aspects before carrying out any comparison.

The values of the two binary rasters representing grassland distribution at the two times were then combined using the Raster Calculator to give four possible change classes:

0 : No change – areas not classified as grassland in both dates

1 : Change – grassland loss between 1954 and 2012

2 : Change – grassland increase between 1954 and 2012

3 : No change – areas that remained grassland throughout the time period

A vector map was also created from this file, since it is more suitable for visualization purposes and for the overlay with other spatial or thematic data.

Grassland loss by altitude range

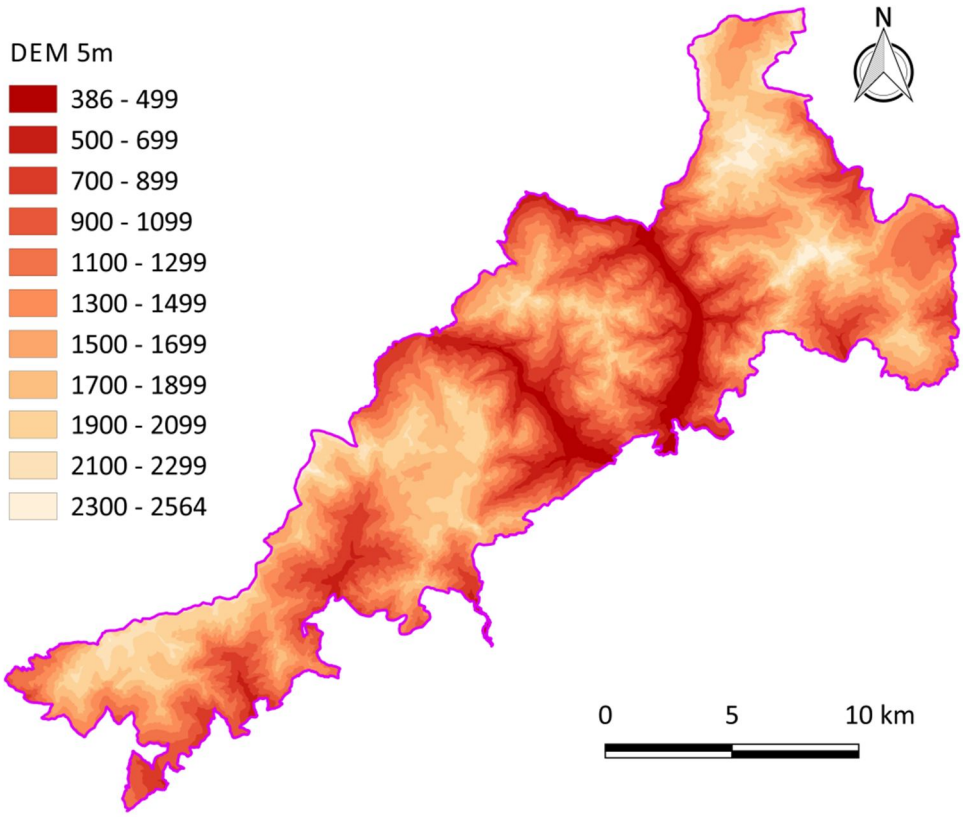

Figure 15: Reclassified DEM

In order to locate and quantify the areas of grassland loss by altitudinal range, the 5 m DEM acquired from the Veneto Region Geoportal was employed. Since the DEM is divided in tiles according to the CTR 10000 cuts, the single tiles were first merged into a single raster and clipped to the study area.

QGIS does not offer a straightforward solution to extract zonal statistics between rasters and to do multi-class zonal statistics, so several steps (described in detail in Appendix A) had to be performed before obtaining the final result.

First, the DEM's pixel values, that originally ranged from 386 to 2564 m, were reclassified into 11 altitudinal bands using the GRASS tool r.reclass, according to the classification system shown in

the legend of Figure 15. Then the resulting raster (Figure 15) was converted to vector through the "Polygonize" tool, and the shapefile obtained from this operation was merged by altitudinal class, in order to obtain only one polygon for each class. In addition, contour lines were extracted from the original raster as a visual aid. From the change classes raster map described in the previous section, three individual rasters (one for each class) were obtained, and each of these rasters was used to calculate zonal statistics for the corresponding class. The same operation was repeated for the original 1954 grassland raster map.

5.4.2 PART 2: Satellite images

Five Landsat 5 images from 2005 (the year with the highest number of reasonably cloud-free scenes for the study area) were used to test for differences in classification results and accuracy by varying the Landsat dates used as input for the classifier and also through the calculation of vegetation indices. Since several high quality ancillary datasets are available as a support in the creation of training areas, a supervised classification was preferred over a non-supervised one. Specifically, a pixel-based semi-automated classification technique with a Maximum Likelihood Classifier (MLC) was employed.

For each image, all spectral bands were used except for the thermal band (band 6), because of its inferior spatial resolution and low sensitivity to the vegetation properties of interest. The list of images used in this study is shown in Table 6.

Satellite/Sensor	Landsat Scene Identifier	Date	Cloud cover
L5/TM	LT51920282005161KIS00	10/06/2005	0,99
L5/TM	LT51920282005209KIS00	28/07/2005	3,06
L5/TM	LT51920282005241KIS00	29/08/2005	8,11
L5/TM	LT51920282005273KIS00	30/09/2005	3,99
L5/TM	LT51920282005289KIS00	16/10/2005	0,61

Table 6: Available Landsat images for the year 2005 with cloud cover less than 10% over the study area

The image dates are distributed throughout the vegetative season, so they should allow to evaluate how classification accuracy varies according to each phenological stage of development of the vegetation. When trying to distinguish between different vegetation land cover types through their spectral properties, it is necessary to make sure of selecting the optimal moment during the vegetative season for enhancing the spectral differences between the land cover types of interest (Esch et al., 2014; Nordberg & Evertson, 2005).

In the case of the Dolomiti Bellunesi National Park study area, it was hypothesized that the late August/early September period may be the best option to obtain a good separability between vegetation types and to distinguish grassland areas, given that usually in this part of the year grasses are already starting to become senescent while shrub and trees are still green. This applies to areas above the treeline as well, where it should be possible to distinguish senescent grasses from evergreen dwarf mountain pine stands (Vettorazzo E., personal communication, June 28, 2015). Boschetti et al. (2007) noted a decrease in biomass production from July to August in alpine grasslands, which could validate the choice of late August as an appropriate period to choose.

Pre-processing

a) Geometric rectification

Landsat scenes from USGS are processed to Standard Terrain Correction (Level 1T "precision and terrain correction") using the Level 1 Product Generation System (LPGS), which provides geometric accuracy by utilizing both ground control points (GCP) and a digital elevation model (DEM). The GCPs used are obtained from the GLS2000 dataset, with a 90 m DEM. The expected error of the GLS2000 dataset is less than one pixel (25 meter RMSE on a per-image basis). The end result is a geometrically rectified product with no sensor, satellite and Earth-related distortions (e.g. view angle effects, Earth rotation and curvature, topographic relief). Landsat standard data products employ the World Geodetic System (WGS) 84 datum as the Earth model and the Universal Transverse Mercator (UTM) map projection.

The geometric correction accuracy given for each Landsat scene is generally high (less than 8 m for the scenes of the study area, see Appendix B), and in addition a Verify Image File is included with the Landsat products, which displays a grid of verification points in various colors to represent the level of geometric accuracy of each part of the scene.

Moreover, the co-registration accuracy between Landsat images and the TELAER 2102 orthophotographs was also assessed, by identifying 11 CPs in both images and computing the RMSE. In this case, RMSE was 0.42 pixel (corresponding to about 13 m), lower than the generally accepted threshold of 0.5 pixel. Proceeding to the co-registration of the images was therefore not considered necessary.

b) Atmospheric correction

The availability at no cost of Landsat Surface Reflectance frees users from the task of having to apply atmospheric correction routines to the images, usually a necessary step to allow for an easier detection and quantification of land surface change. These procedures, especially absolute corrections based on atmospheric modelling, require knowledge of both the sensor spectral profile and the atmospheric properties at the acquisition time, which are difficult and time-consuming to acquire (Du et al., 2002; Xie et al., 2008). SR images are obtained from the processing of Level-1T

Landsat data through the Landsat Ecosystem Disturbance Adaptive Processing System (LEDAPS) (Masek et al., 2006), which applies MODIS absolute atmospheric correction routines to Landsat scenes in a three-step process: 1) conversion of DN to Top-Of-Atmosphere (TOA) reflectance; 2) detection of cloud pixels based on the TOA reflectance; 3) correction to surface reflectance from TOA reflectance and auxiliary data set (ozone, water vapor, geopotential height, aerosol optical thickness and a DEM) to correct for molecular scattering and absorption by atmospheric constituents (USGS, 2015a).

The SR Landsat products were used for every step of this study; one aspect to keep in mind is that SR products (both the bands and the Vegetation Indices) have a scale factor of 0,0001, so the values shown here do not correspond to the real reflectance values.

c)Topographic correction

Topography-induced shading effects generally represent a major problem that affects the accuracy of classifications obtained from satellite imagery in rugged mountain areas (Mihai et al., 2007), and considering the steep terrain of the study area it was decided to carry out a topographic correction procedure on each image. As there is no universally accepted method for evaluating the performance of topographic correction (Balthazar et al., 2012), in this study both the corrected and the uncorrected images were classified and assessed for accuracy, and the classification accuracies for individual land-cover classes were compared to assess the existence of any significant improvement brought by topographic correction.

The first step in the correction of shadows caused by topography is the calculation of the local illumination angle, based on solar geometry (Sun zenith and azimuth angles) of the time and location where the satellite image was acquired and on the topographic slope and aspect angles. For Landsat TM/ETM+ data, a single set of angles can be assumed since the scenes are relatively small. To compute the slope gradient and aspect, a DEM with the same resolution of the images should be used (Balthazar et al., 2012; Richter et al., 2009). To obtain the necessary DEM, the 5 m DEM previously used was first converted to the WGS84/UTM ZONE 32N (EPSG:32632) CRS so as to have the same CRS as the Landsat images, and then resampled to a 30 m pixel size.

QGIS offers the possibility of applying topographic correction to an image through the SAGA geoalgorithm "*Topographic correction*". Among the available methods, the "Minnaert correction

with slope (Law & Nichol, 2004)" method was chosen, as the family of Minnaert correction methods has been shown to give generally acceptable results (Meyer et al., 1993; Richter et al., 2009; Vanonckelen et al., 2013). The values for solar azimuth and elevation were obtained from each Landsat image's metadata file.

The Minnaert constant *k*, which indicates to what extent a surface is Lambertian, was left to the default value of 0,5. The value of k can vary between 0 and 1, where 1 indicates a perfectly Lambertian behaviour and 0 a perfectly or non-Lambertian behaviour, and therefore it is a measure of the roughness of the surface. Using this correction factor helps reducing the problem of over-correction in the areas facing away from the sun typical of methods such as the cosine correction (Law & Nichol, 2004). The topographic correction process is described in more detail in Appendix B.

Cloud cover mask

As it can be observed in Table 6, all the images have variable amounts of cloud cover, which made it necessary to ensure that the same area was classified for each image in order for the classifications to be comparable. Therefore, the first step was to create a cloud mask for 2005 derived from the combination of the cloud cover quality assessment band of each image. In addition to this, considering how some preliminary classification trials showed a great degree of confusion between the class "water" and other land cover classes, it was decided to mask out the water areas as well in order to simplify the classification process and eliminate a source of uncertainty. Within the Dolomiti Bellunesi National Park there are only two water bodies of significant extent (Stua and Mis lakes), so their boundaries were manually digitized. The resulting shapefile was rasterized and

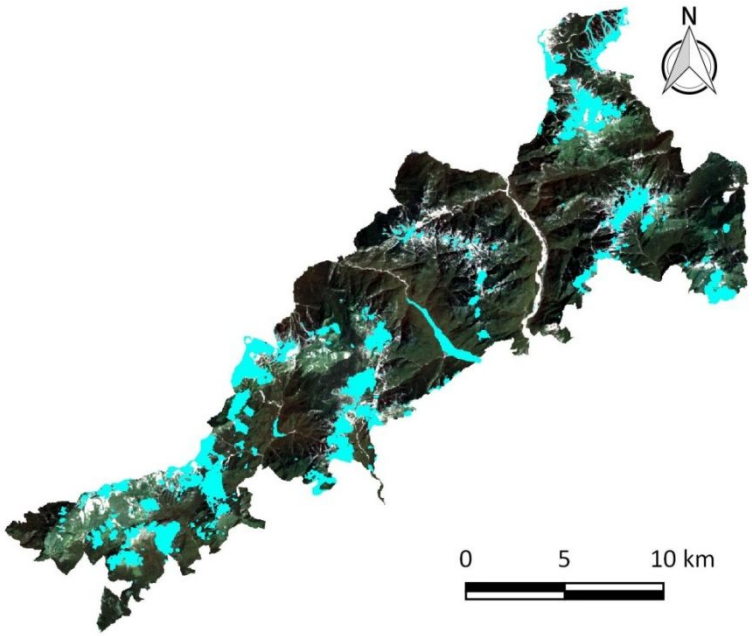

Figure 16: Cloud and water mask (light blue) applied to one of the Landsat 5 images in the 2005 series.

added to the cloud cover mask. This final version of the mask was used to mask each 2005 Landsat scene, in order to keep only those areas that were cloud-free in each of the five dates (Figure 16), on which the classification was performed.

Training area selection

The tool used for image classification was the Semi-Automatic Classification Plugin (SCP) (Congedo & Munafò, 2012), whose functionalities allow to carry out every step of the classification process, from pre-processing to accuracy assessment.

The first step in a semi-automated classification procedure based on the spectral properties of land cover types is the definition and selection of areas of homogeneous land cover, here called Regions of Interest (ROIs), for training the classifier. ROIs are used for the extraction of the spectral signature belonging to each class, which in turn is used for the classification of the whole image.

The land cover categories chosen for the definition of ROIs were based on the IUTI inventory class definitions, which represent the reference data, in order to allow for an easier comparison of the datasets for accuracy assessment purposes (Table 7). Only the class "Forest" was initially divided into two sub-classes (Conifer and Broadleaved) in order to see if their spectral signatures were separable, but in the classification phase the two subclasses were treated as one single class to conform to the IUTI classification.

Macroclass ID	Land cover type	Number of ROIs
1	Grassland	120
2	Shrubs and sparse trees	110
3	Bare/sparsely vegetated areas	72
4	4.1 Conifer Forest	89
	4.2 Broadleaved Forest	107

Table 7: Land cover classes for Landsat image classification and number of training ROIs chosen for each.

In the SCP, the training ROIs can be delineated either manually or through an automated region growing algorithm with user-defined parameters, where it is possible to set the interval which defines the maximum spectral distance between the seed pixel and the surrounding pixels (in radiometry units). Table 7 also shows the number of ROIs chosen for each class, which is a function of the spatial extension of the land cover class and of its perceived spectral separability. For example, the class "shrubs and sparse

trees" was easily confused by the classifier with other land cover types, while the class "bare/sparsely vegetated areas" showed better separability (in addition to being more limited in extent). The choice of ROIs was also guided by the need of capturing the variability present in each land cover category, especially considering that the same ROIs would be used for classifying images from different dates and therefore with different conditions, despite belonging to the same year. This aspect is also important to improve classification using the Maximum Likelihood algorithm.

The creation of ROIs was carried out through the region growing algorithm built into the SCP. A region growing algorithm is a region-based image segmentation method, which examines the neighboring pixels of initial seed points in order to decide whether to add them to the region or not. In this case, the region membership criterion is based on spectral signature similarity (adjustable by the user). The choice of seed points was based on:

- The visualization of the Landsat image under different band combinations, which can highlight different land cover features. The combination used were 3-2-1 (natural color image), 4-3-2 (standard false color) and 4-5-1 (a different false color combination, useful to highlight bare soil) (Figure 18).
- Ancillary data: TELAER 2012 images and 2005 Habitat Map

After selecting each ROI, the ancillary datasets were used again to evaluate the accuracy of each ROI's attribution to a certain class, and all ROIs assigned to the wrong class, of uncertain attribution, or covering more than one land cover type were deleted.

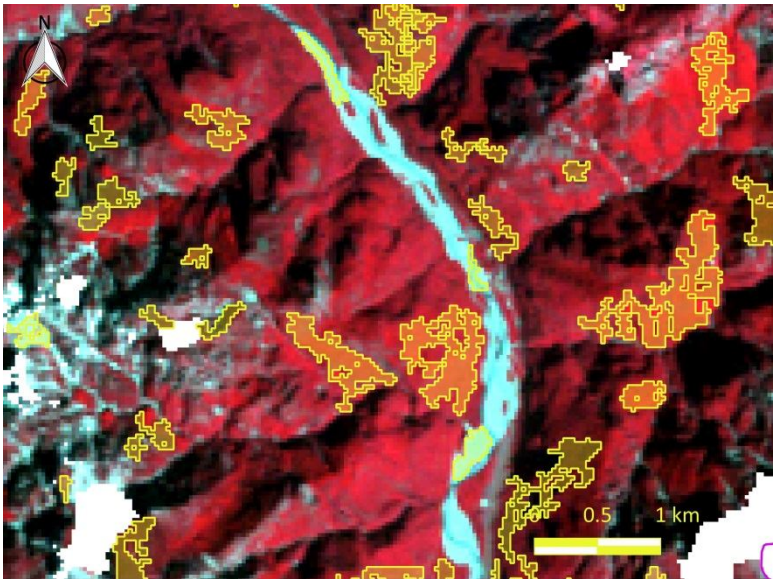

Figure 17: example of ROIs

The choice of appropriate ROIs to train the classifier is partly a trial-and-error process, however, and in some cases even the training areas that are properly assigned to a land cover class (according to visual assessment) do not lead to a good classification result. For this reason, the training was supervised step-by-step by means of classification preview generation in order to

avoid macroscopic errors. Every time the addition of a new ROI caused a detectable worsening of the classification quality, that ROI was deleted and/or re-defined. In total, 498 ROIs were kept for the final classification (Figure 17). The resulting ROI shapefile was also topology-checked to make sure that there was no accidental overlap between ROIs belonging to different classes.

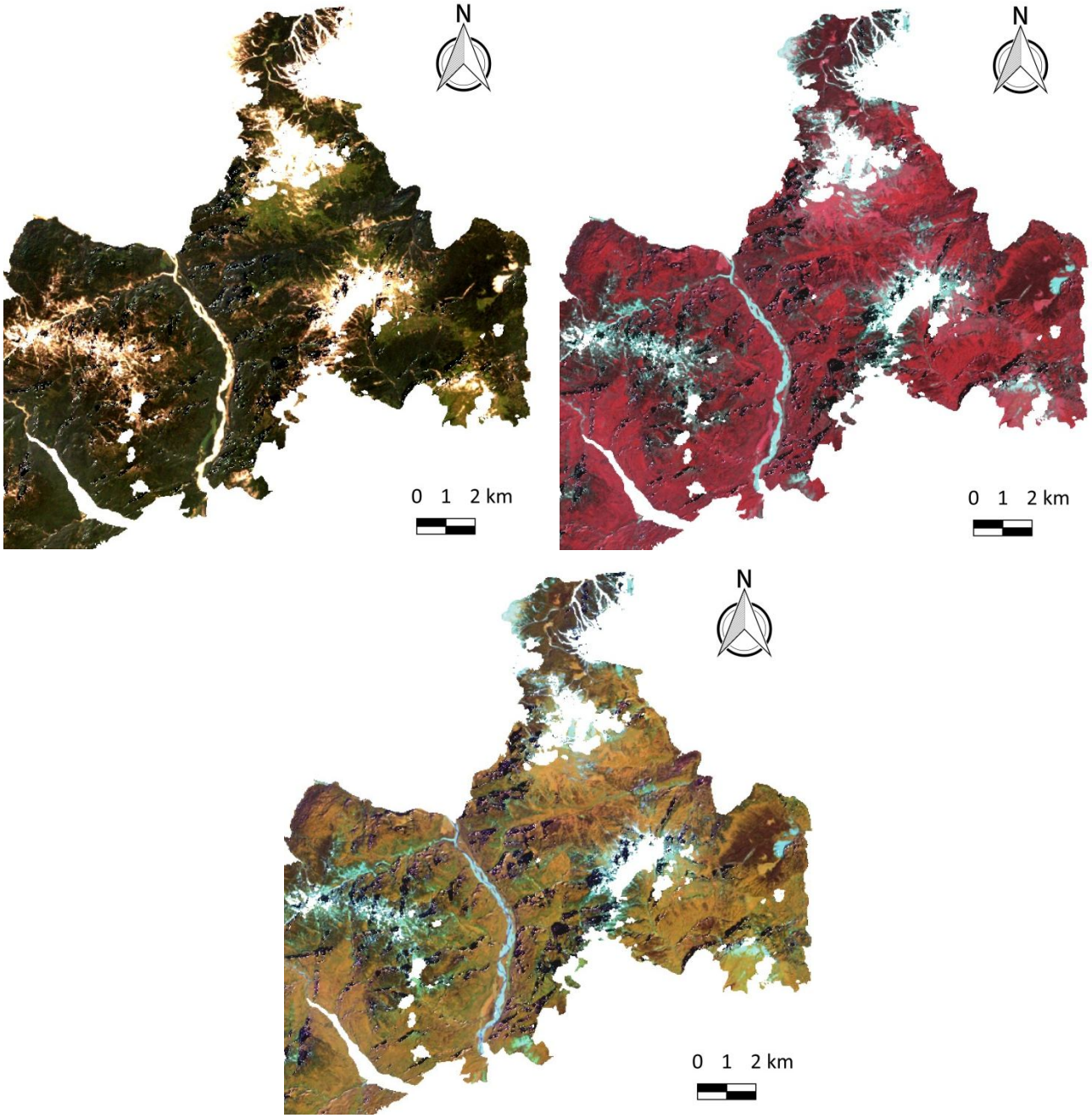

Figure 18: a part of the study area shown in natural color (3-2-1), standard false color (4-3-2) and false color combination 4-5-1.

Vegetation Indices time series

Vegetation Indices (VI), and in particular NDVI, have been widely used as an approximation of vegetation phenology, and several NDVI images obtained from different dates within the same year, or within a vegetative season, can be used to reconstruct the phenological profile of the land cover classes of interest. Plotting time-series vegetation index data produces a temporal curve that summarizes the various stages that green vegetation undergoes during a complete growing season, and that can be used to extract key phenological variables such as the start, the peak and end of the growing season (Simonetti et al., 2014).

In turn, this may be useful for evaluating whether there is a moment in the vegetative season that can be better suited for obtaining a higher classification accuracy due to a greater phenological difference between vegetation types (Senf et al., 2015). The problem with classifying vegetated areas, however, is that the spectral signatures (and consequently VI values) of different vegetation classes can show some significant overlap, and differ according to the phenological stage of development of each vegetation type, so classification results largely depend on the date chosen. Better classification results are often achieved by using two or more VI images as classification input, or combining satellite spectral bands with one or more VI derived from them (Gartzia et al., 2013). This is important for change detection as well, given how land cover with high inter-annual variability affects classification results and can also distort the baseline from which change is measured (Bradley & Mustard, 2005).

The vegetation indices used in this study are NDVI and EVI, both obtained directly from the EROS website as part of the SR Landsat products. NDVI was chosen because it is the most commonly used VI for land cover classification and change detection, and also because it can compensate for topographic effects, while EVI because it should be more sensitive than NDVI to differences in vegetation cover and not become so easily saturated in areas with high biomass. NDVI and EVI are computed for Landsat TM/ETM+ images as (USGS, 2015d):

1) NDVI = (Band 4 – Band 3) / (Band 4 + Band 3).

2) EVI = (Band 4 – Band 3) / (Band 4 + 6 * Band 3 – 7.5 * Band 1 + 1)

A total of 10 VI files were used (5 for NDVI and 5 for EVI, corresponding to the five 2005 Landsat scenes). The VI bands first were masked, and then the NDVI/EVI values corresponding to each

land cover class were extracted from them using the training ROIs created in the classification step (Figure 19). VI statistics (pixel count, mean, minimum and maximum values) were computed for each ROI through the Zonal Statistics tool. Afterwards these statistics were aggregated on a per-class basis, obtaining the mean, maximum and minimum NDVI and EVI values for each class and each date. These data were used to assess the range of NDVI/EVI values for each class and each date, and plotted to create phenological profiles of each vegetation type and observe their changes during the vegetative season.

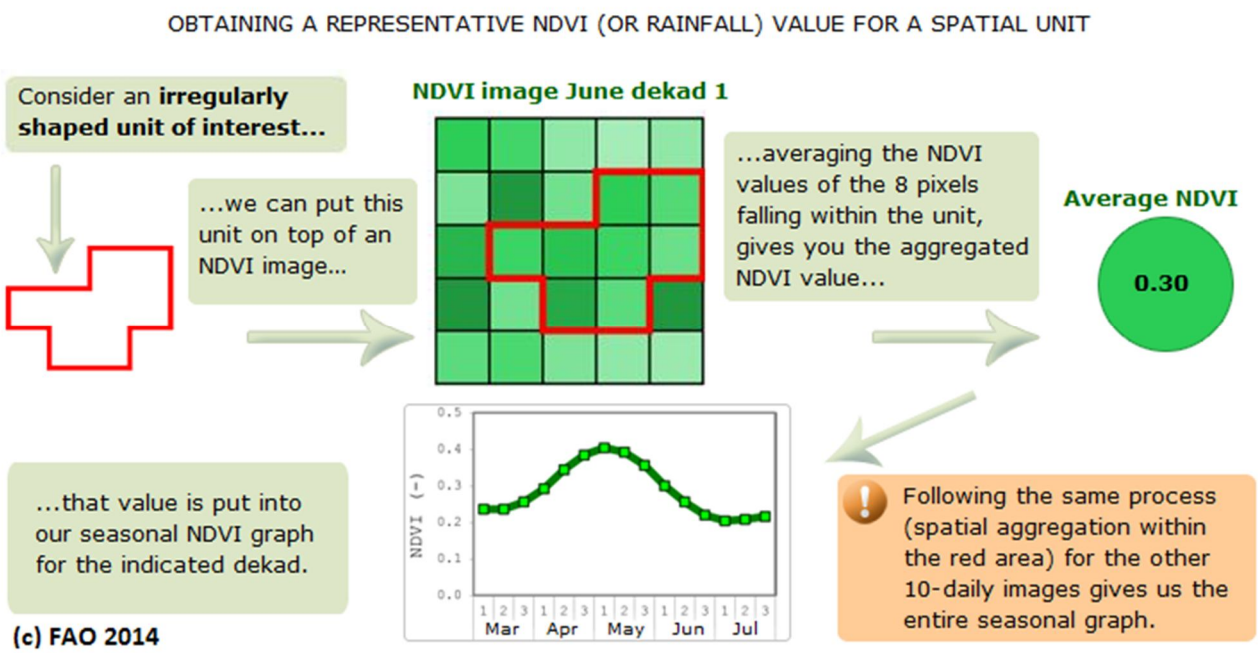

Figure 19: schematic representation of NDVI values extraction

Classification procedure

Workflow

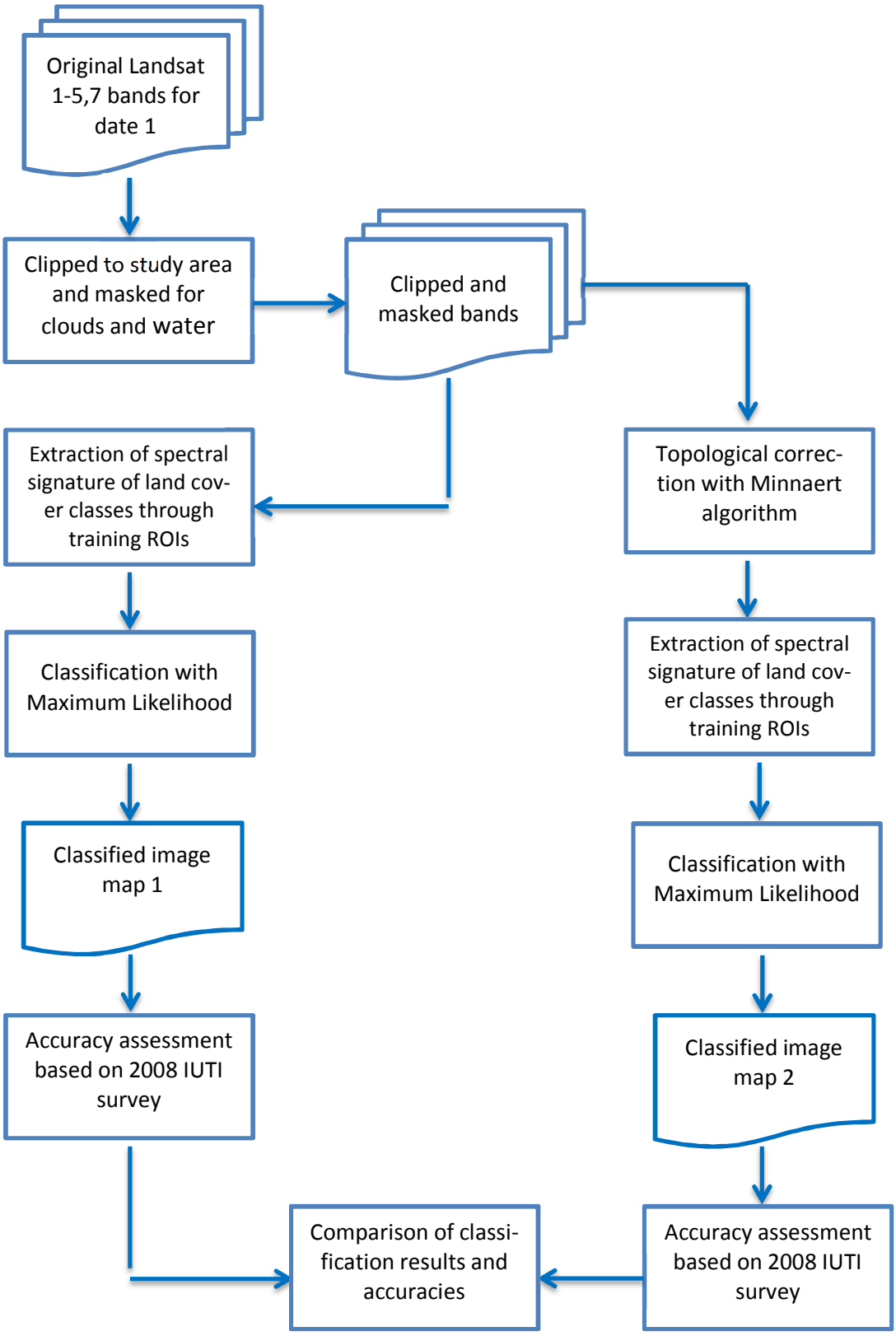

Classification scenarios and signature extraction

The five Landsat images for 2005 were used to create several "classification scenarios" (Table 8), with the purpose of assessing the classification accuracy of 1) single-image classifications for each date and 2) multi-image classifications obtained combining two or more dates or VIs.

For each scenario, a new spectral signature list was extracted for each land cover class, based on the ROIs previously created. Creating a new spectral signature for each scenario ensures that the classification results will not be affected by phenological differences. All the bands of the images/VIs used for each scenario were employed for signature extraction, in order to see if and how the different combinations of images and/or VIs could benefit classification accuracy.

SINGLE-IMAGE CLASSIFICATIONS	
1	2005/06/10
2	2005/07/28
3	2005/08/29
4	2005/09/30
5	2005/10/16
MULTI-IMAGE CLASSIFICATIONS	
6	Landsat - Dates 2 - 5
7	NDVI - All dates
8	NDVI - Dates 2 - 5
9	EVI - All dates
10	EVI - Dates 2 -5
11	Date 2, NDVI, EVI
12	Date 2, NDVI

Table 8: classification scenarios

For each scenario, the signature list so obtained was used to classify the image with the Maximum Likelihood algorithm.

In this classification algorithm, the pixels falling into the ROIs, as representative of each land cover class of interest, are used to estimate the class mean vector and covariance matrix, which are the key inputs to the function. After the class statistics are defined, each pixel is classified on the basis of which class the cell has the highest probability of being a member of. Since it is relatively simple but robust, MLC is one of the most widely employed classification methods. One of the reasons is that it uses means, variances and covariances of training site statistics, where most other decision rules are based on simpler statistics (Vanonckelen et al., 2013). MLC was also chosen because, unlike other available classifiers, it takes into account the spectral variability both between and within classes. No classification threshold was defined, in order to avoid the creation of "unclassified" pixels that later need to be excluded from the accuracy assessment, further diminishing the area available for the cross-validation with IUTI. This is justified by the fact that the land cover classes chosen are representative of all the land cover types present in the study area, and other possible land cover types outside of the classification (in this case only water), have been masked out beforehand.

In addition, to evaluate the effectiveness of the topographic correction both the topographically corrected images obtained with the Minnaert with slope algorithm and the original ones were classified using the same ROIs, but calculating spectral signatures independently. This process was repeated for each of the 5 images used for the study on land cover classification results on 2005 images.

In this case, a full error matrix and therefore a complete accuracy assessment of the resulting classifications could be carried out using the IUTI inventory, again using the 2008 survey as it is the closest in time to the date of the Landsat images.

The error (or confusion) matrix (Figure 20) is an effective way to represent the accuracy of a classification, because it allows to observe the differences between the change map and the reference data based on the number of sample units (i.e., pixels, clusters of pixels, or polygons) assigned to a category in the classification in relation to the actual category derived from the ground truth. The columns usually represent the reference data while the rows indicate the classification obtained from the remotely sensed data (Congalton, 1991; Foody, 2002; Smith et al., 2003).

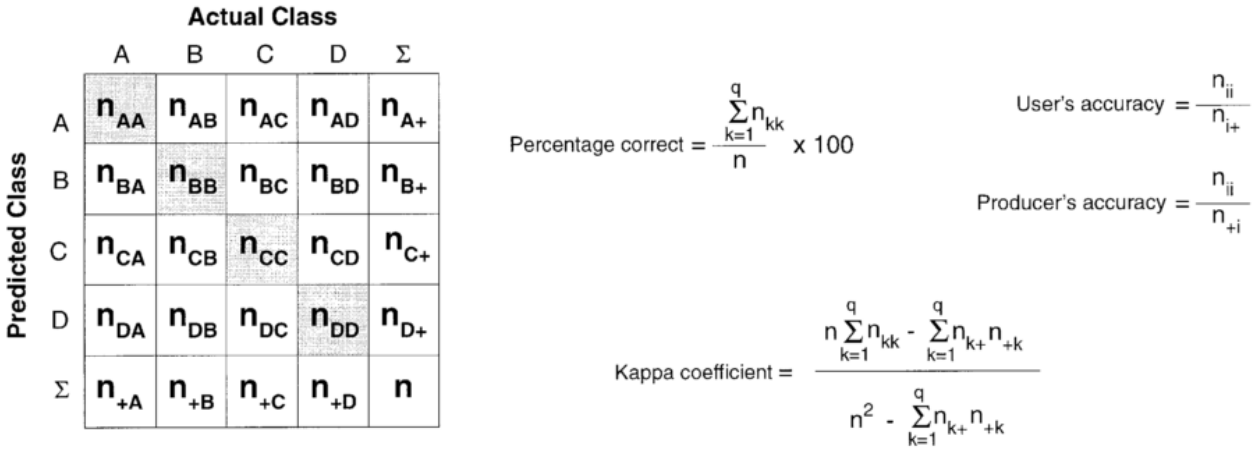

Figure 20: Example of confusion matrix and of the most common accuracy metrics that can be calculated from it. The highlighted elements represent the main diagonal of the matrix (correctly allocated units), while the off-diagonal elements contain the units where there is a disagreement between the classification and the reference data From Foody (2002).

Through the error matrix it is possible to calculate several accuracy metrics, such as overall accuracy, producer's accuracy, user's accuracy and Kappa coefficient. Overall accuracy is the percentage of cases correctly allocated, calculated as the sum of the major diagonal (corresponding to the correctly classified sample units) divided by the total number of sample units in the error matrix. Overall accuracy is a synthetic and easy to interpret metric to express the accuracy of the classification as a whole. Producer's accuracy is obtained by dividing the total number of correctly assigned units in a class by the total number of units for that class present in the reference data (column total), while user's accuracy is calculated by dividing the total number of correctly assigned units in a class by the total number of units classified as that class (row total). It is im-

portant to consider both of these metrics when evaluating the accuracy of a classification, because high producer's accuracies often occur only because too much of the map has been classified as that particular land cover class. User's accuracy on the contrary can show whether there is significant confusion in the attribution of a land cover class, which indicates a problem of the classifier in discriminating between land cover classes. User and Producer's accuracy give information on the two sub-types of error that can occur in a classification: inclusion (commission error) and exclusion (omission error). A commission error occurs when an area is included in an incorrect category, while an omission error occurs when an area is excluded from the category to which it belongs. (Congalton, 1991; Foody, 2002; Morgan et al., 2010).

The Kappa coefficient is an alternative index of classification accuracy, and provides a more conservative but more robust estimation of accuracy than the simple percentage of cases correctly classified, because it takes into account the agreement between classification and the reference data that may occur by chance (Congalton & Green, 2009; Foody, 2002).

Within the SCP it is possible to carry out the accuracy assessment and calculate the error matrix with a dedicated tool (*Post-processing* → *Accuracy*). Before implementing the algorithm, it is necessary to make sure that the two datasets (classification and reference data) have the same thematic classes and code, expressed as a number. The IUTI codes were therefore changed to match those of the classified images (with values from 1 to 4 according to the classification shown in Table 7), and then the file (originally a vector file with point elements) was rasterized with a 30 m pixel size, making sure that the grid of the new raster was aligned to that of Landsat images to minimize positional errors. The error matrix between each classification and the IUTI reference raster and the related statistics were subsequently computed through the SCP and compared.

NDVI image differencing *change detection*

The change information that can be obtained from a change detection technique can be divided in two main types (Lu et al., 2014):

a) Binary change/non-change: provides information only about whether there a land cover change has occurred or not, together with the amount of changed areas and their spatial patterns within a study area for the change detection period considered. Threshold-based methods are commonly used to distinguish changed from non-changed areas.

b) ‘From-to’ change: usually obtained from a post-classification comparison approach, it can provide a complete change matrix. In this case, the definition of a land cover classification system and the accuracy of the classifications are critical to highlight meaningful change trajectories and to exclude apparent change due to misclassification and misregistration.

Image differencing-based change detection methods belong to the change/non change category. When using NDVI bands as the images to difference, the difference image is calculated as:

ΔNDVI[Date2Date1] = NDVI[Date2] – NDVI[Date1]

The pixel values of the difference image in general follow a normal distribution, where pixels in the central region represent no change (near-zero differences) while those within the two tails of the distribution are characterized by significant changes in the vegetation’s properties. In the specific case of this study, where an increase in vegetation biomass and density is expected, subtracting the older date from the most recent one should cause negative values in the difference image to indicate a decrease in green vegetation biomass, while positive values suggest an increase. In the case of grassland to shrubs/trees conversion, an increase is expected (Mancino et al., 2014).

The images chosen for the change detection are the NDVI bands derived from the 27/07/1987 and 18/07/2007 Landsat scenes, respectively. These dates and years were chosen because a)according to the classification and seasonality results, they represented the period with better separability between vegetation classes; b) among the usable images from the same period, they have the lowest cloud cover; c) they can provide the widest temporal gap (20 years), which should give a higher chance of detecting changes.

Before the image differencing procedure itself, the images were pre-processed in order to ensure the best possible comparability. First, the images were masked for clouds (both the cloud cover present in 1987 and 2007) and for water. Second, all negative values were removed, on the basis that only positive values represent soil and vegetation, and moreover the outlying values present in the negative part of the image histograms could introduce artifacts in the difference image.

Finally, the resulting images were normalized through a histogram matching procedure, in order to ensure that the 10-day temporal shift between the images, as well as differences in season-

al temperature/precipitation did not affect the results. After this, the images were subtracted with the raster calculator according to this formula:

ΔNDVI[2007_1987] = NDVI[2007] – NDVI[1987]

Identifying a threshold for detection of vegetation changes is the key issue in change detection methods based on image differencing. The standard deviation (σ) of the pixel values density function in the difference image is one of the most common threshold identification approaches, and has been applied successfully for different natural environments and different remotely sensed imagery (Coppin et al., 2004; Lu et al., 2004; Mancino et al., 2014; Singh, 1989).

The threshold is used to separate three ranges in the normal distribution: (a) the left tail ($\Delta VI < \mu - n\cdot\sigma$); (b) the right tail ($\Delta VI > \mu + n\cdot\sigma$); and (c) the central region of the normal distribution ($\mu - n\cdot\sigma < \Delta VI < \mu + n\cdot\sigma$), where μ represents the mean of the pixel values and *n* defines the range of dispersion around the mean (Mancino et al., 2014). The n value was be identified through a manual trial-and-evaluation procedure, by testing different thresholds and evaluating the change detection results. In the literature, n values generally vary between 1 and 2 (Lu et al., 2004; Singh, 1989). Mancino et al. (2014) found that the optimal n value for a forest expansion change detection problem in a study area comparable to the one of this study was 1,5. In this work, a threshold of $1\cdot\sigma$ was used.

6. RESULTS AND DISCUSSION

6.1 Aerial photographs

Co-registration results

The mean error resulting from the check points was 0.86, which corresponds to less than one pixel, that is to say 1,7 m considering the GAI images' pixel size of 2 m. This represents an improvement from the previous situation, even if it must be taken into account that, considered the distortions present in the images, the same level of accuracy cannot be expected in every part of the images. As noted before, the importance of the GAI 1954 images lies in the possibility of obtaining thematic information from a time period not generally covered by other data sources, rather than in the high spatial accuracy of the results. Despite their spatial and radiometric resolution being poorer compared to the more recent aerial imagery, and the significant distortions caused by the orthorectification process, it would not have been possible to exclude these images from the classification process, given their importance for outlining the situation of semi-natural grasslands land cover at the time preceding abandonment, and thus their role as the foundation on which a temporal series can be built.

After undertaking the task of manually classifying the GAI 1954 images, the difficulties of handling this dataset appeared even more evident, as was the necessity of resorting to a human photointerpreter rather than using an automated classification algorithm. This is especially true for the specific purpose of mapping grasslands, in particular in a complex terrain such as that of the study area. The low level of grey-scale contrast in the GAI 1954/55 images often makes grassland almost indistinguishable from light colored non-vegetated areas, which are common in the rocky mountainous landscape of the Dolomiti Bellunesi National Park; taking a decision about the classification of these areas and the placement of grassland boundaries, was not easy, and often required the comparison with more recent aerial images and thematic cartography to identify the visual characteristics of areas with bare rock (Figure 21).

Similarly, the relatively coarse pixel size and poor radiometric detail may not allow to easily distinguish grassland areas through texture-based classification algorithms, considering that grasslands and sparsely vegetated or rocky areas show similar textural properties as well. An object based classification was attempted in the Regione del Veneto (2011)'s study, but in that case the

target of the classification were forested areas, which have a higher textural contrast. Even in that case, however, it was necessary to employ an interpreter for the visual check of the automated classification's accuracy. Yet another issue is related to the tonal differences among grasslands located at different elevations and aspects within the same photo; in many cases, grasslands in shaded areas appear similar in tone to forests, making it difficult to determine the range of brightness values representing grassland cover in an unambiguous way.

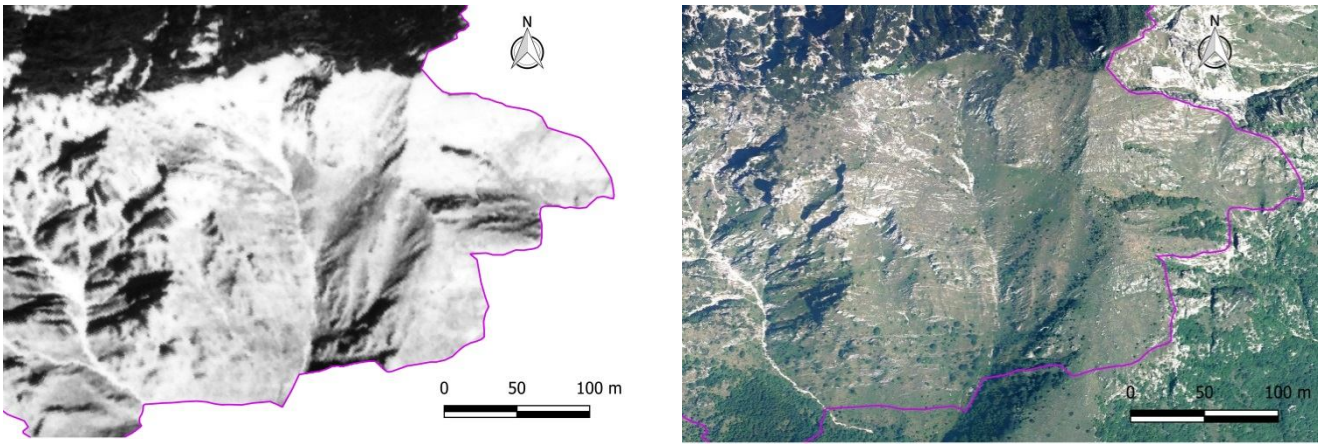

Figure 21: example of a case of uncertain attribution. The bright areas in the 1954 image can be mistaken for bare rock, while in the 2012 image they appear as grassland.

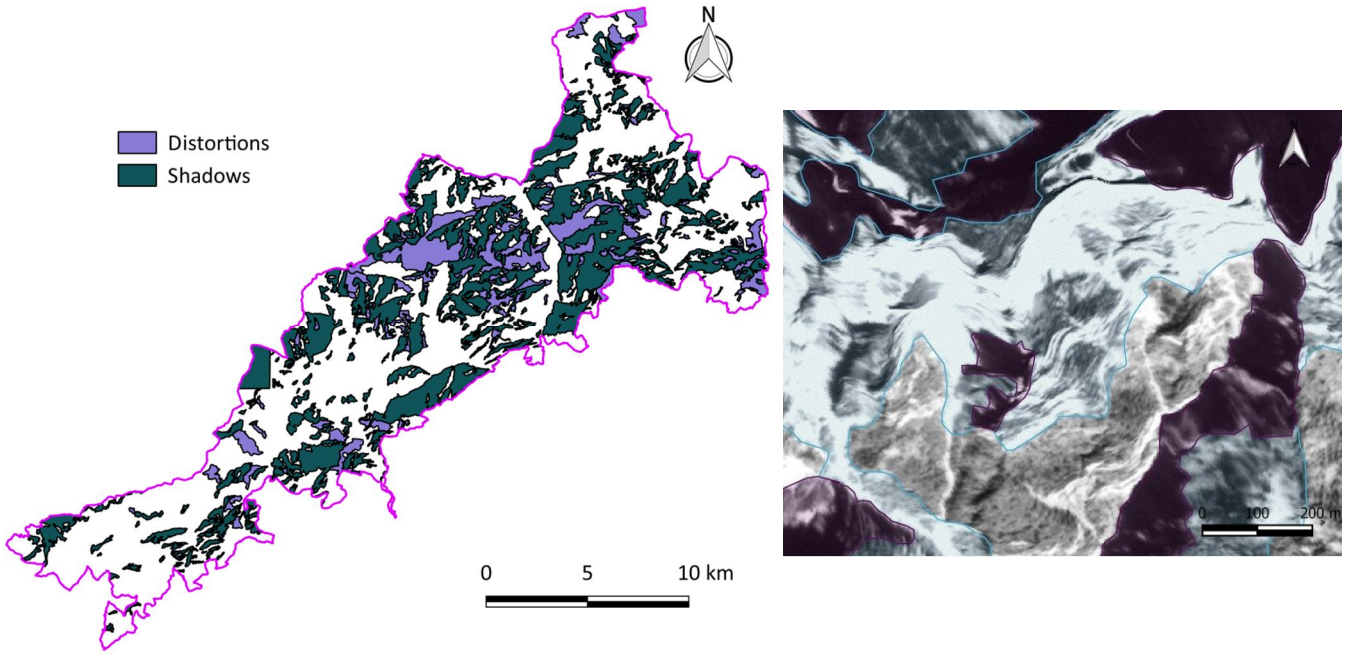

Figure 22: a)Distortions and shadows map based on GAI 1954 images; b)example of an area showing distortions (outlined in blue) and shadows (in purple)

In addition to the classification problems encountered due to the tonal and radiometric characteristics of the images, it is likely that the initial grassland extent for 1954 was underestimated mainly due to the presence of shadows and distortions, as shown in Figure 22. As it can be observed in Table 9, shadows alone occupy almost one third of the study area, so the mapped grassland areas probably represent a conservative estimate of the grassland areas present at that time.

Class	Class Area (ha)	% on total area
Distortions (D)	3313,52	10,69
Shadows (O)	9718,49	31,35

Table 9: percentage of non-classifiable areas in the 1954 aerial images

Grassland distribution maps and change detection results

The cross-validation of the TELAER images with the IUTI inventory yielded a classification accuracy of 86%, corresponding to 102 of the 119 points used for the assessment. These points were classified as “grassland and pastureland” (code 3.1), while of the remaining 17, 8 were assigned to “other wooded land” (3.2), 5 to “arable land” (2.1), 2 to “forest land” (1.1) and one each for settlement (4) and “other land” (6), respectively.

This relatively low classification accuracy, however, is most likely due to the limited sample of IUTI points that could be used, and, even more importantly, to the differences intrinsic in a point sampling compared to a wall-to-wall mapping. Most of the IUTI points classified as “other wooded land”, for example, fell on small sparse shrub or tree stands that were typically enclosed into larger grassland areas that according to the criteria used for the classification of the TELAER images, would have been correctly classified as grassland.

The grassland distribution maps for 1854 and 2012 are shown in Figure 23 a and b, respectively. Table 10 shows the areal extent of grassland habitats at the two times. Overall, about 1578 ha of grassland were lost over the 58-years period, corresponding to almost the 37% of the initial area.

As discussed above, these values do not represent the full extent of grassland habitats in either 1954 or in 2012. The figures for 1954 represent only those grasslands that were not hidden by

shadows or image distortions, while the ones for 2012 represent the grassland areas existing only in the areas visible in both images. This implies that some grassland areas that could be seen in the 2012 images were not included in the count, in order to ensure consistency in the assessment of grassland cover change, otherwise the magnitude of the process may be underestimated due to the greater amount of areas that can be interpreted for 2012.

The pixel-based change detection procedure of combining the two raster distribution maps yielded the change map shown in Figure 24, while Table 11 presents the main statistics of each change class.

	1954	**2012**
Mapped grassland (ha)	4296,35 ha	2717,89 ha
Percentage on total area	13,86 %	8,77 %
Decrease on total area	/	- 1578,45 ha (5,09%)
Decrease on initial grassland area	/	- 36,74 %

Table 10: loss of grassland areas between 1954 and 2012

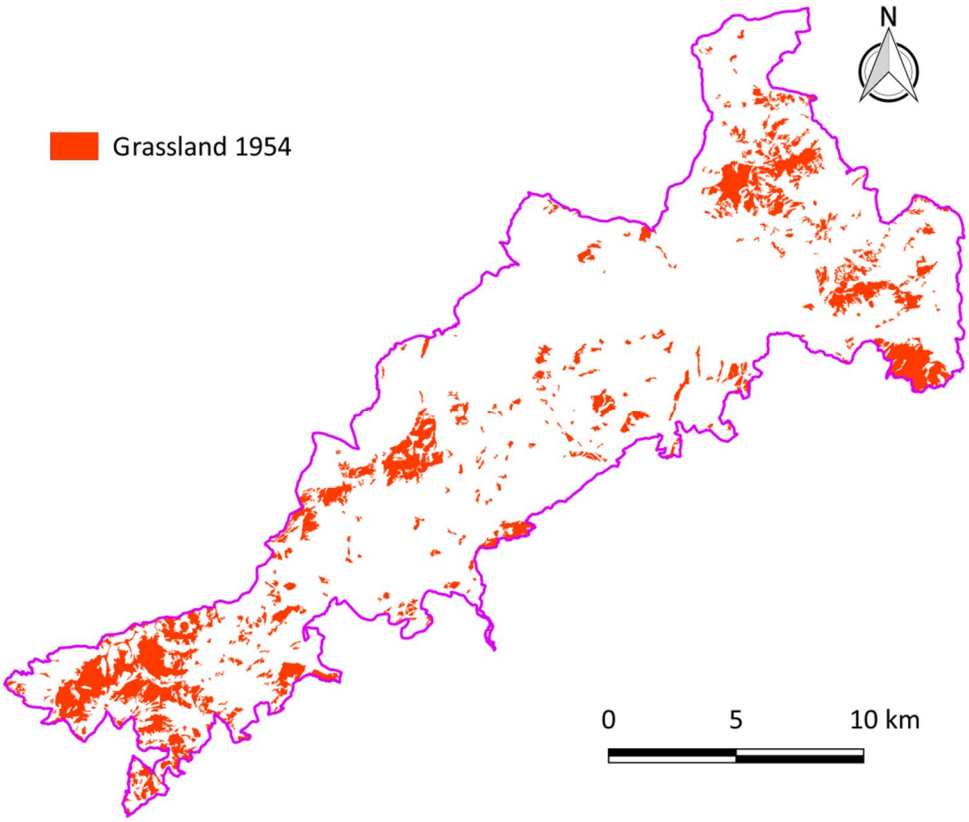

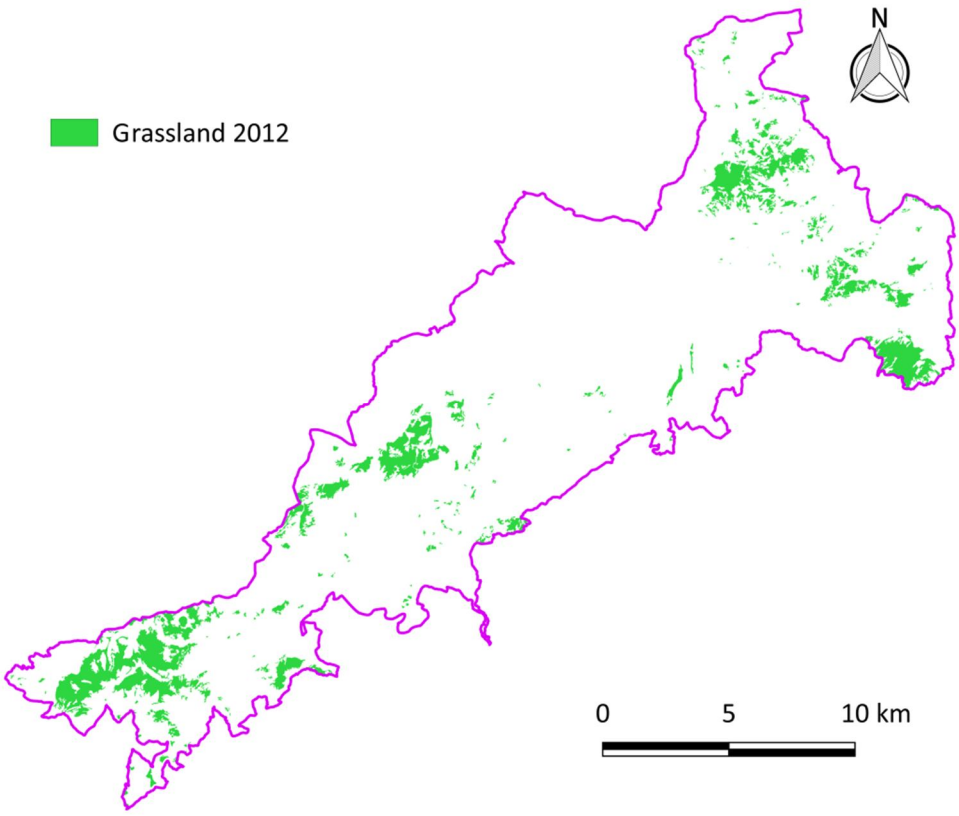

Figure 23: Distribution of mapped grassland areas for 1954 and 2012.

From the change detection results, it can be observed how the amount of grassland that was lost between the two dates is actually higher than what emerged from the simple subtraction of 2012 grassland area from 1954, 41,44% instead of 36,76%. This difference is due to a small amount of grassland increase registered for 2012 (4,71%). It is likely, however, that part of this figure may be caused by misregistration error or by small differences in the delineation of grassland polygons. Misregistration of the boundaries in the different classifications causes the presence of border pixels with false positive or negative changes. In vector format, this problem appears as narrow polygons, the so called “slivers”.

In any case, these results show that inside the Dolomiti Bellunesi National Park’s territory no quantitatively significant phenomenon of grassland expansion is underway, especially if compared to the amount that has been lost since 1954. This can justify the choice of using only the areas included into the original 1954 grassland extension as the basis for future change evaluations involving other time periods, as it has been demonstrated that the reforestation process are clearly prevalent.

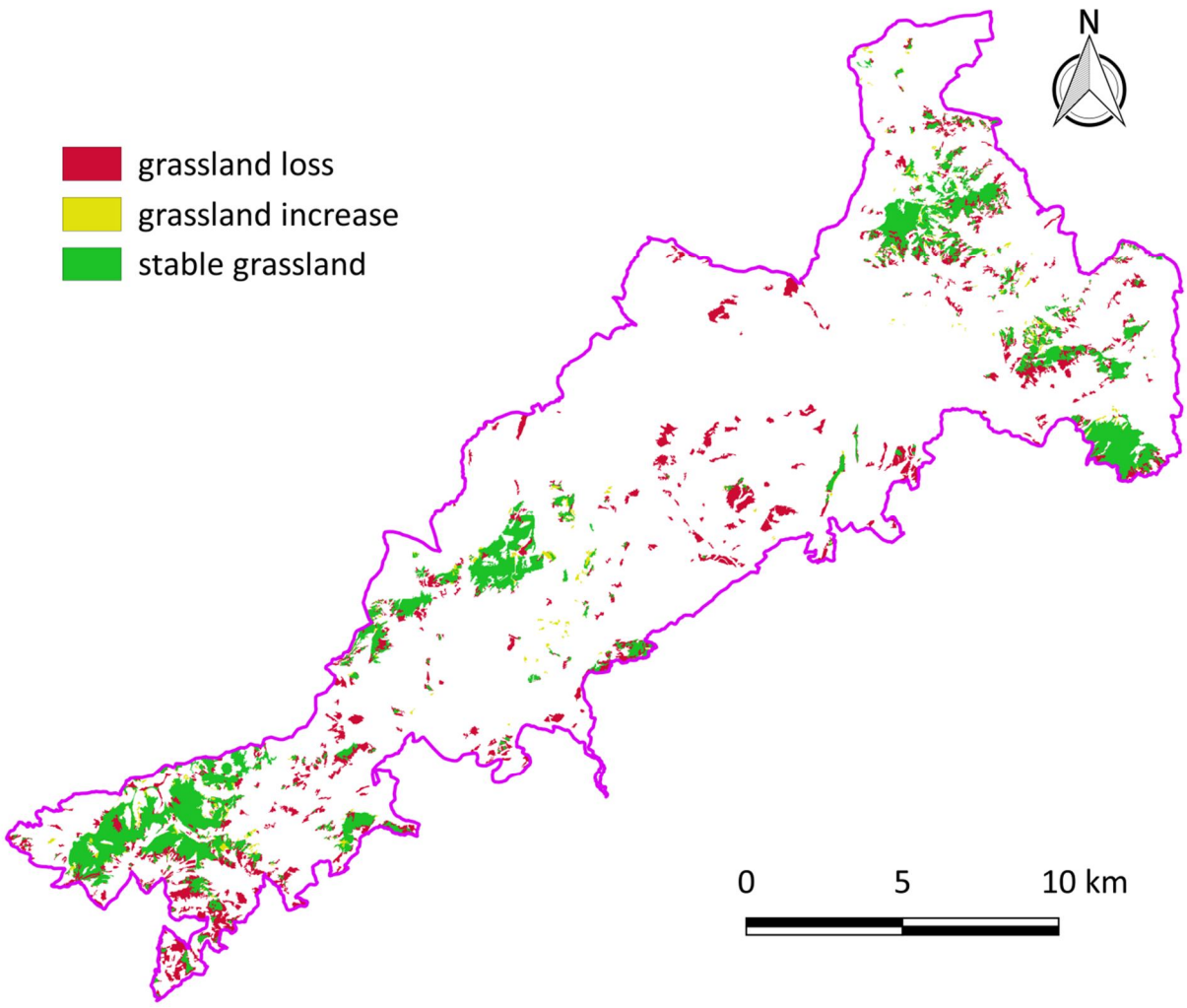

Figure 24: Grassland change map between 1954 and 2012

Change category (code)	Area (ha)	% on total area	% of variation on 1954 grassland
Unchanged – no grassland/not classified (0)	26501,60	85,49	/
Changed – grassland loss (1)	1780,29	5,74	- 41,44
Changed – grassland increase (2)	202,24	0,65	+ 4,71
Unchanged – grassland (3)	2515,71	8,12	58,55

Table 11: post-classification change detection results

Grassland decrease by altitudinal range

From the stratification and comparison of the reclassified DEM and the raster maps of grassland distribution and grassland change, it was possible to derive more specific information about the grassland dynamics within the study area and their distribution according to altitudinal bands (the areas that were not grassland in both of the two dates were not considered).

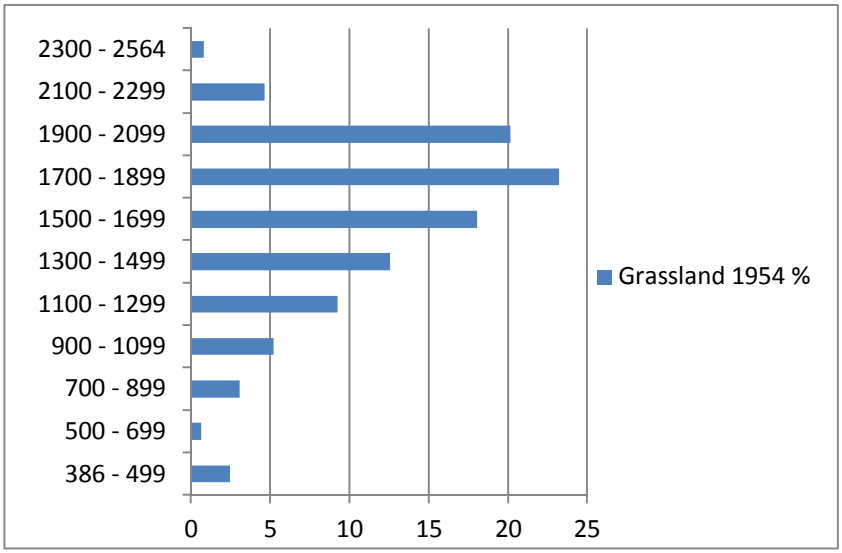

Figure 25: percentage of grassland areas present in each altitudinal band in 1954

Figure 25 shows the way grassland was distributed between altitudinal bands in 1954, expressed in percentage on total 1954 grassland area. It can be observed how the majority of grassland areas are included in the altitudinal band between 1500 and 2100 m. This can be compared with Figure 26, which shows the percentage of increased, unchanged and lost grassland by altitudinal band, calculated on the total area of each change class.

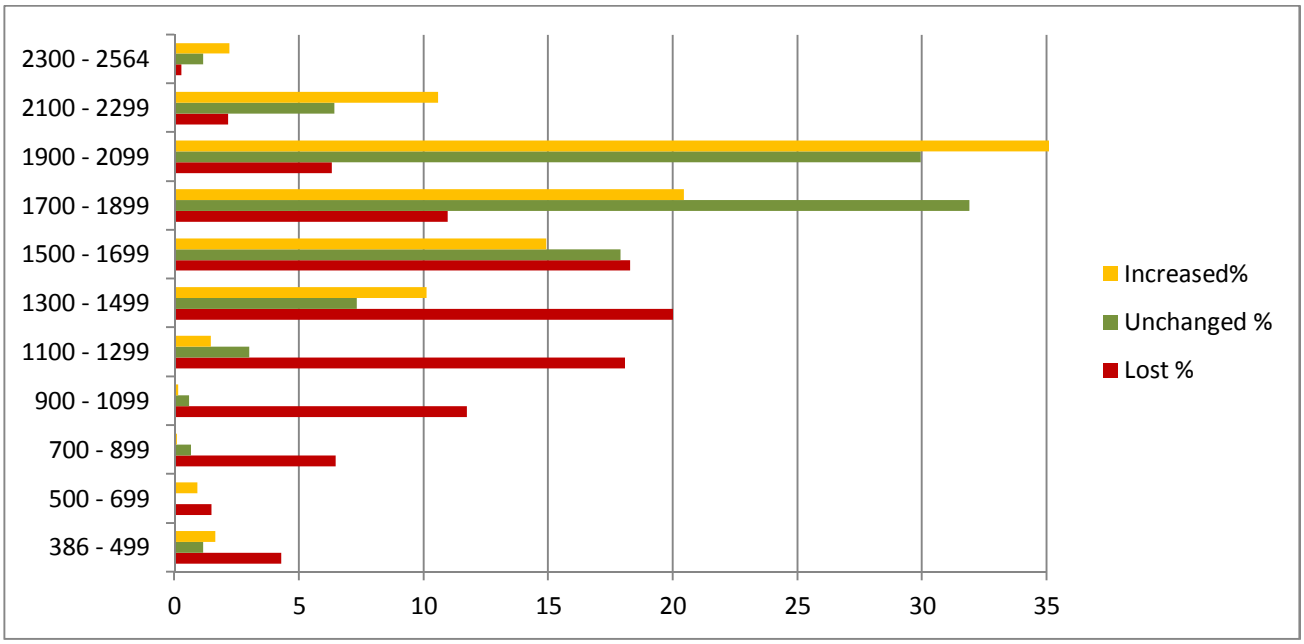

Figure 26: Percentage of increased, unchanged and lost grassland by altitudinal band, calculated on the total area of that class (x axis shows values between 0 and 35 %).

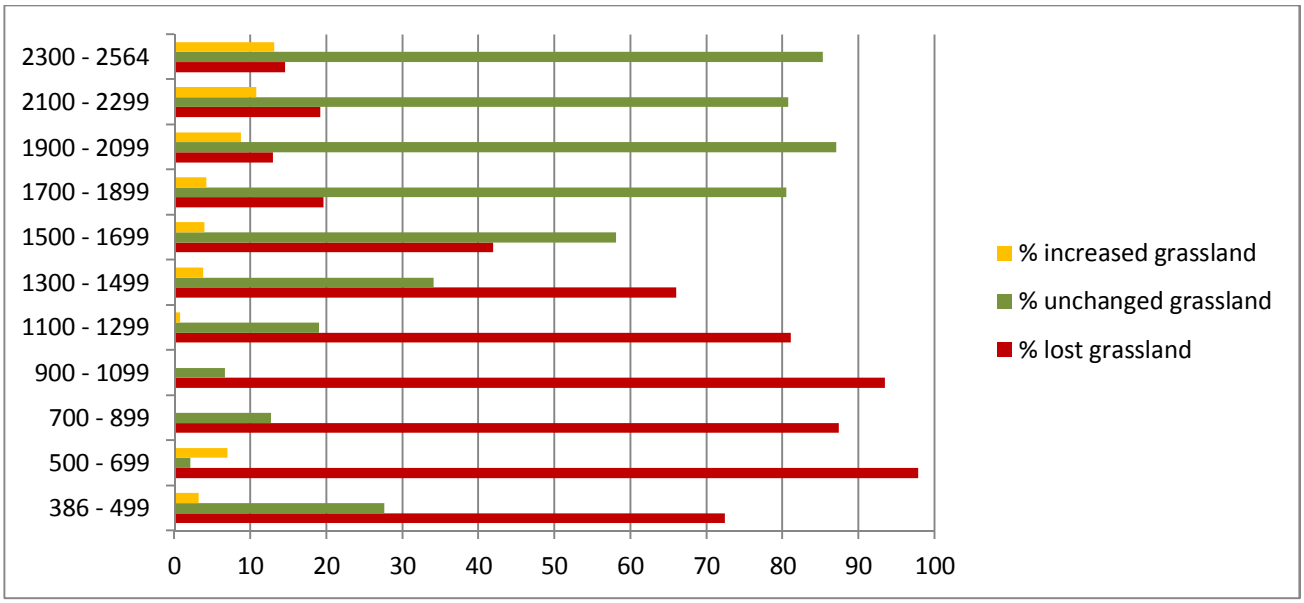

Figure 27: Percentage of increased, unchanged and lost grassland by altitudinal band. Each bar represents the absolute percentage of increase, loss or stability calculated on the initial grassland area, so the three bars do not add up to 100 (x axis shows values between 0 and 100 %).

If the percentage is calculated relatively to the grassland area initially present in each altitudinal band, however (Figure 27), it becomes clearer how the grassland loss dynamics is prevalent on the lower altitudinal bands up to 1500 m, where the forest expansion process led to the disappearance of over the 70% of grasslands. Only the 386-500 elevation band shows a slightly lower loss, with the preservation of a greater amount of grassland areas. This is probably related to the fact that these areas are typically close to the Park's boundaries and to settlements, so they are still managed to some extent.

Conversely, stable grasslands with lower rates of loss are typical of higher altitudes, where natural grassland above the tree line is prevalent (1700-2500). Even in this case, however, the percentage of grassland loss is significant, between 10 and 20%. 1700 m a.s.l. represents the average altitude of the treeline. As is common to most mountain regions, the treeline has been artificially lowered by centuries of anthropic disturbance, therefore it is very likely that the reforestation process has been taking place in the areas above it as well, as observed in similar studies, for example by Gellrich et al. (2007). Moreover, some studies show how the influence of climate change is likely to be contributing to the upward shift of the natural tree line as well, especially due to the expansion of alpine shrub species such as dwarf mountain pine (Dirnböck, Dullinger, & Grabherr, 2003). On the whole, the percentage of grassland present in 1954 above 1700 m was almost 49% of the total grassland area, corresponding to an extent of 2098 ha. Of this, 351 ha, about 17%, had been lost in 2012.

Finally, grassland expansion is a very marginal phenomenon in most cases, and as discussed previously it is likely that a significant part of this perceived increase is due to difference in the delineation of grassland polygons and to residual misregistration. The increase of grassland areas appears more marked at high altitudes (2100-2500 m), where it is higher than 10%. A possible explanation for this is, once again, related to the difference in resolution between the two images: high altitude zones are dominated by areas with sparse grassland interspersed with bare rock, and these two land cover types appear almost identical to each other in the 1954 images, which may have led to an underestimation of the grassland present. The higher radiometric and spatial resolution of the 2012 images allows for a more accurate delineation of the grasslands present in this zones, as previously shown in Figure 21.

6.2 Satellite data

NDVI and EVI time series for 2005

The biggest challenge in obtaining VI time-series from Landsat images is the collection of a cloud-free database covering key dates and seasons throughout the vegetative phase. As it has been shown in this case, it was possible to find enough cloud-free images to cover most of the vegetative season only for one year. Generally, however, the number of dates used for creating VI series is much higher, in order to have a better representation of phenological profiles. By using only 5 images, the resulting profiles were inevitably very coarse, but sufficient to broadly characterize the behaviour of the land cover classes of interest. It is common to create or integrate NDVI time series from other satellite sensors, typically MODIS, which has a higher temporal resolution and therefore provides a greater amount of usable data. The drawback of using MODIS data is the coarse spatial resolution, which was not considered suitable to the scale of this study area and to the fragmentation of the landscape, especially when focusing on grassland areas.

It should also be noted that factors such as climatic variability between years, slope aspect, soil depth and soil capacity of retaining moisture influence the beginning, end, and overall length of the vegetative season, so in order to draw more definitive conclusions about seasonal phenological profiles it would be necessary to compare VI time series across several years and obtain average values. In any case the creation of a VI time series, through showing the approximate period when the vegetative peaks of each land cover type of interest occur, is an essential tool to estimate the most suitable period for classification, and in this case it was used, together with the results of the classification scenarios, for choosing the two images for the change detection procedure. only one or few images are available.

Figure 28 shows the mean NDVI and EVI values obtained by averaging the mean values calculated for each ROI, divided by class and by date. Although the two graphs are not directly comparable, because the range of NDVI and EVI values are very different, NDVI values for all the vegetation classes (Grassland, Shrubs, Conifers and Broadland) are relatively close to each other, with a clear distinction only for the “Bare” class. EVI values, on the contrary, appear to be more spread out within their range, with the exception for the October image. In both cases, however, the average maximum and minimum vegetation peaks (calculated averaging the maximum and minimum values for each date) occur in the July and October image, respectively (see Appendix C). In-

dividual classes show essentially the same trend, with the only exception of the class "Broadleaved", that has higher NDVI and EVI values in the June image. It can also be observed how the Broadleaved and Conifer classes show a very similar profile in the NDVI image, with relatively stable mean NDVI values from June to August, while their EVI values show a different behavior. All the other classes, most notably Grassland show a marked peak in July, followed by a constant decline during the rest of the vegetative season.

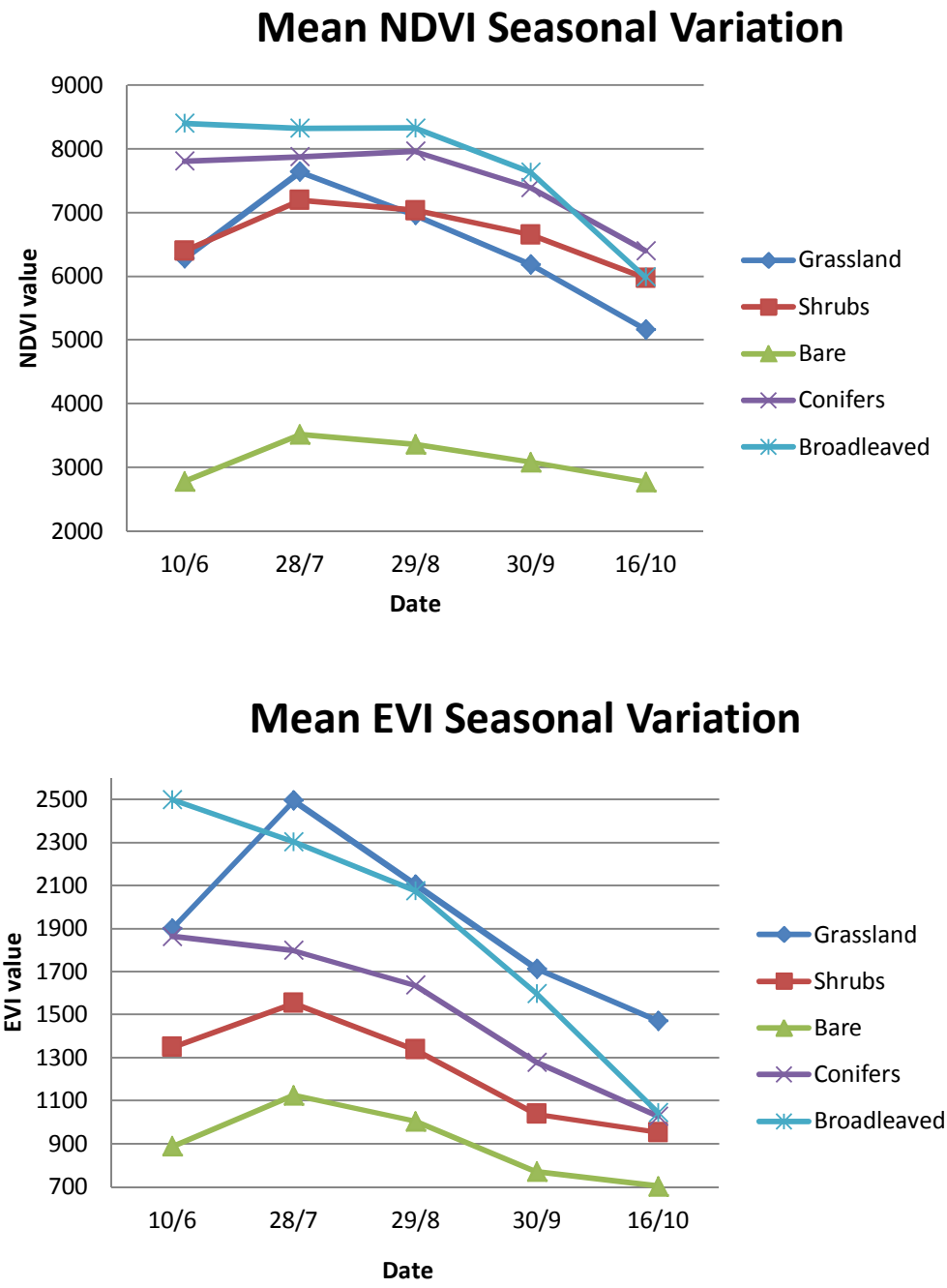

Figure 28: mean NDVI and EVI values for each land cover class, showing the seasonal variation. The values on the x axis represent each the 5 dates used.

Mean values, however, do not give a full picture of the behaviour of the land cover classes in respect to NDVI and EVI values. Figure 29 A-E show the average minimum and maximum values calculated for each date on a per-class basis, which can be compared with the mean NDVI values already shown in Figure 28, now showing also the standard deviation. In many cases, mean NDVI values display a considerable range of variation that causes the classes not to be easily separable according to their mean value. If the range between minimum and maximum mean values is considered as well, class variability becomes even higher, making the definition of NDVI intervals for the separation of vegetation classes even more difficult in practice. The only class that appears clearly separated from the other is, predictably, Bare soil, but even in this case a significant variability can be observed within each date, most likely due to the presence of sparse vegetation. However it should be noticed how in some cases, most notably in the July image, the distance between average maximum and minimum values (and therefore the standard deviation of the mean) is smaller than in others, so it can be speculated that the July image may be better for discriminating between land cover classes because of the smaller within-class variability.

On the contrary, the minimum-maximum range for EVI values is remarkably close to the interval of variability of EVI mean (Figure 30 A-E), and the standard deviation values are lower than NDVI, showing less within-class variability. Similarly to NDVI, however, EVI values for most land cover classes display the narrowest range between maximum and minimum values for the July image, as can be noticed observing Figure 29A and Figure 30A.

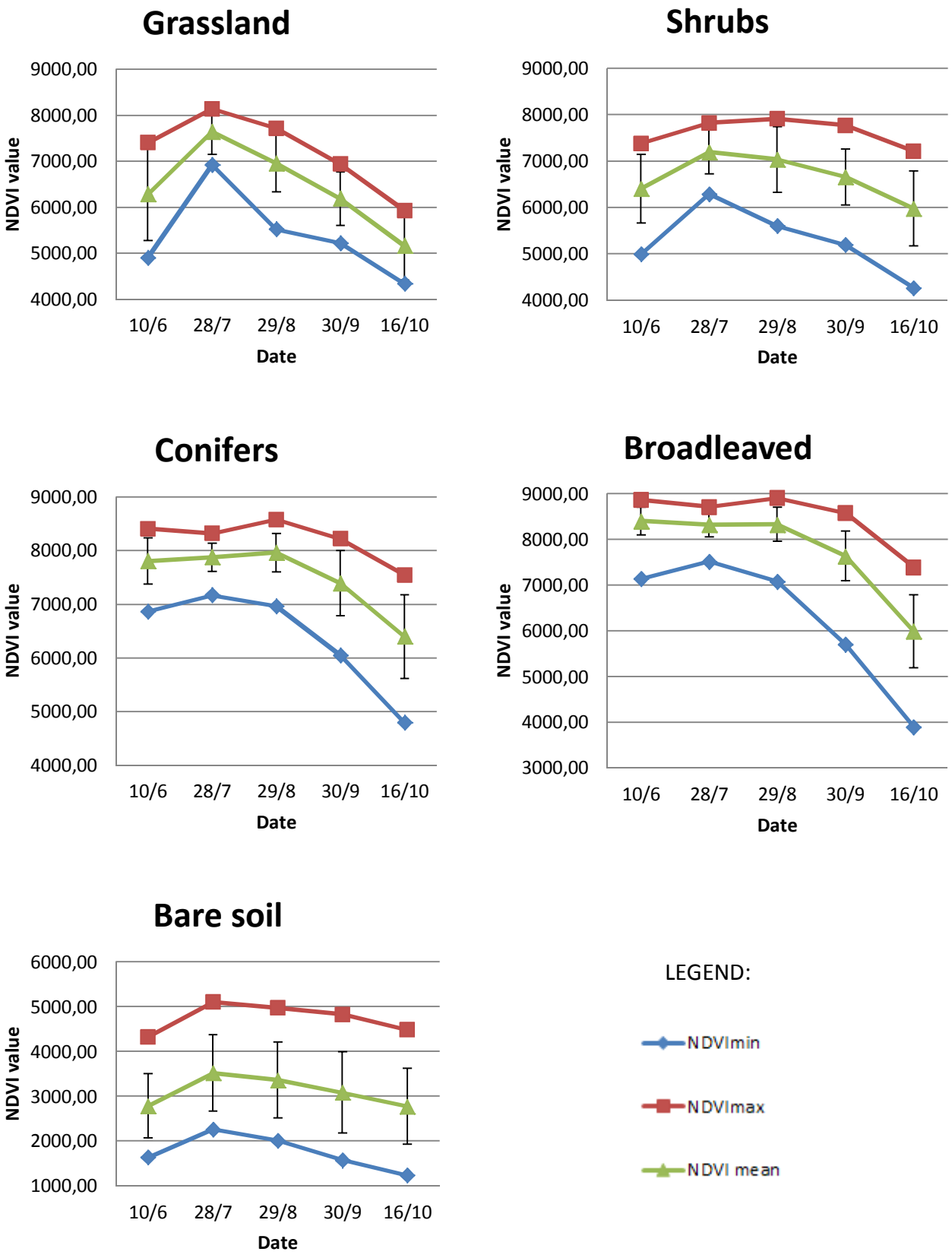

Figure 29 A-E: for each land cover class, the average minimum and maximum NDVI values are shown, as well as the mean NDVI with its standard deviation. Y axis value range varies between the images.

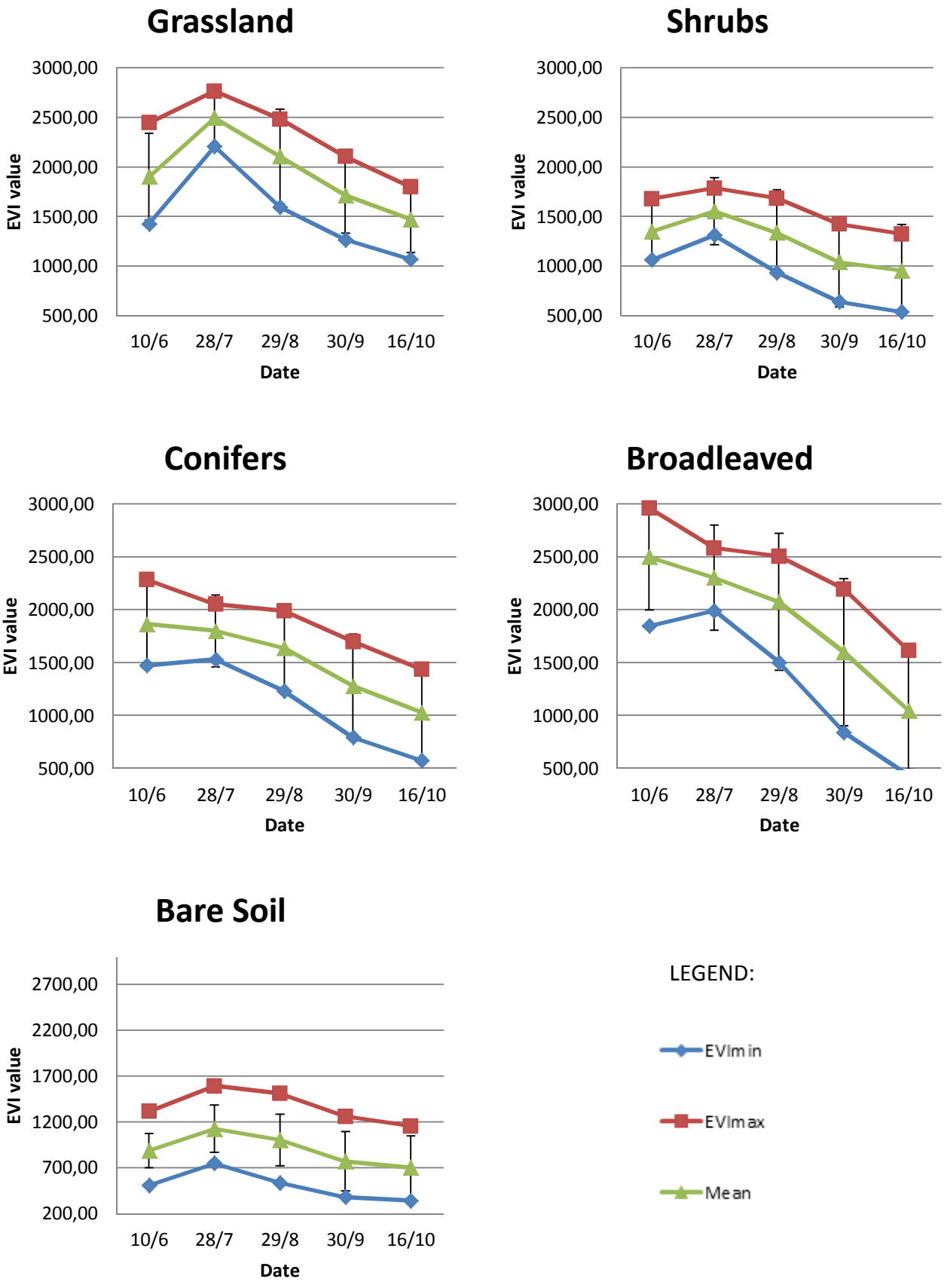

Figure 30 A-E: for each land cover class, the average minimum and maximum EVI values are shown, as well as the mean EVI with its standard deviation. Y axis value range is 500-3000 for all land cover classes except Bare soil (200-3000).

Results of classification scenarios

Based on the VI time series and on the results of the individual classifications of each 2005 Landsat scene, different classification scenarios were investigated.

			ACCURACY									
			GRASSLAND		SHRUBS		BARE SOIL		FOREST		Overall	Kappa
	Date		PA	UA	PA	UA	PA	UA	PA	UA		
1	2005/06/10	U	60,71	50,30	56,28	43,28	53,33	35,96	77,45	93,05	70,20	0,50
		C	62,86	50,00	55,74	44,93	58,33	38,46	77,89	93,25	**70,96**	**0,51**
		D	*2,14*	*-0,30*	*-0,55*	*1,66*	*5,00*	*2,51*	*0,45*	*0,20*	*0,76*	*0,01*
2	2005/07/28	U	62,86	65,67	47,54	33,59	60,00	25,17	70,77	91,55	65,09	0,44
		C	**63,57**	**70,08**	44,26	38,57	75,00	27,44	75,96	92,09	68,78	0,48
		D	*0,71*	*4,41*	*-3,28*	*4,98*	*15,00*	*2,26*	*5,19*	*0,53*	*3,69*	*0,05*
3	2005/08/29	U	58,57	54,30	57,92	31,45	48,33	28,71	65,28	94,02	62,16	0,41
		C	60,71	52,80	58,47	34,74	56,67	30,63	68,25	96,44	64,90	0,45
		D	*2,14*	*-1,51*	*0,55*	*3,29*	*8,33*	*1,92*	*2,97*	*2,42*	*2,74*	*0,04*
4	2005/09/30	U	58,57	52,90	60,11	25,52	35,00	24,42	51,86	90,89	53,22	0,31
		C	63,57	39,21	8,74	23,53	45,00	26,47	77,41	79,06	61,84	0,32
		D	*5,00*	*-13,70*	*-51,37*	*-1,99*	*10,00*	*2,05*	*25,56*	*-11,83*	*8,62*	*0,01*
5	2005/10/16	U	65,00	56,52	51,91	25,75	35,00	28,00	55,79	83,19	55,16	0,30
		C	65,00	68,42	54,10	25,32	35,00	25,93	56,68	84,51	56,10	0,32
		D	*0,00*	*11,90*	*2,19*	*-0,43*	*0,00*	*-2,07*	*0,89*	*1,33*	*0,95*	*0,01*
6	**Landsat - Dates 2 - 5**		**64,29**	**76,27**	42,62	40,41	75,00	27,78	79,08	91,27	**70,58**	**0,50**
7	**NDVI - All dates**		60,71	51,52	50,82	42,86	88,33	36,05	74,48	95,08	69,35	0,50
8	**NDVI - Dates 2 - 5**		46,43	26,42	37,70	43,13	88,33	33,76	67,06	91,50	60,45	0,38
9	**EVI - All dates**		58,57	58,99	27,32	37,31	86,67	28,73	79,67	89,05	68,21	0,46
10	**EVI - Dates 2 -5**		52,14	23,93	30,60	29,63	85,00	24,06	39,61	76,07	42,29	0,18
11	**Date 2, NDVI, EVI**		**62,86**	**75,86**	50,27	39,15	85,00	32,08	76,11	93,78	**70,39**	**0,51**
12	**Date 2, NDVI**		**63,57**	**72,95**	48,63	43,41	86,67	32,10	79,23	94,01	**72,28**	**0,54**

Table 12: Producer's Accuracy (PA) and User's Accuracy (UA) for each land cover class, calculated for each classification scenario. For individual images (1-5), the classification was performed on the original uncorrected (U) and topographically corrected (C) bands, and the Difference (D = C - U) is shown. The table also shows the overall accuracy and Kappa coefficient for each classification.

Table 12 shows the accuracy assessment results for each Classification scenario. Single-date classification (1-5) are obtained by classifying a single Landsat scene (bands 1-5 and 7), and were

run twice, the first time on the original image not corrected for topographic effects, and the second time on the topographically corrected image. Classification 6 was created by stacking the July and October scenes (topographically corrected) and performing the classification on the 12 bands thus obtained. Classifications 7-10 are based solely on VIs, while Classifications 11-12 are based on the combination of the July image (topographically corrected) and VIs. In the case of classifications using two dates of imagery, the July and October images were used because they represent the vegetative maximum and minimum. Complete data for each classification are reported in Appendix C.

The results obtained from the classifications are not always easy to interpret, since they vary depending on the specific accuracy metric taken into account and often do not seem to follow a specific pattern. Differences in the average values of accuracy metrics between the original and corrected images are also shown (calculated as the difference between corrected – uncorrected), to help evaluating the performance of the topographic correction routine.

As for overall accuracy, if the traditional threshold of 85% is considered as the minimum level of overall accuracy for evaluating the classifier's performance, then none of the classifications can be considered satisfactory, given how the highest value (obtained for Classification 12) only reaches 72%. In general, however, it can be observed how using stacks of VIs (Classifications 7 and 9), stacked Landsat bands (Classifications 6) or combinations of one Landsat scene with VIs (Classifications 11 and 12) gives better results than single date classifications both in terms of overall accuracy and of Kappa value.

In the case of the Grassland class, which is the main focus of interest, Classification 6 gives the best results both in terms of PA and UA, followed by Classifications 11 and 12. High PA values are not necessarily significant, as they may mean simply that the classifier overestimated the extent of grassland areas, so it is important to have accompanying high UA values as well. Of the single band classifications, only the July image gives good results, that seem to have been further improved by topographic correction.

As for the other classes, Shrubs and Bare soil are the most problematic, and in generally they exhibit very low accuracies. High PA values are likely to be the result of overestimation, considering how they are always accompanied by poor UA values. A look at the error matrices (Appendix C) shows a lot of confusion in the assignation of the Shrubs land cover class, which is often misclassified as Bare soil or Forest, suggesting that the training ROIs used for this class are not adequate to properly characterize this class, or that a spectral-based classification technique is not suitable for

mapping this class. Conversely, the class Forest shows high accuracies for almost all the classifications, with UA values above 90% in the majority of cases. The error matrix for Classification 6 (July-October), the most accurate one, is shown in Table 13:

	REFERENCE				
CLASSIFICATION	**Grassland**	**Shrubs**	**Bare**	**Forest**	**Total**
Grassland	**90**	14	0	14	**118**
Shrubs	8	**78**	8	99	**193**
Bare	38	51	**45**	28	**162**
Forest	4	40	7	**533**	**584**
Total	**140**	**183**	**60**	**674**	**1057**

Table 13: error matrix for Classification 6 (July-October)

A consideration of a different nature concerning classification accuracy is related to the reference data used. The IUTI inventory is based on point sampling, but in order to be able to carry out the accuracy assessment procedure, the original point was transformed into a 30 x 30 m pixel; this implies the possibility of introducing a source of error, especially in fragmented areas or at the boundary between different land cover types.

Concerning the evaluation of the best period for classification when no multi-season images are available, the results seem to indicate that the end of July (Date 2) can give the best results both in terms of overall accuracy and for the identification of grassland areas, and that the classification is significantly improved by adding both NDVI and EVI (or alternatively, just NDVI) to the Landsat bands used for the classification. Topographic correction prior to classification has a positive effect on classification accuracy as well. The addition of VIs to the Landsat image bands improves grassland classification accuracy only marginally, but in general it has a positive effect on each class' accuracy, leading to a higher overall accuracy (+3,5%) and especially to an improvement of the classification of the "problematic" classes Shrubs and Bare soil.

	GRASSLAND			
CLASSIFICATION	PA	UA	Percentage %	Area (ha)
2012 Grassland	100,00	86,00	7,67	2381,13
July-October	64,29	76,27	11,31	3039,66
July+NDVI	63,57	72,95	12,06	3244,05
July+NDVI+EVI	62,86	75,86	11,33	3046,05
July	63,57	70,08	12,19	3278,52

Table 14: Percentage and area of grassland habitats as mapped by the semi-automated classifiers and by the manual classification

Table 14 shows the extent of grassland areas mapped by the four classification with the highest accuracy in respect to this class, and the extent of grassland calculated from the manual classification performed on the TELAER 2012 images. The values shown here for 2012 represent the full mapped extent, (including the areas previously excluded because they corresponded to unclassifiable areas in 1954), but masked for clouds like the 2005 Landsat images in order to be comparable with the latter. The percentages show that, despite the efforts in improving classification accuracy, the classifier still significantly overestimates grassland areas.

Moreover, the classification results showed a lot of noise, resulting in a salt-and-pepper effect. To try to reduce this effect, the raster resulting from the July-October classification was filtered to eliminate the small areas (1 or 2 pixels wide) that are most likely the result of misclassification. This was accomplished using the utility gdal_sieve, which allows to filter out small clusters of pixel by using four (diagonal pixels are not considered directly connected) or eight (diagonal pixels are considered directly connected) connectedness to determine polygons. It is also possible to set a threshold value which defines the minimum number of pixels a cluster must have to be preserved, otherwise it will be merged with the neighboring clusters. Several trials were made by using four and eight connectedness and 2, 3 and 4 pixels as a threshold, respectively. Using 4 connectedness yielded better results than eight, and the results of the accuracy assessment conducted on each of the three filtered classifications are presented in Table 15.

	2 pixels threshold	3 pixels threshold	4 pixels threshold
Overall accuracy [%]	**72,19**	**73,04**	**73,04**
Overall Kappa	**0,53**	**0,54**	**0,54**
Grassland PA	63,57	63,57	62,14
Grassland UA	78,07	77,39	76,32
Shrubs PA	45,36	44,81	45,36
Shrubs UA	42,78	44,57	45,11
Bare Soil PA	78,33	81,67	80,00
Bare Soil UA	30,13	31,82	31,79
Forest PA	80,71	81,90	82,20
Forest UA	91,74	91,39	91,12

Table 15: accuracy assessment results of 4x4 filtered classifications (PA: Producer's Accuracy; UA: User's Accuracy).

"Cleaning" the raster did bring some improvements, especially in terms of overall accuracy and overall kappa (70,58% and 0,50 respectively in the original classification). The filtering using a

2 pixel threshold also showed the best results in improving grassland's UA (76,27% in the original classification.

Figure 31 shows the full classification obtained from the stack of July and October Landsat bands before and after the application of a 4x4 sieve with 2 pixel threshold, while in Figure 32 only the grassland areas are shown for both, and the 2012 grassland areas superimposed to them in order to give an idea of the amount of misclassification from the automated classifier. The red areas correspond to the pixels classified as grassland by the semi-automated classification but not by the photointerpreter, while the green areas are those classified as grassland by both.

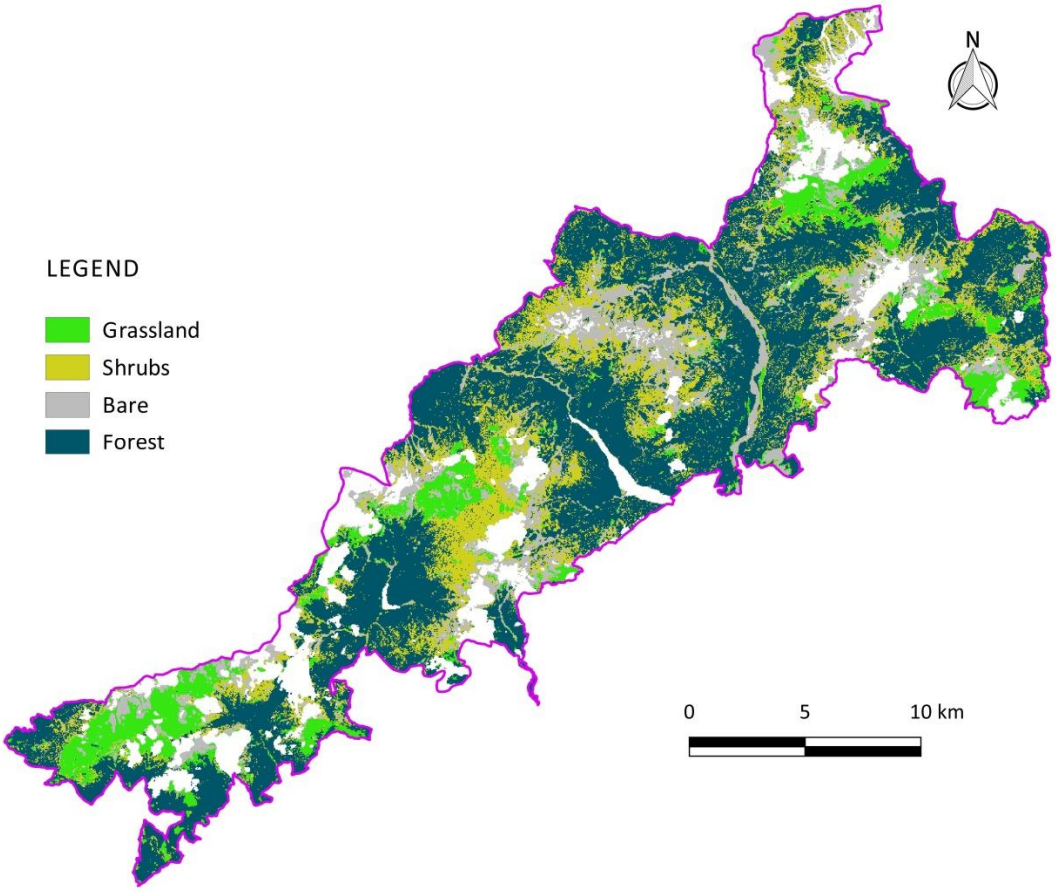

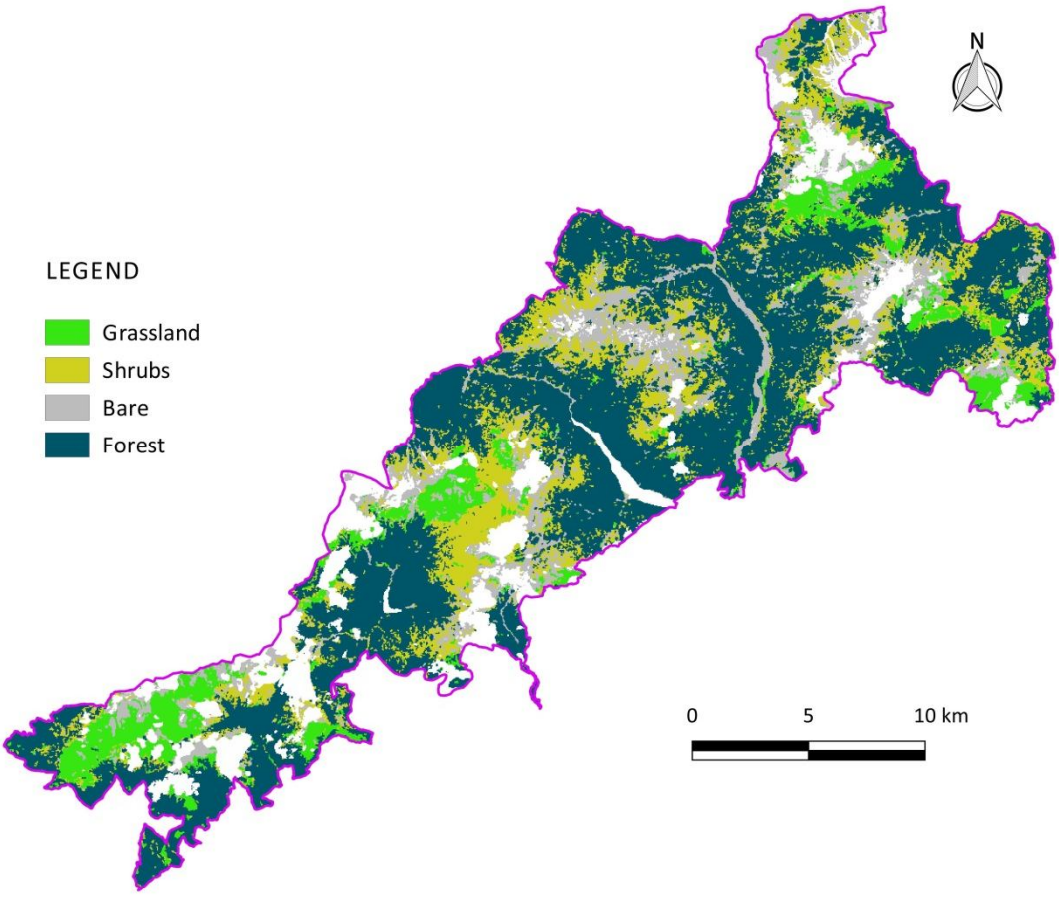

Figure 31: Land cover classification obtained from Classification 6 (July and October Landsat images)

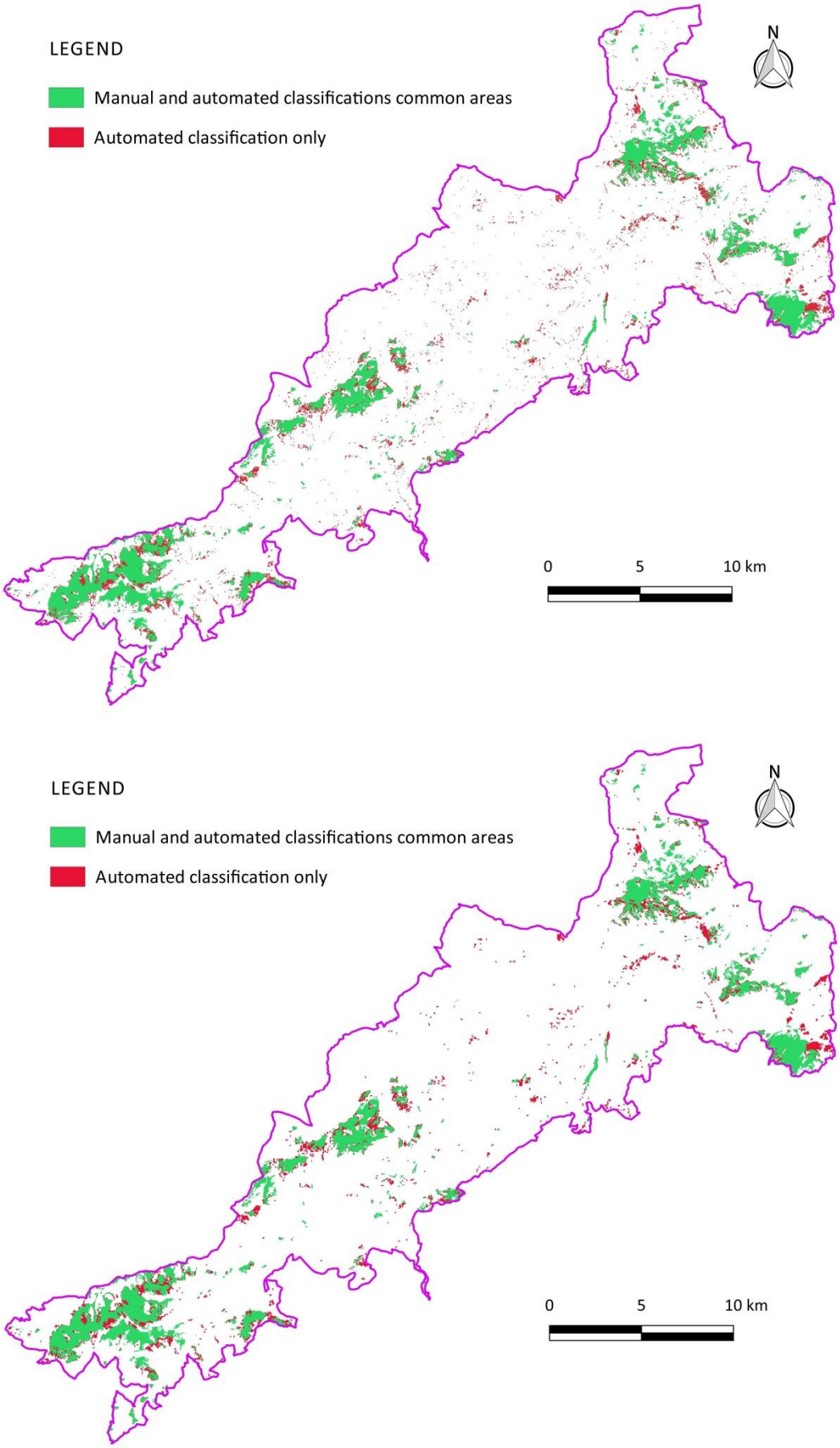

Figure 32: comparison between grassland areas mapped by the July-October classification and by manual photointerpretation.

Effect of topographic correction

An example of the images resulting from the Minnaert topographic correction is shown in Figure 33. The first image shows a part of the uncorrected July scene, while the second image the topographically corrected area from the same date. This can be further compared to the third image, taken from the corrected October scene. The images are shown in false color composite (RGB bands 4-3-2) for easier visual interpretation, because the effect of topographic correction appears more evident in near- and middle-IR bands. It can be observed how in the July image the Minnaert algorithm achieved a good topographic correction effect (at least visually), that appears as a "flattening" of the relief. In general, only the most deeply shadowed areas that exhibited almost no reflectance were not improved by topographic correction, and some artifacts were introduced along the mountain ridges, corresponding to pixels in self-shadow being divided by zero. This is most likely due to the use of a single default k value, that doesn't take into account the variability of the terrain and of the land cover present in the image. Considering one single Minnaert constant value for the entire dataset is unrealistic, since the terrain is not uniform and thus reflects solar energy

differently. For a more accurate topographic correction, a specific k value for each band should be computed, and a separation between land cover types should be considered as well to further improve correction results. Successful applications of the Minnaert correction employed different k values based both on land cover types and on topographic slopes (Lu et al., 2008), but this requires a priori knowledge of the land-cover and increases the complexity and time required for image processing.

Another factor to consider is that semi-empirical methods such as the Minnaert correction and the other methods available in QGIS consider only direct solar irradiance, and it is also likely that more evident topographic effect due to the lower sun angle may contribute to the lower quality of the classification in the later images. The poor results of the Minnaert correction can be observed in the October image, which shows many uncorrected shadows and artifacts); and have been previously reported in the case of images taken when solar elevation angles are lower than 40◦ (Hantson & Chuvieco, 2011). The effects of poor topographic correction on classification accuracy, however, are harder to assess. Positive effects of topographic correction can be observed especially for the first three dates, while for the last two images there doesn't seem to be a recognizable pattern.

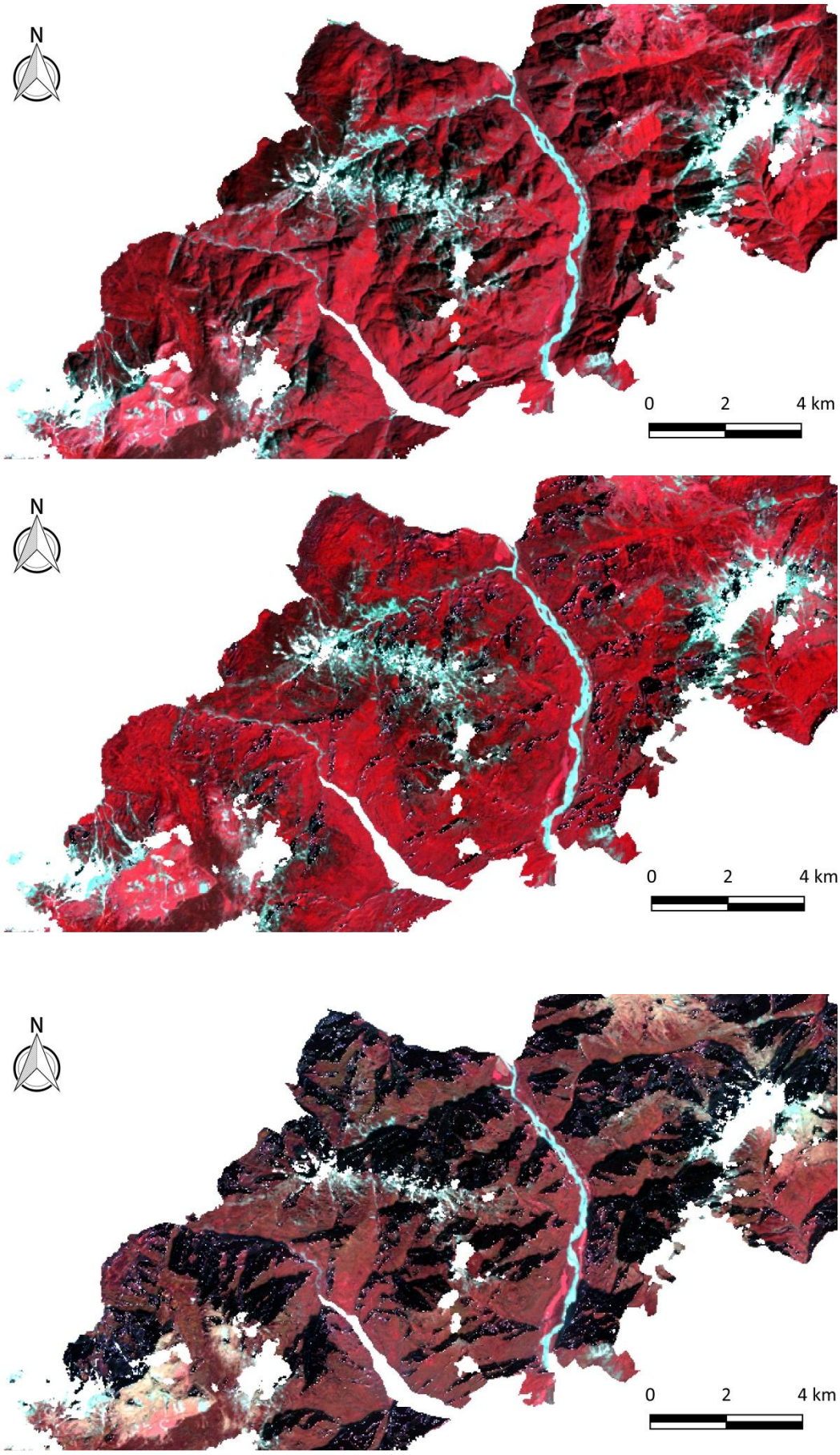

Figure 33: a portion of the study area shown for the July scene before (image a) and after (image b) the application of topographic correction. The topographically corrected October image is shown for comparison (image c).

NDVI image differencing change detection results

Figure 34 shows the histograms of the NDVI images for 1987 and 2007. As it can be observed, the 1987 has higher mean values compared to the 2007. The mean of the 1987 image is 7079, while the mean of the 2007 image is 6791. Through the histogram matching procedure, the 2007 histogram was "shifted" to match the 1987 one (Figure 34, bottom right).

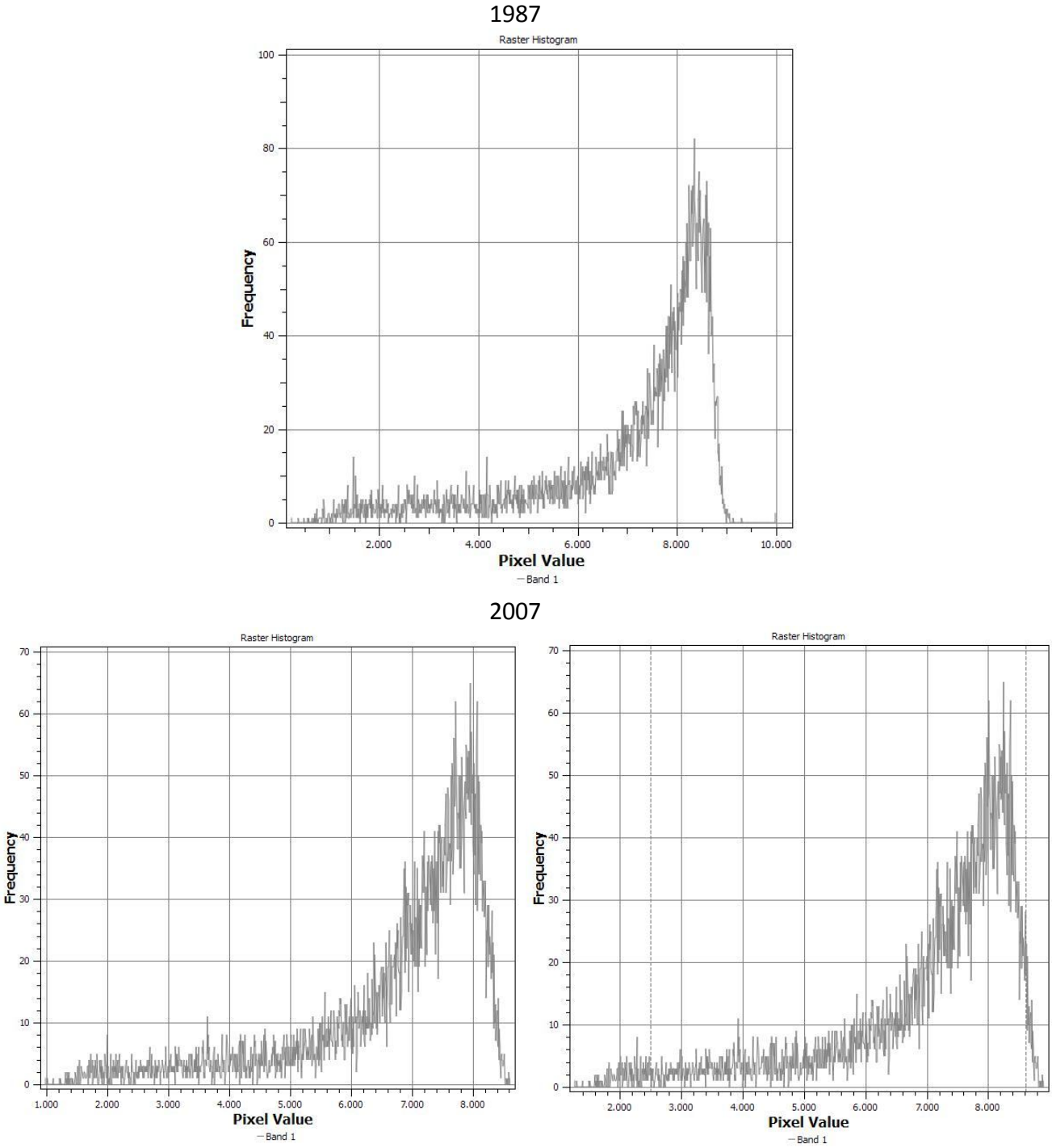

Figure 34: 1987 NDVI image histogram (top), 2007 NDVI image histogram before (left) and after (right) normalization

After the preprocessing phase, the 1987 NDVI image was subtracted from the 2007, to give the difference image. As expected, the resulting values are normally distributed.

The mean and standard deviation were calculated to obtain the threshold for classification, obtaining a value of 0 for the mean and of 777 for the standard deviation. By using a n value equal to 1, the distribution of values of the difference image were reclassified into three classes:

NDVI decrease ($\Delta NDVI < \mu - n \cdot \sigma$)	$\Delta NDVI < -777$
NDVI stability ($\mu - n \cdot \sigma < \Delta NDVI < \mu + n \cdot \sigma$)	$-776 < \Delta NDVI < 777$
NDVI increase ($\Delta NDVI > \mu + n \cdot \sigma$)	$\Delta NDVI > 778$

The reclassified image is shown in Figure 35.

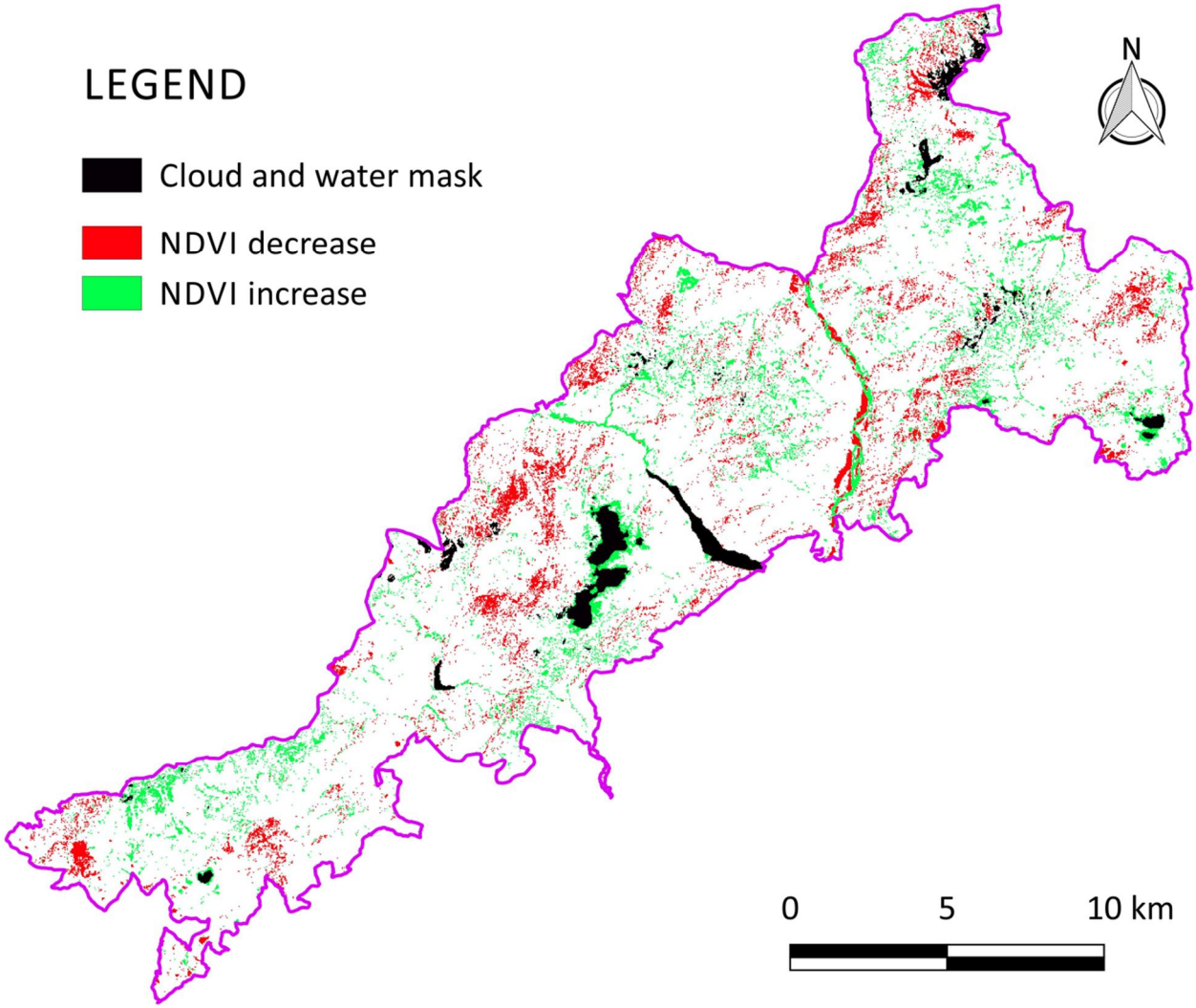

Figure 35: result of the reclassification procedure of the difference image, showing NDVI increase and decrease.

Contrarily to expectations, however, it was not possible to observe a clear correlation between the areas of NDVI increase and the areas of forest expansion. Shows a detail of the reclassified difference image with the 1954 polygons superimposed to it.

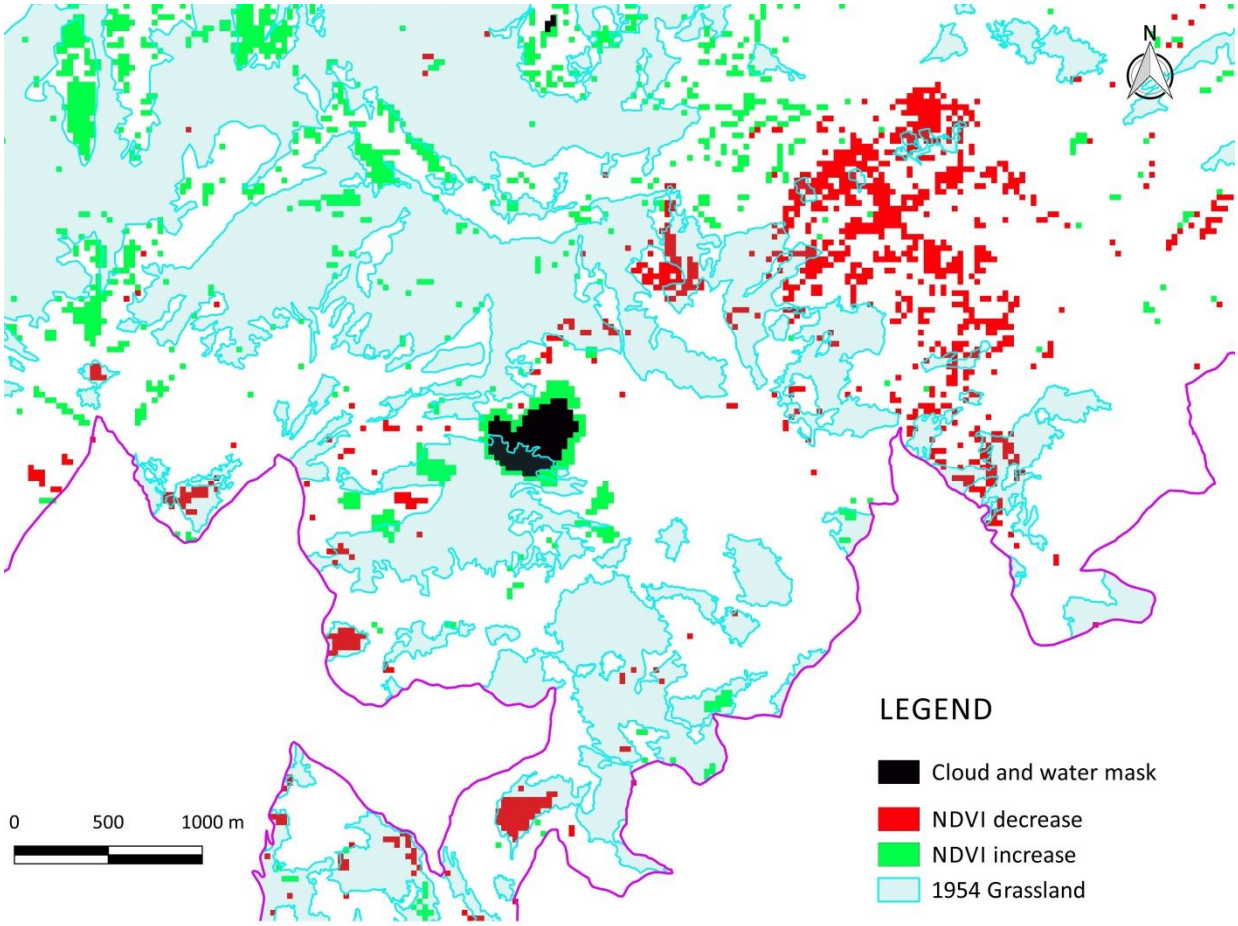

According to the anticipated results, it should be possible to observe a NDVI increase along the borders of the grassland polygons where forest expansion has been taking place, but in reality it is not so. This may be due to the fact that in 1987, when the oldest Landsat scene was taken, the reforestation process was already too advanced to be clearly observed at the spatial resolution of the Landsat images. Given how it was not possible to find any data source that could provide information on the grassland cover in the period between 1954 and the 1980s at the scale of interest, it is difficult to define the evolution of land cover, but it can be presumed that the greatest amount of change may have taken place in this period. A similar kind of fast recolonization dynamics following abandonment of grassland management has been reported in other studies (Garbarino & Pividori, 2006; Roura-Pascual et al., 2005; Urbinati et al., 2004).

An interesting consideration that can be made observing the difference image, however, is how a lot of the NDVI increase (and consequently of the vegetation increase) can be observed in the areas above the treeline (about 1700 m). This could suggest an increase related to the effects of climate change, which has been reported in several studies carried out in the alpine region. This was not the topic of this study, however, so the phenomenon has not been analyzed further.

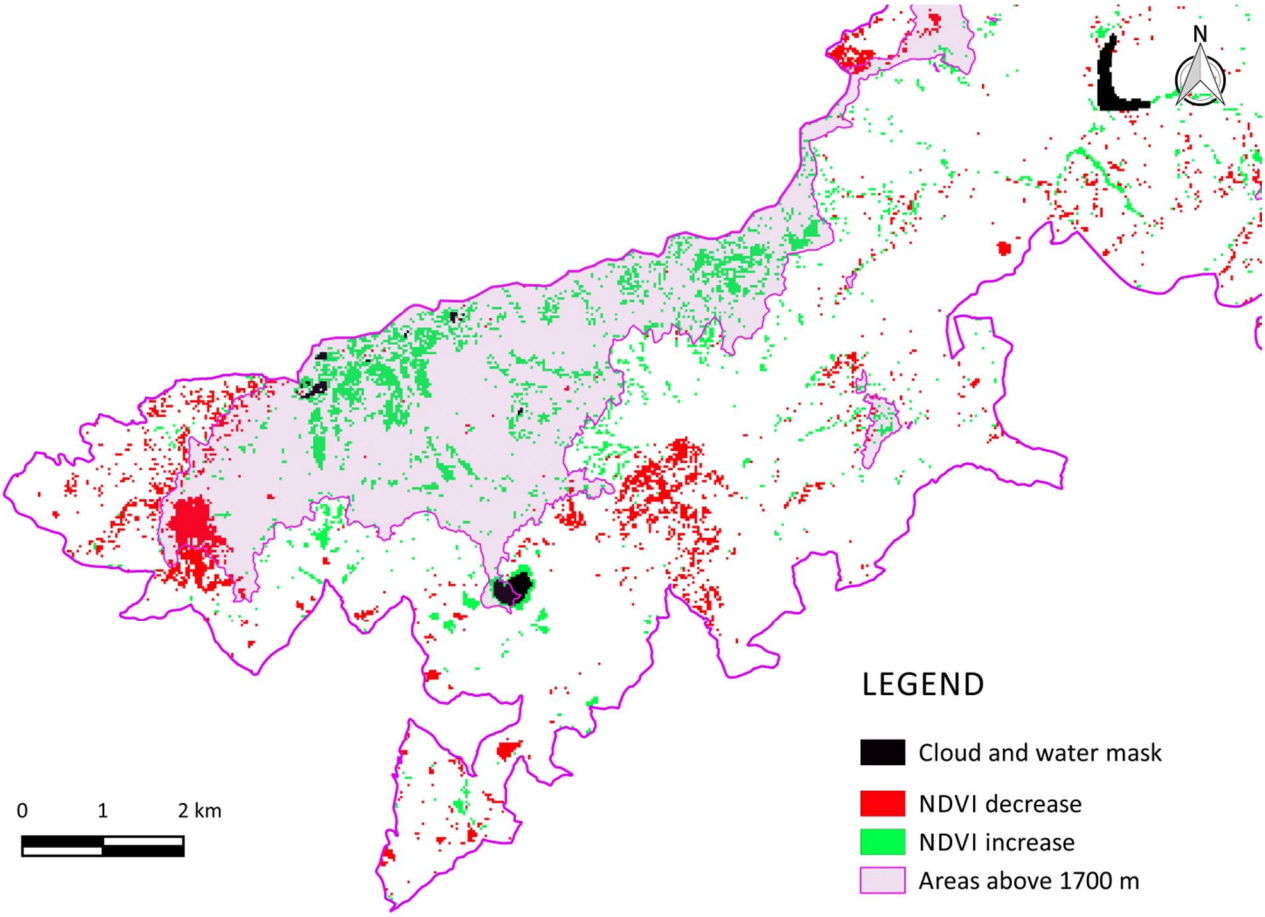

Figure 36: Detail of the reclassified difference image where the the areas with elevation above 1700 m are highlighted.

CONCLUSIONS

This work has tried to characterize and quantify, through the use of different types of remote sensing data, a land cover change phenomenon that is of primary importance not only within the Dolomiti Bellunesi National Park but also, as other studies have shown (Giupponi et al., 2006), in the entire Belluno Province. As shown in this study, the disappearance of grassland areas following forest expansion has been advancing at a rapid pace, and this evolutionary trend is destined to continue, considering both the dependence of semi-natural grasslands on active management and the still uncertain threats posed by climate change.

While other studies have been previously carried out about the land cover change dynamics in this area, their focus was mainly on forest extension and expansion, while the present study, by focusing explicitly on grassland decrease allowed for a more in-depth evaluation of the magnitude of the problem and the most critical areas of change.

Overall, it was possible to obtain a significant amount of information, in particular thanks to the use of multi-sensor and multi-source data. This implies several drawbacks as well, such as the impossibility of collecting clear images (either cloud-free, in the case of satellite images, or free from distortions, in the case of historical aerial images), or the limited possibilities offered by medium-resolution data such as Landsat images. Considered the various issues involved in long time series analyses such as this one, the use of a GIS to interrelate both the original data and the ones created in the course of the study was fundamental to have an overview of the characteristics and dynamics of the phenomenon of interest. This represents the basic tool that can be used for future evaluations and to aid in the definition of priority areas where to focus conservation and management efforts.

Protected areas such as the Dolomiti Bellunesi National Park play a fundamental role in biodiversity conservation, and therefore it is important to reconstruct the evolution of the landscape and its biodiversity-rich habitats in order to create a quantitative framework to support conservation planning and restoration activities at different spatial scales (Ciolli et al., 2007). Understanding land-use change dynamics is a requirement for making informed decision about management and conservation activities in relation to the different functions carried out by semi-natural grassland habitats, and mountain ecosystems as a whole: not only biodiversity conservation, but also preservation of the local cultural heritage and aesthetic beauty, and the productive activities based on the utilization of these functions and resources.

Traditionally, these habitats have been influenced by human activities, and it was the complex interaction between human and natural systems that shaped those aspects that are now considered worth preserving. This is the reason why, in such an environment, or at least in some parts of it, anthropic activities must be taken into account when developing conservation strategies, making sustainable landscape management itself a conservation tool. This aspect has already been recognized by the Dolomiti Bellunesi National Park, through the development of programs for the revitalization of traditional mountain activities, in particular extensive livestock systems (Parco Nazionale Dolomiti Bellunesi, 2003).

As it is often the case when dealing with formerly managed semi-natural environments characterized by high conservation and/or aesthetic value, the choice of whether to restore or maintain a situation of low-level anthropic disturbance or to leave the area to its natural evolution towards true "wilderness" can be a matter of debate. While it is true that the landscape mosaic created by traditional mountain activities fosters higher biodiversity levels than a uniform extent of forest, it is also true that forests represents the climax stage of natural successions in most subalpine mountain areas.

At the same time, however, it is not possible to disregard the potentialities offered by the conservation of the existing landscape mosaic in supporting local economy, in particular regarding the sustainable tourism sector. For this reason, striving to keep a balance between letting successional processes shape the environment towards a more natural state and maintaining landscape diversity in those areas where habitat loss may cause a significant loss of biodiversity and of attractiveness, seems to be the best course of action, at least in the case of protected areas such as the Dolomiti Bellunesi National Park, where conservation is seen as an objective to reach also through the preservation of the harmonious relationship that once existed between the mountains and the people who depended on them for their livelihood.

ACKNOWLEDGMENTS

I would like to thank Professor Carlo Giupponi, my supervisor, for the help and guidance he has given me during the course of my thesis, and Fabio Cian for the technical support and for giving me very useful advice on how to improve my thesis.

My gratitude also goes to Daniele Savio for his encyclopedic knowledge about aerial photography and the precious information and guidance he gave me at the beginning of my work. In this respect, I would like to acknowledge and thank the Veneto Region as well for providing the data without which this study would have been impossible.

Heartfelt thanks to Enrico Vettorazzo and all the Dolomiti Bellunesi National Park staff for all the help and companionship during the months I spent working there.

Many thanks to my parents, who helped and supported me in every way they could, and to my grandparents for lighting candles for me even if they still don't understand what my thesis is about.

And thank you to Meng, for the unfailing love and support, and for encouraging me through every step of the way. Thank you for always being there.

BIBLIOGRAPHY

Agnoletti, M. (2007). The degradation of traditional landscape in a mountain area of Tuscany during the 19th and 20th centuries: Implications for biodiversity and sustainable management. *Forest Ecology and Management*, *249*(1-2), 5–17. doi:10.1016/j.foreco.2007.05.032

Aldrich, R. C. (1979). *Remote Sensing of Wildland Resources : A State-of-the-Art Review*.

Allen, T. R. (2000). Topographic Normalization of Landsat Thematic Mapper Data in Three Mountain Environments. *Geocarto International*, *15*(2), 15–22. doi:10.1080/10106049908542148

Améztegui, A., Brotons, L., & Coll, L. (2010). Land-use changes as major drivers of mountain pine (Pinus uncinata Ram.) expansion in the Pyrenees. *Global Ecology and Biogeography*, *19*(5), 632–641. doi:10.1111/j.1466-8238.2010.00550.x

Anderson, J. J., & Cobb, N. S. (2004). Tree Cover Discrimination in Panchromatic Aerial Imagery of Pinyon-Juniper Woodlands. *Photogrammetric Engineering and Remote Sensing*, *70*(9), 1063–1068.

Andreatta, G. (2007). Selvicoltura all'interno delle aree protette : la gestione dei tagli boschivi nel Parco Nazionale delle Dolomiti Bellunesi. *Forest@*, *4*(4), 355–364.

Balletti, C. (2006). Georeference in the analysis of the geometric content of early maps. *E-Perimetron*, *1*(1), 32–42.

Balthazar, V., Vanacker, V., & Lambin, E. F. (2012). Evaluation and parameterization of ATCOR3 topographic correction method for forest cover mapping in mountain areas. *International Journal of Applied Earth Observation and Geoinformation*, *18*(1), 436–450. doi:10.1016/j.jag.2012.03.010

Bender, O., Boehmer, H. J., Jens, D., & Schumacher, K. P. (2005). Using GIS to analyse long-term cultural landscape change in Southern Germany. *Landscape and Urban Planning*, *70*(1–2), 111–125. doi:10.1016/j.landurbplan.2003.10.008

Berti, C. (2008). Tra l ' Arno e il Calambrone. L'evoluzione del paesaggio nella pianura meridionale pisana tra Otto e Novecento. In C. Masetti, Brigati, & Genova (Eds.), *Primo Seminario di studi storico-cartografici "Dalla mappa ai GIS"* (pp. 349–377). Roma, 5-6 marzo 2007.

Bitelli, G., Ferrari, C., Girelli, V., Gusella, L., Mognol, A., & Pezzi, G. (2005). Integrazione di immagini multitemporali aeree e satellitari per lo studio del pattern della vegetazione nell'Appennino: un caso di studio. In *Conferenza Nazionale ASITA, 9th edition*.

Boschetti, M., Bocchi, S., & Brivio, P. A. (2007). Assessment of pasture production in the Italian Alps using spectrometric and remote sensing information. *Agriculture, Ecosystems and Environment*, *118*(1-4), 267–272. doi:10.1016/j.agee.2006.05.024

Boyd, D. S., & Foody, G. M. (2011). An overview of recent remote sensing and GIS based research in ecological informatics. *Ecological Informatics*, *6*(1), 25–36. doi:10.1016/j.ecoinf.2010.07.007

Bradley, B. a., & Mustard, J. F. (2005). Identifying land cover variability distinct from land cover change: Cheatgrass in the Great Basin. *Remote Sensing of Environment*, *94*(2), 204–213. doi:10.1016/j.rse.2004.08.016

Brandt, J. J. E., Bunce, R. G. H., Howard, D. C., & Petit, S. (2002). General principles of monitoring land cover change based on two case studies in Britain and Denmark. *Landscape and Urban Planning*, *62*(1), 37–51. doi:10.1016/S0169-2046(02)00095-6

Brandtberg, T. (1999). *Remote sensing for forestry applications - a historical retrospect*. Retrieved from http://homepages.inf.ed.ac.uk/rbf/CVonline/LOCAL_COPIES/BRANDTBERG/UK.html

Briggs, J. M., Knapp, A. K., Blair, J. M., Heisler, J. L., Hoch, G. A., Lett, M. S., & McCarron, J. K. (2005). An ecosystem in transition: causes and consequences of the conversion of mesic grassland to shrubland. *BioScience*, *55*(3), 243–254. doi:10.1641/0006-3568(2005)055[0243:AEITCA]2.0.CO;2

Brovelli, M. A., & Minghini, M. (2012). Georeferencing old maps: a polynomial-based approach for Como historical cadastres. *E-Perimetron*, *7*(3), 97–110.

Campbell, J., & Shin, M. (2011). *Essentials of Geographic Information Systems*. FlatWorldKnowledge.com. Retrieved from http://2012books.lardbucket.org/pdfs/geographic-information-system-basics.pdf

Campos, N., Lawrence, R., McGlynn, B., & Gardner, K. (2011). Using Quickbird and Landsat imagery to analyze temporal changes in mountain resort development: Big Sky, Montana 1990–2005. *Journal of Applied Remote Sensing*, *5*(1), 053541. doi:10.1117/1.3615998

Carmel, Y., Dean, D. J., & Flather, C. H. (2001). Combining location and classification error sources for estimating multi-temporal database accuracy. *Photogrammetric Engineering & Remote Sensing*, *67*(7), 865–872.

Chirici, G., & Martino, P. Di. (2009). Tecniche avanzate di cartografia degli ambienti forestali su base tipologica in italia centrale, 989–994. Retrieved from http://www.researchgate.net/publication/233386440_Tecniche_avanzate_di_cartografia_degli_ambienti_forestali_su_base_tipologica_in_italia_centrale/file/5046352cbc4447e444.pdf

Ciolli, M., Serafini, M., & Tattoni, C. (2007). Storia della copertura forestale nel Parco di Paneveggio Pale di S. Martino. *Dendronatura*, *28*(1), 9–15. Retrieved from http://www.legnotrentino.it/documenti/Pubblicazioni/2007/ASFOR_Op_DNatura01_2007_09_15.pdf

Comber, A., Fisher, P., & Wadsworth, R. (2005). Comparing statistical and semantic approaches for identifying change from land cover datasets. *Journal of Environmental Management*, *77*(1), 47–55. doi:10.1016/j.jenvman.2005.02.009

Congalton, R. G. (1991). A review of assessing the accuracy of classifications of remotely sensed data. *Remote Sensing of Environment*, *37*(1), 35–46. doi:10.1016/0034-4257(91)90048-B

Congalton, R. G., & Green, K. (2009). *Assessing the accuracy of Remotely Sensed Data* (Second.). Boca Raton, FL: CRC Press, Taylor & Francis Group.

Congedo, L., & Munafò, M. (2012). *Development of a Methodology for Land Cover Classification in Dar es Salaam using Landsat Imagery*. Rome. Retrieved from http://www.planning4adaptation.eu/

Coop, J. D., & Givnish, T. J. (2007). Spatial and temporal patterns of recent forest encroachment in montane grasslands of the Valles Caldera, New Mexico, USA. *Journal of Biogeography*, *34*(5), 914–927. doi:10.1111/j.1365-2699.2006.01660.x

Coppin, P. O. L. R., & Bauer, M. E. (1996). Change Detection in Forest Ecosystems with Remote Sensing Digital Imagery. *Remote Sensing Reviews*, *13*, 207–234.

Coppin, P. O. L. R., Jonckheere, I., Nackaerts, K., Muys, B., & Lambin, E. (2004). Digital change detection methods in ecosystem monitoring: a review. *International Journal of Remote Sensing*, *25*(9), 1565–1596. doi:10.1080/0143116031000101675

Corona, P., Pompei, E., & Scarascia Mugnozza, G. (2005). Stima probabilistica del tasso di espansione annua e del valore al 1990 della superficie forestale nella Regione Abruzzo. *Forest@*, *2*(2), 178–184.

Culvenor, D. S. (2002). TIDA: an algorithm for the delineation of tree crowns in high spatial resolution remotely sensed imagery. *Computers & Geosciences*, *28*(1), 33–44. doi:10.1016/S0098-3004(00)00110-2

Dai, X., & Khorram, S. (1998). The effects of image misregistration on the accuracy of remotely sensed change detection. *IEEE Transactions on Geoscience and Remote Sensing*, *36*(5), 1566–1577. doi:10.1109/36.718860

De Natale, F., Gasparini, P., Puzzolo, V., & Tosi, V. (2003). Stima del grado di copertura forestale da ortofoto e applicazione della definizione di bosco negli inventari forestali. *L'Italia Forestale E Montana*, *4*, 289–300.

Di Gregorio, A., & Jansen, L. J. M. (2005). *Land Cover Classification System Classification concepts and user manual*. Rome: Food and Agriculture Organization of the United Nations. Retrieved from http://www.fao.org/docrep/008/y7220e/y7220e00.htm#Contents

Didier, L. (2001). Invasion patterns of European larch and Swiss stone pine in subalpine pastures in the French Alps. *Forest Ecology and Management*, *145*(1–2), 67–77. doi:10.1016/S0378-1127(00)00575-2

Dirnböck, T., Dullinger, S., & Grabherr, G. (2003). A regional impact assessment of climate and land-use change on alpine vegetation. *Journal of Biogeography*. Retrieved from http://onlinelibrary.wiley.com/doi/10.1046/j.1365-2699.2003.00839.x/full

Dixon, A. P., Faber-Langendoen, D., Josse, C., Morrison, J., & Loucks, C. J. (2014). Distribution mapping of world grassland types. *Journal of Biogeography*, *41*, 2003–2019. doi:10.1111/jbi.12381

Du, Y., Teillet, P. M., & Cihlar, J. (2002). Radiometric normalization of multitemporal high-resolution satellite images with quality control for land cover change detection. *Remote Sensing of Environment*, *82*(1), 123–134. Retrieved from <Go to ISI>://000177475900011

Eberly, D. (2011). Thin-Plate Splines. Geometric Tools, LLC. Retrieved from http://www.geometrictools.com/

Ekstrand, S. (1996). Landsat TM-Based Forest Damage Assessment: Correction for Topographic Effects. *Photogrammetric Engineering & Remote Sensing*, *62*(2), 151–161.

Esch, T., Metz, A., Marconcini, M., & Keil, M. (2014). Combined use of multi-seasonal high and medium resolution satellite imagery for parcel-related mapping of cropland and grassland. *International Journal of Applied Earth Observation and Geoinformation*, *28*(1), 230–237. doi:10.1016/j.jag.2013.12.007

European Commission. (2008). *LIFE and Europe's grasslands: Restoring a forgotten habitat*. doi:10.2779/23028

Fahsi, A., Tsegaye, T., Tadesse, W., & Coleman, T. (2000). Incorporation of digital elevation models with Landsat-TM data to improve land cover classification accuracy. *Forest Ecology and Management*, *128*(1-2), 57–64. doi:10.1016/S0378-1127(99)00272-8

FAO (Food and Agricultural Organisation of the United Nations). (2005). *Grasslands of the World*. (J. M. Suttie, S. G. Reynolds, & C. Batello, Eds.)*Plant Production and Protection Series*.

FAO (Food and Agricultural Organisation of the United Nations). (2010). *GLOBAL FOREST RESOURCES ASSESSMENT 2010 - TERMS AND DEFINITIONS*. Retrieved from http://www.fao.org/docrep/014/am665e/am665e00.pdf

Fichera, C. R., Modica, G., & Pollino, M. (2012). Land Cover classification and change-detection analysis using multi-temporal remote sensed imagery and landscape metrics. *European Journal of Remote Sensing*, *45*, 1–18. doi:10.5721/EuJRS20124501

Foody, G. M. (2002). Status of land cover classification accuracy assessment. *Remote Sensing of Environment*, *80*, 185–201.

Frate, L., Saura, S., Minotti, M., Di Martino, P., Giancola, C., & Carranza, M. (2014). Quantifying Forest Spatial Pattern Trends at Multiple Extents: An Approach to Detect Significant Changes at Different Scales. *Remote Sensing*, *6*(10), 9298–9315. doi:10.3390/rs6109298

Garbarino, M., & Pividori, M. (2006). Le dinamiche del paesaggio forestale : evoluzione temporale del bosco di neoformazione sui pascoli di Corte Pogallo - Parco nazionale della Val Grande (VB). *Forest@*, *3*(2), 213–221.

Garbarino, M., Sibona, E., Lingua, E., & Motta, R. (2014). Decline of traditional landscape in a protected area of the southwestern Alps: The fate of enclosed pasture patches in the land mosaic shift. *Journal of Mountain Science*, *11*(2), 544–554. doi:10.1007/s11629-013-2666-9

Gartzia, M., Alados, C. L., Pérez-cabello, F., & Bueno, C. G. (2013). Improving the Accuracy of Vegetation Classifications in Mountainous Areas - A case study in the central Pyrenees. *Mountain Research and Development*, *33*(1), 63–74.

Gellrich, M., Baur, P., Koch, B., & Zimmermann, N. E. (2007). Agricultural land abandonment and natural forest re-growth in the Swiss mountains: A spatially explicit economic analysis. *Agriculture, Ecosystems & Environment*, *118*(1-4), 93–108. doi:10.1016/j.agee.2006.05.001

Gellrich, M., & Zimmermann, N. E. (2007). Investigating the regional-scale pattern of agricultural land abandonment in the Swiss mountains: A spatial statistical modelling approach. *Landscape and Urban Planning*, *79*(1), 65–76. doi:10.1016/j.landurbplan.2006.03.004

Gerard, F., Petit, S., Smith, G., Thomson, A., Brown, N., Manchester, S., … Feranec, J. (2010). Land cover change in Europe between 1950 and 2000 determined employing aerial photography. *Progress in Physical Geography*, *34*(2), 183–205. doi:10.1177/0309133309360141

Giupponi, C., Ramanzin, M., Sturaro, E., & Fuser, S. (2006). Climate and land use changes, biodiversity and agri-environmental measures in the Belluno province , Italy. *Environmental Science & Policy*, *9*, 163–173. doi:10.1016/j.envsci.2005.11.007

Gu, Y., Wylie, B. K., Howard, D. M., Phuyal, K. P., & Ji, L. (2013). NDVI saturation adjustment: A new approach for improving cropland performance estimates in the Greater Platte River Basin, USA. *Ecological Indicators*, *30*, 1–6. doi:10.1016/j.ecolind.2013.01.041

Halpern, C. B., Antos, J. A., Rice, J. M., Haugo, R. D., & Lang, N. L. (2010). Tree invasion of a montane meadow complex: temporal trends, spatial patterns, and biotic interactions. *Journal of Vegetation Science*, *21*(4), 717–732. Retrieved from http://onlinelibrary.wiley.com/doi/10.1111/j.1654-1103.2010.01183.x/full

Hang, N. T., & Canh, P. X. (2014). A comparison of vegetation spectral indices derived from Landsat 8 and previous Landsat generations. In *35th Asian Conference on Remote Sensing*.

Hantson, S., & Chuvieco, E. (2011). Evaluation of different topographic correction methods for landsat imagery. *International Journal of Applied Earth Observation and Geoinformation*, *13*(5), 691–700. doi:10.1016/j.jag.2011.05.001

Hayes, D. J., & Sader, S. a. (2001). Comparison of ChangeDetection Techniques for Monitoring Tropical Forest Clearing and Vegetation Regrowth in a Time Series. *Photogrammetric Engineering & Remote Sensing*, *67, No. 9*, 1067–1075. doi:citeulike-article-id:7954186

Höchtl, F., Lehringer, S., & Konold, W. (2005). " Wilderness ": what it means when it becomes a reality — a case study from the southwestern Alps. *Landscape and Urban Planning*, *70*, 85–95. doi:10.1016/j.landurbplan.2003.10.006

Hori, S., Hayashi, M., Matsubara, Y., Awaya, Y., & Iehara, T. (2007). Detection of Afforestation, Reforestation and Deforestation (ARD) by Visual Photo Interpretation of High Spatial Resolution Images : A Fundamental Case Study. *Journal of Forest Planning*, *13*(1), 109–123. Retrieved from http://ci.nii.ac.jp/naid/110009357710/en/

Hostert, P., Röder, A., & Hill, J. (2003). Coupling spectral unmixing and trend analysis for monitoring of long-term vegetation dynamics in Mediterranean rangelands. *Remote Sensing of Environment*, *87*(2-3), 183–197. doi:10.1016/80034-4257(03)00145-7

Huete, A. R., & Jackson, R. D. (1988). Soil and atmosphere influences on the spectra of partial canopies. *Remote Sensing of Environment*, *25*(1), 89–105. doi:10.1016/0034-4257(88)90043-0

Hussain, M., Chen, D., Cheng, A., Wei, H., & Stanley, D. (2013). Change detection from remotely sensed images: From pixel-based to object-based approaches. *ISPRS Journal of Photogrammetry and Remote Sensing*, *80*, 91–106. doi:10.1016/j.isprsjprs.2013.03.006

Im, J., Jensen, J. R., & Tullis, J. a. (2008). Object-based change detection using correlation image analysis and image segmentation. *International Journal of Remote Sensing*, *29*(2), 399–423. doi:10.1080/01431160601075582

IPCC. (2003). *Intergovernmental Panel on Climate Change Good Practice Guidance for Land Use, Land-Use Change and Forestry*. Retrieved from http://www.ipcc-nggip.iges.or.jp/public/gpglulucf.html

Jackson, R. D., & Huete, A. R. (1991). Interpreting vegetation indices. *Preventive Veterinary Medicine*. doi:10.1016/S0167-5877(05)80004-2

Jelinski, D. E., & Wu, J. (1996). The modifiable areal unit problem and implications for landscape ecology. *Landscape Ecology*, *11*(3), 129–140. doi:10.1007/BF02447512

Jianya, G., Haigang, S., Guorui, M., & Qiming, Z. (2008). A Review of Multi-Temporal Remote Sensing Data Change Detection. *The International Archives of the Photogrammetry, Remote Sensing and Spatial Information Sciences*, *37*(B7), 757–762. doi:10.1016/j.isprsjprs.2003.10.002

Kadmon, R., & Harari-Kremer, R. (1999). Studying Long-Term Vegetation Dynamics Using Digital Processing of Historical Aerial Photographs. *Remote Sensing of Environment*, *68*(2), 164–176. doi:10.1016/S0034-4257(98)00109-6

Kremer, N. J., Halpern, C. B., & Antos, J. A. (2014). Conifer reinvasion of montane meadows following experimental tree removal and prescribed burning. *Forest Ecology and Management*, *319*, 128–137. doi:10.1016/j.foreco.2014.02.002

Laliberte, A. S., Rango, A., Havstad, K. M., Paris, J. F., Beck, R. F., McNeely, R., & Gonzalez, A. L. (2004). Object-oriented image analysis for mapping shrub encroachment from 1937 to 2003 in southern New Mexico. *Remote Sensing of Environment*, *93*(1–2), 198–210. doi:10.1016/j.rse.2004.07.011

Langley, S. K., Cheshire, H. M., & Humes, K. S. (2001). A comparison of single date and multitemporal satellite image classifications in a semi-arid grassland. *Journal of Arid Environments*, *49*(2), 401–411. doi:10.1006/jare.2000.0771

Law, K. H., & Nichol, J. (2004). Topographic correction for differential illumination effects on Ikonos satellite imagery. *ISPRS Archives*, *35*(B3), 641–646.

Lega, P., & Vincini, M. (2003). *Studio della dinamica forestale e colturale nell' Appennino piacentino con l' impiego di immagini multitemporali e multisensore.* Piacenza.

Lillesand, T. M., Kiefer, R. W., & Chipman, J. W. (2004). *Remote sensing and image interpretation*. (J. W. & Sons, Ed.) (5th ed.).

Lu, D. ., Li, G. ., & Moran, E. (2014). Current situation and needs of change detection techniques. *International Journal of Image and Data Fusion*, *5*(1), 13–38. doi:10.1080/19479832.2013.868372

Lu, D., Ge, H., He, S., Xu, A., Zhou, G., & Du, H. (2008). Pixel-based Minnaert Correction Method for Reducing Topographic Effects on a Landsat 7 ETM+ Image. *Photogrammetric Engineering and Remote Sensing*, *74*(11), 1343–1350.

Lu, D., Mausel, P., Brondízio, E., & Moran, E. (2004). Change detection techniques. *International Journal of Remote Sensing*, *25*(12), 2365–2401. doi:10.1080/0143116031000139863

Lunetta, R. S., Ediriwickrema, J., Johnson, D. M., Lyon, J. G., & McKerrow, A. (2002). Impacts of vegetation dynamics on the identification of land-cover change in a biologically complex community in North Carolina, USA. *Remote Sensing of Environment*, *82*(2-3), 258–270. doi:10.1016/S0034-4257(02)00042-1

Lyon, J. G., Yuan, D., Lunetta, R. S., & Elvidge, C. D. (1998). A Change Detection Experiment Using Vegetation Indices. *Photogrammetric Engineering & Remote Sensing*, *64*(2), 143–150. doi:citeulike-article-id:7262520

MacDonald, D., Crabtree, J. . R., Wiesinger, G., Dax, T., Stamou, N., Fleury, P., … Gibon, A. (2000). Agricultural abandonment in mountain areas of Europe: Environmental consequences and policy response. *Journal of Environmental Management*, *59*(1), 47–69. doi:10.1006/jema.1999.0335

Mancino, G., Nolè, A., Ripullone, F., & Ferrara, A. (2014). Landsat TM imagery and NDVI differencing to detect vegetation change: Assessing natural forest expansion in Basilicata, southern Italy. *IForest*, *7*(2), 75–84. doi:10.3832/ifor0909-007

Marchetti, M., Bertani, R., Corona, P., & Valentini, R. (2012). Changes of forest coverage and land uses as assessed by the inventory of land uses in Italy. *Forest@ - Rivista di Selvicoltura ed Ecologia Forestale*, *9*(4), 170–184. doi:10.3832/efor0696-009

Mas, J.-F. (1999). Monitoring land-cover changes: a comparison of change detection techniques. *International Journal of Remote Sensing*, *20*(1), 139–152. doi:10.1080/014311699213659

Masek, J. G., Vermote, E. F., Saleous, N., Wolfe, R., Hall, F. G., Huemmrich, F., … Lim, T. K. (2006). A Landsat surface reflectance data set for North America, 1990-2000. *IEEE Geoscience and Remote Sensing Letters*, *3*, 68–72.

Mašková, Z., Zemek, F., & Květ, J. (2008). Normalized difference vegetation index (NDVI) in the management of mountain meadows. *Boreal Environment Research*, *13*(5), 417–432.

Mast, J. N., Veblen, T. T., & Hodgson, M. E. (1997). Tree invasion within a pine/grassland ecotone: an approach with historic aerial photography and GIS modeling. *Forest Ecology and Management*, *93*(3), 181–194. doi:10.1016/S0378-1127(96)03954-0

Matsushita, B., Yang, W., Chen, J., Onda, Y., & Qiu, G. (2007). Sensitivity of the Enhanced Vegetation Index (EVI) and Normalized Difference Vegetation Index (NDVI) to Topographic Effects: A Case Study in High-density Cypress Forest. *Sensors*, *7*(11), 2636–2651. doi:10.3390/s7112636

Meyer, P., Itten, K. I., Kellenberger, T., Sandmeier, S., & Sandmeier, R. (1993). Radiometric corrections of topographically induced effects on Landsat TM data in an alpine environment. *ISPRS Journal of Photogrammetry and Remote Sensing*, *48*(4), 17–28. doi:10.1016/0924-2716(93)90028-L

Mihai, B., Savulescu, I., & Sandric, I. (2007). Change Detection Analysis (1986–2002) of Vegetation Cover in Romania. *Mountain Research and Development*, *27*(3), 250–258. doi:10.1659/mred.0645

Mognol, A. (2007). Analisi di immagini aerofotogrammetriche e telerilevate per la caratterizzazione qualitativa e quantitativa di ecosistemi forestali e della loro evoluzione. Retrieved from http://amsdottorato.cib.unibo.it/308/

Morgan, J. L., Gergel, S. E., & Coops, N. C. (2010). Aerial Photography: A Rapidly Evolving Tool for Ecological Management. *BioScience*, *60*(1), 47–59. doi:10.1525/bio.2010.60.1.9

Mottet, A., Ladet, S., Coqué, N., & Gibon, A. (2006). Agricultural land-use change and its drivers in mountain landscapes: A case study in the Pyrenees. *Agriculture, Ecosystems & Environment*, *114*(2–4), 296–310. doi:10.1016/j.agee.2005.11.017

Neteler, M., & Mitasova, H. (2008). *Open Source GIS: A GRASS GIS Approach* (3nd Editio.). Springer, New York.

Niedrist, G., Tasser, E., Luth, C., Dalla Via, J., & Tappeiner, U. (2009). Plant diversity declines with recent land use changes in European Alps. *Plant Ecology*, *202*, 195–210. doi:10.1007/s11258-008-9487-x

Nordberg, M. L., & Evertson, J. (2003). Monitoring change in mountainous dry-heath vegetation at a regional scale using multitemporal Landsat TM data. *Ambio*, *32*(8), 502–509. doi:10.1579/0044-7447-32.8.502

Nordberg, M. L., & Evertson, J. (2005). Vegetation index differencing and linear regression for change detection in a swedish mountain range using landsat tm (r) and etm+((r)) imagery. *Land Degradation & Development*, *16*(2), 139–149. doi:Doi 10.1002/Ldr.660

Northrop, A. (2015). IDEAS – LANDSAT Products Description Document.

Olsson, E. G. A., Austrheim, G., & Grenne, S. N. (2000). Landscape change patterns in mountains, land use and environmental diversity, Mid-Norway 1960 – 1993. *Landscape Ecology*, *15*, 155–170.

Paine, D. P., & Kiser, J. D. (2012). *Aerial photography and image interpretation*. (John Wiley & Sons, Ed.) (3rd ed.). Hoboken, New Jersey. doi:10.1002/9781118110997

Parco Nazionale Dolomiti Bellunesi. (2003). *Progetto speciale riqualificazione malghe, gestione prati e pascoli*. Retrieved September 1, 2015, from http://www.dolomitipark.it/it/page.php?id=448

Parco Nazionale Dolomiti Bellunesi. (2015). *Parco Nazionale Dolomiti Bellunesi: l'area protetta*. Retrieved September 1, 2015, from http://www.parks.it/parco.nazionale.dol.bellunesi/par.php

Payero, J. O., Neale, C. M. U., & Wright, J. L. (2004). Comparison of Eleven Vegetation Indices for Estimating Plant Height of Alfalfa and Grass. *Applied Engineering in Agriculture*, *20*(3), 385–393. doi:10.13031/2013.16057

Pelorosso, R., Leone, A., & Boccia, L. (2009). Land cover and land use change in the Italian central Apennines: A comparison of assessment methods. *Applied Geography*, *29*(1), 35–48. doi:10.1016/j.apgeog.2008.07.003

Petit, C. C., & Lambin, E. F. (2001). Integration of multi-source remote sensing data for land cover change detection. *International Journal of Geographical Information Science*, *15*(8), 785–803. doi:10.1080/13658810110074483

Poschlod, P., & WallisDeVries, M. F. (2002). The historical and socioeconomic perspective of calcareous grasslands—lessons from the distant and recent past. *Biological Conservation*, *104*(3), 361–376. doi:10.1016/S0006-3207(01)00201-4

Pouliot, D. . A., King, D. . J., Bell, F. . W., & Pitt, D. . G. (2002). Automated tree crown detection and delineation in high-resolution digital camera imagery of coniferous forest regeneration. *Remote Sensing of Environment*, *82*(2-3), 322–334. doi:10.1016/S0034-4257(02)00050-0

Poyatos, R., Latron, J., & Llorens, P. (2003). Land Use and Land Cover Change After Agricultural Abandonment. *Mountain Research and Development*, *23*(4), 362–368. doi:10.1659/0276-4741(2003)023[0362:LUALCC]2.0.CO;2

Price, J. N., & Morgan, J. W. (2008). Woody plant encroachment reduces species richness of herb-rich woodlands in southern Australia. *Austral Ecology*, *33*(3), 278–289. doi:10.1111/j.1442-9993.2007.01815.x

Price, K. P., Guo, X., & Stiles, J. M. (2003). Comparison of landsat TM and ERS-2 SAR data for discriminating among grassland types and treatments in eastern Kansas. *Computers and Electronics in Agriculture*, *37*(1-3), 157–171. doi:10.1016/S0168-1699(02)00110-2

QGis 2.0 User Manual. (2014). *QGis 2.0 User Manual*. Retrieved December 21, 2014, from http://docs.qgis.org/2.0/en/docs/user_manual/plugins/plugins_georeferencer.html

QGIS Development Team. (2015). QGIS Geographic Information System. Open Source Geospatial Foundation Project. Retrieved from http://qgis.osgeo.org

Radke, R. J., Andra, S., Al-Kofahi, O., & Roysam, B. (2005). Image change detection algorithms: a systematic survey. *IEEE Transactions on Image Processing: A Publication of the IEEE Signal Processing Society*, *14*(3), 294–307. doi:10.1.1.5.291

Regione del Veneto. (2011). *L'evoluzione dei boschi veneti – Analisi delle dinamiche spaziali dei popolamenti forestali regionali*. Regione del Veneto - Unità di Progetto Foreste e Parchi. Retrieved from http://www.regione.veneto.it/static/www/agricoltura-e-foreste/evoluzione_boschi_veneti_smaller.pdf

Richter, R., Kellenberger, T., & Kaufmann, H. (2009). Comparison of topographic correction methods. *Remote Sensing*, *1*(3), 184–196. doi:10.3390/rs1030184

Rocchini, D. (2004). Misleading information from direct interpretation of geometrically incorrect aerial photographs. *The Photogrammetric Record*, *19*(106), 138–148.

Rocchini, D. ., Metz, M. ., Frigeri, A., Delucchi, L., Marcantonio, M., & Neteler, M. (2012). Robust rectification of aerial photographs in an open source environment. *Computers & Geosciences*, *39*, 145–151. doi:10.1016/j.cageo.2011.06.002

Rocchini, D., & Di Rita, A. (2005). Relief effects on aerial photos geometric correction. *Applied Geography*, *25*(2), 159–168. doi:10.1016/j.apgeog.2005.03.002

Rogan, J., & Chen, D. (2004). Remote sensing technology for mapping and monitoring land-cover and land-use change. *Progress in Planning*, *61*(4), 301–325. doi:10.1016/S0305-9006(03)00066-7

Rogan, J., Franklin, J., & Roberts, D. A. (2002). A comparison of methods for monitoring multitemporal vegetation change using Thematic Mapper imagery. *Remote Sensing of Environment*, *80*(1), 143–156. doi:10.1016/S0034-4257(01)00296-6

Roura-Pascual, N., Pons, P., Etienne, M., & Lambert, B. (2005). Transformation of a Rural Landscape in the Eastern Pyrenees Between 1953 and 2000. *Mountain Research and Development*, *25*(3), 252–261.

Roy, D. P. (2000). The impact of misregistration upon composited wide field of view satellite data and implications for change detection. *IEEE Transactions on Geoscience and Remote Sensing*, *38*(4), 2017–2032. doi:10.1109/36.851783

Salvadori, I., Pilli, R., & Anfodillo, T. (2006). Proposta di una metodologia di analisi della variazione di superficie boscata tramite foto aeree per l' applicazione del protocollo di Kyoto: il caso della Comunità Montana del Grappa (TV). *Forest@*, *3*(3), 339–350. Retrieved from http://www.sisef.it/forest@/contents/?id=efor0393-0030339

Sankey, T. T., & Germino, M. J. (2008). Assessment of Juniper Encroachment With The Use of Satellite Imagery and Geospatial Data. *Rangeland Ecology & Management*, *61*(4), 412–418. doi:10.2111/07-141.1

Sant, E., Simonds, G., Ramsey, R., & Larsen, R. (2014). Assessment of sagebrush cover using remote sensing at multiple spatial and temporal scales. *Ecological Indicators*, *43*, 297–305. Retrieved from http://www.sciencedirect.com/science/article/pii/S1470160X14001162

Schroeder, T. a., Cohen, W. B., Song, C., Canty, M. J., & Yang, Z. (2006). Radiometric correction of multi-temporal Landsat data for characterization of early successional forest patterns in western Oregon. *Remote Sensing of Environment*, *103*(1), 16–26. doi:10.1016/j.rse.2006.03.008

Senf, C., Leitão, P. J., Pflugmacher, D., van der Linden, S., & Hostert, P. (2015). Mapping land cover in complex Mediterranean landscapes using Landsat: Improved classification accuracies from integrating multi-seasonal and synthetic imagery. *Remote Sensing of Environment*, *156*, 527–536. doi:10.1016/j.rse.2014.10.018

Serra, P., Pons, X., & Saurì, D. (2003). Post-classification change detection with data from different sensors: some accuracy considerations. *International Journal of Remote Sensing*, *24*(16), 3311–3340.

Sgarbossa, A. (2010). *Evoluzione del paesaggio e cambiamenti di uso del suolo dal 1954 al 2006 nelle foreste di Tovanella e Cajada (Dolomiti-Belluno)*. Retrieved from http://www.tesionline.it/default/tesi.asp?idt=35339

Shepherd, J. D., & Dymond, J. R. (2003). Correcting satellite imagery for the variance of reflectance and illumination with topography. *International Journal of Remote Sensing*, *24*(17), 3503–3514. doi:10.1080/01431160210154029

Simonetti, E., Simonetti, D., & Preatoni, D. (2014). *Phenology-based land cover classification using Landsat 8 time series*. doi:10.2788/15561

Singh, A. (1989). Digital change detection techniques using remotely-sensed data. *International Journal of Remote Sensing*, *10*(6), 989–1003.

Sitzia, T., Semenzato, P., & Trentanovi, G. (2010). Natural reforestation is changing spatial patterns of rural mountain and hill landscapes: A global overview. *Forest Ecology and Management*, *259*(8), 1354–1362. doi:10.1016/j.foreco.2010.01.048

Smith, J. H., Stehman, S. V, Wickham, J. D., & Yang, L. (2003). Effects of landscape characteristics on land-cover class accuracy. *Remote Sensing of Environment*, *84*, 342–349.

Song, C., Woodcock, C., Seto, K. C., Lenney, M. P., & Macomber, S. a. (2001). Classification and change detection using Landsat TM Data- When and how to correct atmospheric effects? *Remote Sensing of Environment*, *75*(2), 230–244. doi:10.1016/S0034-4257(00)00169-3

Stanga, P., & Zbinden, N. (2004). Evoluzione della copertura vegetale in aree alpestri del Canton Ticino nel periodo 1971–2001. *Schweiz. Z. Forstwes*, *155*(7), 284–289.

Stow, D. A. (1999). Reducing the effect of misregistration on pixel level change detection. *International Journal of Remote Sensing*, *12*, 2477–2483.

Stow, D. A., & Chen, D. M. (2002). Sensitivity of multitemporal NOAA AVHRR data of an urbanizing region to land-use/land-cover changes and misregistration. *Remote Sensing of Environment*, *80*, 297–307.

Strahler, A. H., Boschetti, L., Foody, G. M., Friedl, M. A., Hansen, M. C., Herold, M., … Woodcock, C. E. (2006). *Global Land Cover Validation: Recommendations for Evaluation and Accuracy Assessment of Global Land Cover Maps*.

Strand, G.-H., Dramstad, W., & Engan, G. (2002). The effect of field experience on the accuracy of identifying land cover types in aerial photographs. *International Journal of Applied Earth Observation and Geoinformation*, *4*(2), 137–146. doi:10.1016/S0303-2434(02)00011-9

Tasser, E., & Tappeiner, U. (2002). Impact of land use changes on mountain vegetation. *Applied Vegetation Science*, *5*(2), 173–184. doi:10.1111/j.1654-109X.2002.tb00547.x

Tasser, E., Walde, J., Tappeiner, U., Teutsch, A., & Noggler, W. (2007). Land-use changes and natural reforestation in the Eastern Central Alps. *Agriculture, Ecosystems & Environment*, *118*(1–4), 115–129. doi:10.1016/j.agee.2006.05.004

Tattoni, C., Ciolli, M., Ferretti, F., & Cantiani, M. G. (2010). Monitoring spatial and temporal pattern of Paneveggio forest (Northern Italy) from 1859 to 2006. *IForest*, *3*, 72–80. doi:10.3832/ifor0530-003

Townshend, J. R. G., Justice, C. O., Gurney, C., & McManus, J. (1992). The impact of misregistration on change detection. *IEEE Transactions on Geoscience and Remote Sensing*, *30*(5), 1054–1060. doi:10.1109/36.175340

Traub, B., Kohl, M., Paivinen, R., & Kugler, O. (1998). Effects of different definitions on forest area estimation in national forest inventories in Europe. In *Integrated Tools for Natural Resources Inventories in the 21st Century* (pp. 176–184). Boise, Idaho.

Turner, D. P., Cohen, W. B., Kennedy, R. E., Fassnacht, K. S., & Briggs, J. M. (1999). Relationships between leaf area index and Landsat TM spectral vegetation indices across three temperate zone sites. *Remote Sensing of Environment*, *70*(1), 52–68. doi:10.1016/S0034-4257(99)00057-7

Turner II, B. L., Lambin, E. F., & Reenberg, A. (2008). The emergence of land change science for global environmental change and sustainability. *PNAS*, *105*(7).

Turner, M. G. (1990). Spatial and temporal analysis of landscape patterns. *Landscape Ecology*, *4*(1), 21–30. doi:10.1007/BF02573948

Ünsalan, C., & Boyer, K. L. (2003). *Multispectral satellite image understanding*. Springer London.

Urbinati, C., Benetti, R., Viola, F., & Ferrari, C. (2004). Dinamismi della copertura forestale in Val di Tovel dal 1860 ad oggi. *Studi Trent. Sci. Nat., Acta Biol.*, *81*(2), 39–52.

USGS. (2015a). Landsat 4-7 Climate Data Record (Cdr) Surface Reflectance - Product Guide. doi:10.1080/1073161X.1994.10467258

USGS. (2015b). *Landsat 7 Long Term Acquisition Plan (LTAP-7)*. Retrieved September 5, 2015, from https://landsat.usgs.gov/tools_da_LTAP.php

USGS. (2015c). *Landsat Missions Timeline*. Retrieved September 1, 2015, from http://landsat.usgs.gov/about_mission_history.php

USGS. (2015d). LANDSAT Surface Reflectance-derived Spectral Indices. Department of the Interior- U.S. Geological Survey. doi:10.1080/1073161X.1994.10467258

Vacchiano, G., Garbarino, M., Lingua, E., & Motta, R. (2006). Le pinete di pino silvestre come testimoni delle trasformazioni del paesaggio montano in Piemonte e Valle d'Aosta. Retrieved from http://www.academia.edu/2977889/Le_pinete_di_Pino_silvestre_come_testimoni_delle_trasformazioni_del_paesaggio_montano_in_Piemonte_e_Val_dAosta

Van Lynden, G. W. J., & Mantel, S. (2001). The role of GIS and remote sensing in land degradation assessment and conservation mapping: some user experiences and expectations. *JAG*, *3*(1), 61–68.

Van Niel, T. G., McVicar, T. R., Li, L., Gallant, J. C., & Yang, Q. (2008). The impact of misregistration on SRTM and DEM image differences. *Remote Sensing of Environment*, *112*(5), 2430–2442. doi:10.1016/j.rse.2007.11.003

Vanonckelen, S., Lhermitte, S., & Van Rompaey, A. (2013). The effect of atmospheric and topographic correction methods on land cover classification accuracy. *International Journal of Applied Earth Observation and Geoinformation*, *24*(1), 9–21. doi:10.1016/j.jag.2013.02.003

Verburg, P. H., Neumann, K., & Nol, L. (2011). Challenges in using land use and land cover data for global change studies. *Global Change Biology*, *17*(2), 974–989. doi:10.1111/j.1365-2486.2010.02307.x

Verbyla, D. L., & Boles, S. H. (2000). Bias in land cover change estimates due to misregistration. *International Journal of Remote Sensing*, *21*(18), 3553–3560.

Vicente-Serrano, S. M., Pérez-Cabello, F., & Lasanta, T. (2008). Assessment of radiometric correction techniques in analyzing vegetation variability and change using time series of Landsat images. *Remote Sensing of Environment*, *112*(10), 3916–3934. doi:10.1016/j.rse.2008.06.011

Vittek, M., Brink, A., Donnay, F., Simonetti, D., & Desclée, B. (2013). Land cover change monitoring using landsat MSS/TM satellite image data over west Africa between 1975 and 1990. *Remote Sensing*, *6*(1), 658–676. doi:10.3390/rs6010658

WallisDeVries, M. F., Poschlod, P., & Willems, J. H. (2002). Challenges for the conservation of calcareous grasslands in northwestern Europe: integrating the requirements of flora and fauna. *Biological Conservation*, *104*(3), 265–273. doi:10.1016/S0006-3207(01)00191-4

Walton, J. T., Nowak, D. J., & Greenfield, E. J. (2008). Assessing Urban Forest Canopy Cover Using Airborne or Satellite Imagery. *Arboriculture & Urban Forestry*, *34*(6), 334–340.

Wang, H., & Ellis, E. C. (2005). Image Misregistration Error in Change Measurements. *Photogrammetric Engineering & Remote Sensing*, *71*(9), 1037–1044. doi:10.14358/PERS.71.9.1037

Waser, L. T., & Schwarz, M. (2006). Comparison of large-area land cover products with national forest inventories and CORINE land cover in the European Alps. *International Journal of Applied Earth Observation and Geoinformation*, *8*(3), 196–207. doi:10.1016/j.jag.2005.10.001

Whiteman, G., & Brown, J. R. (1998). Assessment of a method for mapping woody plant density in a grassland matrix. *Journal of Arid Environments*, *38*(2), 269–282. doi:10.1006/jare.1997.0325

Willhauck, G., Schneider, T., De Kok, R., & Ammer, U. (2000). Comparison of object oriented classification techniques and standard image analysis for the use of change detection between SPOT multispectral

satellite images and aerial photos . *ISPRS Archives*, *XXXIII*(Supplement B3), 214–221. Retrieved from http://www.isprs.org/proceedings/XXXIII/congress/part3/214_XXXIII-part3.pdf

Willneff, J., & Poon, J. (2006). Georeferencing From Orthorectified and Non-Orthorectified High-Resolution Satellite Imagery. In *The 13th Australasian Remote Sensing and Photogrammetry Conference*. Canberra, Australia.

Xian, G., Homer, C., & Fry, J. (2009). Updating the 2001 National Land Cover Database land cover classification to 2006 by using Landsat imagery change detection methods. *Remote Sensing of Environment*, *113*(6), 1133–1147. doi:10.1016/j.rse.2009.02.004

Xie, Y., Sha, Z., & Yu, M. (2008). Remote sensing imagery in vegetation mapping: a review. *Journal of Plant Ecology*, *1*(1), 9–23. doi:10.1093/jpe/rtm005

Yuan, D., & Elvidge, C. D. (1996). Comparison of relative radiometric normalization techniques. *ISPRS Journal of Photogrammetry and Remote Sensing*, *51*(3), 117–126. doi:10.1016/0924-2716(96)00018-4

Yuan, F., Sawaya, K. E., Loeffelholz, B. C., & Bauer, M. E. (2005). Land cover classification and change analysis of the Twin Cities (Minnesota) metropolitan area by multitemporal Landsat remote sensing. *Remote Sensing of Environment*, *98*(2-3), 317–328. doi:10.1016/j.rse.2005.08.006

Ziliotto, U., Andrich, O., Lasen, C., & Ramanzin, M. (2004). *Tratti Essenziali della tipologia Veneta dei Pascoli di Monte e Dintorni*. Venezia: Regione del Veneto.

APPENDIX A. AERIAL PHOTOGRAPHS

All the operations described in this and in the following section have been carried out using QGIS version 2.10.

N.B.: it is advisable to change the default language to English through *Settings → Options → Locale → Override system locale*, because the majority of the documentation and tutorials are available in English, and having the interface in a different language can be confusing.

A. PROCESSING AND ANALYSIS OF AERIAL IMAGES

A1. A note on the reference systems used in Italy

The geodetic system (datum) used for most of the Italian cartography (and for the majority of the data acquired in this study) is ROMA40/Gauss–Boaga. The grid system is based on the Roma 1940 datum, whose origin lies at Monte Mario near Rome. The projection is split into a western (EPSG 3003) and eastern zone (EPSG 3004). The western zone, used in this study, is used for the areas west of the 12 °E longitude, and is also referred to as Monte Mario / Italy zone 1 or Rome 1940 / Italy zone 1 (source: http://www.epsg-registry.org/).

In QGIS, several projection definitions all corresponding to Monte Mario/Italy zone 1 are available:

1) Monte Mario/Italy zone 1 (EPSG:3003)

```
+proj=tmerc +lat_0=0 +lon_0=9 +k=0.9996 +x_0=1500000 +y_0=0 +ellps=intl
+towgs84=-104.1,-49.1,-9.9,0.971,-2.917,0.714,-11.68 +units=m +no_defs
```

2) Monte Mario/Italy zone 1 (EPSG:102091)

```
+proj=tmerc +lat_0=0 +lon_0=9 +k=0.9996 +x_0=1500000 +y_0=0 +ellps=intl
+units=m +no_defs
```

QGIs may not recognize EPSG:102091 as it is not, in fact, an official EPSG definition but an ESRI one, and set it as a custom SR, like so:

```
Generated CRS for telaer: user 100000
 +proj=tmerc +lat_0=0 +lon_0=9.000000000000002 +k=0.9996 +x_0=1500000
+y_0=0 +ellps=intl +units=m +no_defs
```

The only difference between EPSG:3003 and EPSG:102091 is that the first one has a datum shift for conversion to WGS84 (+towgs84) defined in the projection, while the second doesn't. EPSG:102091 is generally associated to files produced with ESRI software, where datum shifts are not written into projection definitions, but kept separate. With QGIS it is advisable to use the first one, especially if the data need to be reprojected on-the-fly or converted to a CRS using WGS84, like WGS84/UTM zone 32N (EPSG: 32632) for Italy. Using the projection without datum shift causes a shift of up to 100 m between the input image and the target image.

3) Monte Mario (Rome)/Italy zone 1 (deprecated) EPSG:26591

```
+proj=tmerc +lat_0=0 +lon_0=-3.45233333333333 +k=0.9996 +x_0=1500000
+y_0=0 +ellps=intl +towgs84=-104.1,-49.1,-9.9,0.971,-2.917,0.714,-11.68
+pm=rome +units=m +no_defs
```

(deprecated by EPSG because associated with incorrect datum resulting in map projection longitude being incompatible with prime meridian).

In these cases, it is better to open the layer in QGIS, use *Right click →Set Layer CRS*, then save under another name. For raster files, a better option is to use *Raster → Conversion → Translate (gdal_translate)*, which allows not only to set the CRS but also the compression parameters to avoid overly big files.

Useful links:

http://paologis.blogspot.it/2009/06/sistemi-di-riferimento-un-po-di-teoria.html

http://blog.spaziogis.it/2007/10/06/persi-nel-mare-dei-sistemi-di-coordinate/

http://gis.stackexchange.com/questions/102541/any-difference-between-epsg3003-and-epsg102091

http://www.rigacci.org/wiki/doku.php/tecnica/gps_cartografia_gis/gauss_boaga_wgs84

http://spatialreference.org/

http://docs.oracle.com/cd/B19306_01/appdev.102/b14255/sdo_cs_concepts.htm#CIHGEICG

A2. Data conversions

One of the most common operations that is executed on digital data is conversion. They may be format conversions, SR conversions, data type conversions, resolution conversions, and so on. Sometimes conversions are associated to merging, as it is the case when processing batches of data to create image mosaics. For raster data QGIS offers many conversion options through GDAL. GDAL (Geospatial Data Abstraction Library) is an open source library for reading and writing raster geospatial data formats. The GDAL Tools plugin is integrated in QGIS to offer a GUI to the collection of tools in the GDAL library.

Some useful Gdal utilities are:

gdal_translate: can be used to convert raster data between different formats, performing some operations like subsettings, resampling, and rescaling pixels in the process.
(http://www.gdal.org/gdal_translate.html)

gdal_warp: image mosaicing, reprojection and warping utility. The program can reproject to any supported projection, and can also apply GCPs stored with the image if the image is "raw" with control information.
(http://www.gdal.org/gdalwarp.html)

gdal_merge: This utility will automatically mosaic a set of images. All the images must be in the same coordinate system and have a matching number of bands, but they may be overlapping, and at different resolutions. In areas of overlap, the last image will be copied over earlier ones.
N.B.: gdal_merge does not support projection conversions, so it is not possible to merge a batch of rasters and to change their projection at the same time.
(http://www.gdal.org/gdal_merge.html)

All three are accessible from the *Raster* menu of QGIS, or from *Processing* → *Toolbox* → *GDAL/OGR*. From the processing toolbox more options are available, but the command line is not editable manually, while from the raster menu it can be edited, so the latter ends up being the best choice to customize the output results. If working in batch mode, however, the command line will not be editable.

Some of the most frequently used options:

-of *format*

Selects the format to create the new file as. GeoTIFF is the default. The list of all format codes can be listed with the **--formats** switch. Only formats list as "(rw)" (read-write) can be written. The .ecw (Enhanced Compression Wavelet) format, for example, commonly used for aerial and satellite images, is a proprietary compression image format, and as such can only be read but not written.

-ot *type*

Assigns the indicated data type to the output bands. Data type can be defined as *Byte/Int16/UInt16/UInt32/Int32/Float32/Float64/CInt16/CInt32/CFloat32/CFloat64*. Data type definition is extremely important, because the default is often Float32 or Float64, which is excessive for most data types and can lead to problems when executing raster operations (for example with the Raster Calculator).

-a_nodata *value***:**

Assigns a specified nodata value to the output bands. Can be set to *none* to avoid setting a nodata value to the output file if one exists for the source file. If the input dataset has a nodata value, this does not cause pixel values that are equal to that nodata value to be changed to the value specified with this option.

-co *NAME=VALUE*

Optional creation options that vary depending on the chosen output format. In the case of the GeoTIFF format (which is the one most common in practice), the creation options can be used to control compression, and whether the file should be tiled or not

-a_srs *SRS*

Specifies the coordinate system of the output file.

-r *resampling_method*

Allows to select the resampling method.

Useful links:

http://docs.qgis.org/2.2/en/docs/user_manual/plugins/plugins_gdaltools.html

http://www.gdal.org/gdal_utilities.html

http://www.geos.ed.ac.uk/~smudd/TopoTutorials/html/tutorial_raster_conversion.html

A3. Rasterization of vector files

This operation can be executed through *Raster → Conversion → Rasterize (gdal_rasterize)*

Some examples of the conversions used for the files in this work:

a. To convert the vector distribution map of grassland in 1954 images to a binary raster containing the values 1 (for grassland) and 0 (no grassland):

```
gdal_rasterize -burn 1 -te 1713966.4223998808301985 5102780.3500143056735396
1751609.1579887964762747 5134454.5267424853518605 -tr 2.0 2.0 -ot Int16 -l Cata-
stoPratiPascoli_1954_prati
J:\TesiNuovo\02_ProducedData\PerimetrazioniPrati_150820\CatastoPratiPascoli_1954
\CatastoGAI54_pratiMergedFINAL\CatastoPratiPascoli_1954_prati.shp
J:/TesiNuovo/02_ProducedData/PerimetrazioniPrati_150820/CatastoPratiPascoli_1954
/CatastoGAI54_pratiMergedFINAL/CatastoGAI54_finalRASTER/Prati1954raster.tif
```

b. Conversion of point vector (IUTI inventory) to raster:

```
gdal_rasterize -a COD08_new -te 1713966.4223998808301985
5102780.3500143056735396 1751609.1579887964762747 5134454.5267424853518605 -tr
2.0 2.0 -ot Int16 -l iuti_3003_2012AA
J:/TesiNuovo/02_ProducedData/IUTI/Iuti_3003_2012Accuracy/iuti_3003_2012AA.shp
J:/TesiNuovo/02_ProducedData/IUTI/Iuti_3003_2012Accuracy/iuti_3003_2012AAraster.
tif
```

-burn 1: all pixels inside the vector will be assigned the value “1”. This is useful to override vector attribute values, or when the vector’s attributes are not important because only one class exists, like in the first example.

-a COD08_new: in this case, the pixels of the new raster will be assigned the value corresponding to the column called "COD08_new" in the original vector's attribute table. This can be used when the attribute value needs to be passed on to the raster file.
N.B.: it is necessary to be careful about the original data type of the attribute value, For example, the original data type for IUTI codes was String, even if expressed by a numerical code like 3.1, 3.2, etc… If the data type is not changed beforehand, however, the resulting raster values will be 3 for both 3.1 and 3.2, resulting in a loss of thematic information.

-a_nodata: it is possible to assign a no data value. If -a_nodata is omitted, gdal_rasterize will give the value 0 to what is outside the vector geometries, but it will not be read as nodata. This choice depends on the kind of operations that have to be performed with the raster. In the case of the 1954 grassland raster, the nodata value was not assigned because a 0 value was needed to combine it with the 2012 grassland raster in the Raster Calculator and create the change map.

-te 1713966.4223998808301985 5102780.3500143056735396 1751609.1579887964762747 5134454.5267424853518605: this set georeferenced extent, so that the new raster will align with a base raster defined by the user. If not defined, the raster grids will not be aligned, which is a problem for calculations involving more than one raster, like change detection. In this case, the extent of the original GAI 1954 images was chosen for all rasterized files.

-tr 2.0 2.0: sets pixel resolution (in georeferenced units, in this case meters). 2 m was used because it is the resolution of the coarser images (GAI 1954).

After rasterizing, it is necessary to clip the raster to the study area (unless it is a rectangle), because otherwise the extension of the output raster is that of the bounding box of the study area itself). Use *Raster → Extraction → Clipper (gdalwarp)*
A problem with the gdalwarp clipper is that it doesn't deal with compression well and creates raster files with huge sizes. A solution is to clip first then use gdal_translate for compression.
It is also possible to gdalwarp to a .vrt (virtual raster) first, which is faster, with the option **`-of`** `vrt`, then use gdal_translate to convert to GeoTIFF with the -co COMPRESS=LZW option for compression.

N.B.: Any operation using gdalwarp or the raster calculator with bring a compressed raster back to its original huge file size, and possibly also assign an inappropriate data format, so the transformation may have to be applied several times.

An alternative to gdal_rasterize is *Processing toolbox → Saga → shapes to grid* , which also allows to set the extent of the rasterized layer according to the user's needs).

A4. Raster reclassification

Example: working with the 5m DEM downloaded from the Veneto Region's Geoportal
- Ascii format (.txt)
- Cut on CTR 10000 sections (25 separate files for the study area)
- No assigned coordinate system

First, *Raster → Miscellaneous → Build virtual raster* was used to create a virtual raster (.vrt) where all the single rasters appear as one.

Then the .vrt was converted to GeoTIFF and assigned to the EPSG:3003 CRS with gdal_translate:

```
gdal_translate -a_srs EPSG:3003 -a_nodata -9999 -ot Int16 -of GTiff -co
COMPRESS=LZW      J:/TesiNuovo/All_AncillaryData/DTM5m/DTM5m_catalogo.vrt
J:/TesiNuovo/All_AncillaryData/DTM5m/DTM5m_merged.tif
```

Finally, the raster was clipped to the study area. The DEM values range from 386 to 2564 m, but they need to need to be reclassified to obtain discrete values so it will be possible to polygonize the raster into altitudinal bands.

The reclassification of a raster's pixel values can be performed by using GRASS through the *Processing → Toolbox → GRASS commands → Raster → r.reclass* module.
GRASS user manual on how to use r.reclass:
https://grass.osgeo.org/grass64/manuals/r.reclass.html

Important:

r.reclass only works on an *integer* input raster map; if the input map is floating point data, *r.reclass* will round the raster values down to the next integer.
r.reclass does not generate any new raster map layers, but instead creates a **reclass table** which is used to reclassify the original raster map layer each time the reclassed map name is requested. If the original raster map layer is removed, *r.reclass* map layer will no longer be accessible unless it had been converted to a raster beforehand.

Reclassification rules .txt file used for the DEM:

```
386 thru 499 = 1
500 thru 699 = 2
700 thru 899 = 3
900 thru 1099 = 4
1100 thru 1299 = 5
1300 thru 1499 = 6
1500 thru 1699 = 7
1700 thru 1899 = 8
1900 thru 2099 = 9
2100 thru 2299 = 10
2300 thru * = 11
```

N.B.: the option “open output file after running algorithm” MUST BE DISABLED because otherwise GRASS inexplicably gives an error message and the reclassified raster is not created. The reclassified file can be added manually afterwards.

The reclassified raster was then polygonized, and the polygons thus obtained were dissolved (*Vector → Geoprocessing Tools → Dissolve*) in order to obtain one polygon for each altitude class.

Unfortunately, it seems like an option to make QGIS calculate zonal statistics divided by raster class (ex. calculating how many pixels of EACH class fall into a given polygon) doesn’t exist yet. The output result is always calculated on all pixels falling inside the shapefile, regardless of their value. Therefore it is necessary to use a workaround, creating a separate raster for each class of interest first. In this case, luckily only 3 classes were involved. From the change classes raster, the change class of interest can be extracted using the Raster Calculator with a simple expression of this kind:
filename@1 = 1

This extracts all pixels with value 1 (corresponding to the Class "grassland loss") to a new raster defined by the user.
From this raster it is possible to extract the zonal statistics needed with *Raster → Zonal Statistics*, setting as *polygon containing the zones* the altitudinal band shapefile previously created.
In this specific case, only the pixel count was extracted, because other statistics would be meaningless.

A5. Useful plugins for working with vector files

These plugins have to be downloaded manually from the plugin repository, but are very useful for expanding QGIS possibilities in working with vector files and modify/export attributes.
N.B.: when doing vector operations (e.g. clipping, difference, etc.) make sure the CRS is the same. Reprojecting the files to the same CRS with on-the-fly is not enough.

QuickmultiAttributeEdit → assigns the same attribute value to a chosen attribute field of selected geometries in a vector file.

TableManager: info on attributes' data type and possibility of moving columns.
(Retrieving information about vector files can be done also through the *Processing Toolbox → OGR Miscellaneous → Information*)

XY Tools: export attribute table to csv and other formats

GroupStats: makes it easy to calculate statistics for feature groups in a vector layer and export them. Tutorial: http://anitagraser.com/2013/02/02/group-stats-tutorial/

APPENDIX B. LANDSAT IMAGES

B1. Landsat specifications

Table 1-A Differences between Landsat 4–7 and Landsat 8 Surface Reflectance algorithms

6S Second Simulation of a Satellite Signal in the Solar Spectrum, AOT Aerosol Optical Thickness, CFmask C Version of Function Of Mask, CMA Climate Modeling Grid - Aerosol, CMG Climate Modeling Grid, DDV Dark Dense Vegetation, DEM Digital Elevation Model, ETM+ Enhanced Thematic Mapper Plus, GSFC Goddard Space Flight Center, INT Integer, MEaSUREs Making Earth Science Data Records for Use in Research Environments, MODIS Moderate Resolution Imaging Spectroradiometer, N/A Not Applicable, NASA National Aeronautics and Space Administration, NCEP National Centers for Environmental Prediction, OLI Operational Land Imager, OMI Ozone Monitoring Instrument, QA Quality Assurance, SR Surface Reflectance, TIRS Thermal Infrared Sensor, TM Thematic Mapper, TOA Top of Atmosphere Reflectance, TOMS Total Ozone Mapping Spectrometer, XML Extensible Markup Language

Parameter	Landsat 4–5, 7 (LEDAPS)	Landsat 8 OLI (L8SR)
(Original) research grant	NASA GSFC, MEaSUREs (Masek)	NASA GSFC
Global coverage	Yes	Yes
TOA	Visible (1–5,7) + Brightness temp (6) bands	Visible (1–7, 9) +Thermal (10–11) bands
SR	Visible (1–5,7) bands	Visible (1–7) bands (OLI/TIRS only)
Radiative transfer model	6S	Internal algorithm
Thermal correction level	TOA only	TOA only
Thermal band units	Kelvin	Kelvin
Pressure	NCEP Grid	Surface pressure is calculated internally based on the elevation
Water vapor	NCEP Grid	MODIS CMA
Air temperature	NCEP Grid	MODIS CMA
DEM	Global Climate Model DEM	Global Climate Model DEM
Ozone	OMI/TOMS	MODIS CMG Coarse resolution ozone
AOT	Correlation between chlorophyll	MODIS CMA
	absorption and bound water absorption of scene	
Sun angle	Scene center from input metadata	Scene center from input metadata
View zenith angle	From input metadata	Hard-coded to 0
Undesirable zenith angle correction	N/A	SR not processed when solar zenith angle > 76 degrees
Pan band processed?	No	No
XML metadata?	Yes	Yes
Brightness temperature calculated	Yes (Band 6 TM/ETM+)	Yes (Bands 10 & 11 TIRS)
Cloud mask	CFmask	CFmask
Data format	INT16	INT16
Fill values	-9999	-9999
QA bands	Cloud Adjacent cloud Cloud shadow DDV Fill Land water Snow Atmospheric opacity	Cloud Adjacent cloud Cloud shadow Aerosols Cirrus

Figure 37: List of Landsat specifications for SR products and differences between Landsat 4-7 and Landsat 8. From (USGS, 2015a)

B2. List of Landsat 4-7 images with cloud cover < 10%

Satellite/Sensor	Landsat Scene Identifier	Date	% cloud cover
L5/TM	LT51920281986221AAA03	09/08/1986	3,65
L5/TM	**LT51920281987208AAA02**	**27/07/1987**	**1,86**
L4/TM	LT41920281989205XXX01	24/07/1989	3,41
L4/TM	LT41920281991227AAA02	15/08/1991	3,67
L5/TM	LT51920281994195AAA02	14/07/1994	2,66
L7/ETM+	*LE71920282000236EDC00*	*23/08/2000*	*10,46*
L7/ETM+	*LE71920282001238EDC00*	*26/08/2001*	*6,90*
L7/ETM+	LE71920282002209EDC00	28/07/2002	*4,32*
L7/ETM+	LE71920282002225NSG00	13/08/2002	2,05
L5/TM	**LT51920282005161KIS00**	**10/06/2005**	**0,99**
L5/TM	**LT51920282005209KIS00**	**28/07/2005**	**3,06**
L5/TM	**LT51920282005241KIS00**	**29/08/2005**	**8,11**
L5/TM	**LT51920282005273KIS00**	**30/09/2005**	**3,99**
L5/TM	**LT51920282005289KIS00**	**16/10/2005**	**0,61**
L5/TM	LT51920282006212MOR00	31/07/2006	7,46
L5/TM	LT51920282006244MOR00	01/09/2006	2,35
L5/TM	**LT51920282007199MOR00**	**18/07/2007**	**0,62**
L5/TM	LT51920282009204MOR00	23/07/2009	5,71
L5/TM	LT51920282010191MOR00	10/07/2010	7,79
L5/TM	LT51920282010223MOR00	11/08/2010	4,86
L5/TM	LT51920282010255MOR00	12/09/2010	5,35
L5/TM	LT51920282011178MOR00	27/06/2011	7,59

B3. Visualization

Each Landsat image is formed by 7 spectral bands (in this case 6, since band 6, thermal infrared, was not used). To visualize the scene as a single image and be able to create band combinations, the most convenient and memory-saving option is to create a multi-spectral virtual raster.

Raster → Miscellaneous > Build Virtual Raster (catalog) ; the Landsat bands have to be selected in according to their band order, and the "Separate" option must be checked, so that the bands will not be fused together to give a singleband image. From the Properties menu of the virtual raster it is possible to create band combinations, for example 3-2-1 for natural color and 4-3-2 for standard false color.

B4. Geometric accuracy of Landsat-TELAER 2012 co-registration

Table with CP positions and residuals obtained from the assessment of the registration accuracy between Landsat images and TELAER 2012 ortophotographs.

Some points had to be individuated outside of the study area due to the lower spatial resolution of Landsat images, that didn't allow the identification of enough points inside of the Dolomiti Bellunesi National Park's boundaries. The operation was therefore carried out before clipping the Landsat images to the study area's extent.

GCP table

Visible	ID	Source X	Source Y	Dest. X	Dest. Y	dX (pixels)	dY (pixels)	Residual (pixels)
✖	0	713729	5,10708e+06	713734	5,10708e+06	-0,126746	-0,101142	0,162155
✖	1	722246	5,1057e+06	722273	5,10569e+06	0,467504	0,445049	0,645467
✖	2	718843	5,11319e+06	718841	5,11318e+06	-0,304643	0,0197573	0,305283
✖	3	727411	5,11308e+06	727414	5,11309e+06	-0,190092	-0,202131	0,277474
✖	4	736726	5,11089e+06	736734	5,1109e+06	-0,15798	-0,0214913	0,159435
✖	5	732496	5,12444e+06	732504	5,12443e+06	0,184636	0,250633	0,3113
✖	6	729924	5,11765e+06	729928	5,11767e+06	-0,0833482	-0,318922	0,329634
✖	7	741450	5,11638e+06	741474	5,11639e+06	0,437404	-0,280246	0,519481
✖	8	739305	5,12518e+06	739311	5,12519e+06	0,0367622	0,0298846	0,0473767
✖	9	750374	5,12504e+06	750368	5,12504e+06	-0,480965	0,214272	0,526536
✖	10	742365	5,13389e+06	742371	5,1339e+06	0,217468	-0,0356641	0,220373

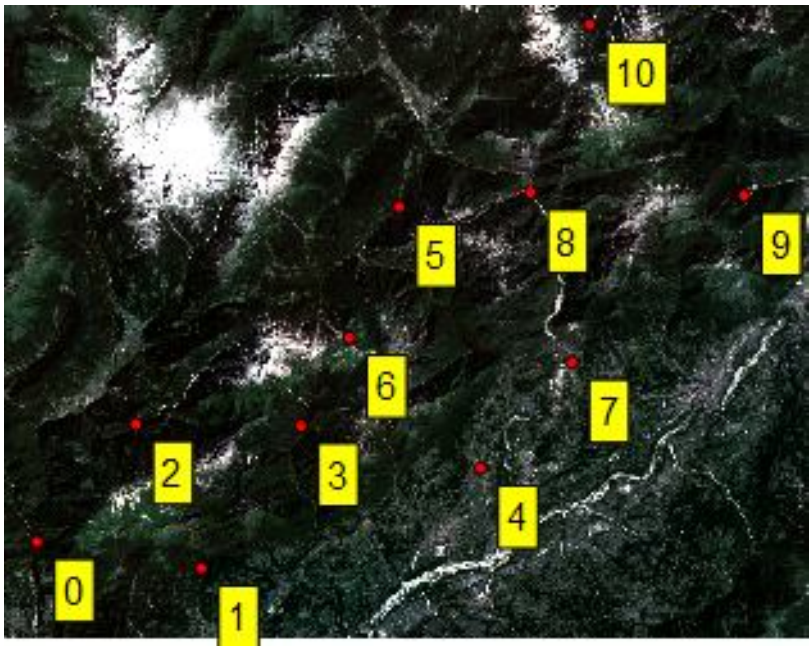

B5. Topographic correction of Landsat images

To create the 30 m DEM in EPSG:32632 from the original 5 m DEM (EPSG: 3003) gdalwarp can be used to reproject and resample to 30 m at the same time, making sure that the new DEM's grid is aligned to that of the Landsat images:

```
gdalwarp -overwrite -s_srs EPSG:3003 -t_srs EPSG:32632 -te 713925.0000000000000000 5102745.0000000000000000 751575.0000000000000000 5134425.0000000000000000 -tr 30 30 -ot Int16 -r cubic -dstnodata -9999 -of GTiff -co COMPRESS=LZW -multi J:\TesiNuovo\02_ProducedData\DTM5m\DTM5m_merged_clip.tif J:/TesiNuovo/02_ProducedData/DTM5m/DTM_forLandsat/DTM5m_merged_clip32632gdalwarp.tif
```

The "Topographic correction" utility is available from the *Processing Toolbox → SAGA → Terrain Analysis – Lighting →Topographic correction.* The available topographic correction methods are:

[0] Cosine Correction

[1] Cosine Correction

[2] Minnaert Correction

[3] Minnaert Correction with Slope

[4] Minnaert Correction with Slope (Law & Nichol, 2004)

[5] C Correction

[6] Normalization

The Azimuth and Elevation parameters needed were obtained from each Landsat scene's metadata, and are shown in Table 16:

DATE	SCENE_CENTER_TIME	SUN_AZIMUTH	SUN_ELEVATION
10/06/2005	09:45:52.3210560Z	135,86	61,24
28/07/2005	09:46:16.2680560Z	137,31	56,89
29/08/2005	09:46:28.1410630Z	146,46	48,81
30/09/2005	09:46:26.8090190Z	155,67	38,27
16/10/2005	09:46:23.9390000Z	158,97	32,70

Table 16: Solar Azimuth and Elevation of the Landsat scenes used

B6. Creation of cloud and water mask for Landsat 2005 images

Each cloud cover band is a binary file containing the values 0 (no data) and 255 (cloud pixels). These files can be combined into a single file with *Processing Toolbox → Grass →r.series ,* using "maximum" to extract the maximum cell value. In this way, the resulting file is a raster with the value 0 (no data) when all the files have the value 0, and 255 where at least one of the cloud cover files has the value 255. The option "propagate nulls" must be unchecked.

https://grass.osgeo.org/grass70/manuals/r.series.html?page=manuals/html70_user/r.series.html

The rasterized water mask file was added to the mask in the same way.

N.B: It is important to pay attention that all files have the same number set as null value.

Each Landsat image was masked with the tool bandcalc included in the Semi Automated Classification Plugin:

```
np.where("CloudAndWaterMASK_32float" == 255, 0,
"clipPNDB_LT51920282005209KIS00_sr_band1")
np.where("CloudAndWaterMASK_32float" == 255, 0,
"clipPNDB_LT51920282005209KIS00_sr_band2")
np.where("CloudAndWaterMASK_32float" == 255, 0,
"clipPNDB_LT51920282005209KIS00_sr_band3")
np.where("CloudAndWaterMASK_32float" == 255, 0,
"clipPNDB_LT51920282005209KIS00_sr_band4")
np.where("CloudAndWaterMASK_32float" == 255, 0,
"clipPNDB_LT51920282005209KIS00_sr_band5")
np.where("CloudAndWaterMASK_32float" == 255, 0,
"clipPNDB_LT51920282005209KIS00_sr_band7")
```

Enable "use no data value = 0" to set all the masked areas as "no data", so that they will not be considered in the classification.

B7. Training ROIs and Classification with SCP

After loading the multiband image that will be used for the classification and before starting the training ROI selection, it is necessary to define the band set used as input and set the center wavelength of each band, which is required for spectral signature calculation. The center wavelength depends on the type of data used, and for the most common satellite data can be chosen directly from the "quick wavelength settings" dropdown menu in SCP's "*Band Set*" window.

This was followed by the creation of Training ROIs using the region growing functionality and using TELAER 2012 ortophotographs and the Natura 2000 habitat map as reference data to check the algorithm's accuracy. The masked Landsat images were used even in the ROI definition stage, in order not to choose any ROI falling partially or completely into the areas made not classifiable by the presence of clouds.

It is possible to run classification previews during ROI selection, which allow to quickly assess the classification accuracy and to delete or modify any ROI giving abnormal results.

Land cover class spectral signatures are extracted from the training ROIs previously created, and can be plotted to assess the differences between class signatures. The SCP also calculates three different types of distance between spectral signatures: Jeffries-Matusita Distance, Euclidean Distance, Spectral Angle and Bray-Curtis similarity, that are useful to evaluate the separability of the Land cover classes chosen.

After running the Maximum Likelihood classifier, the classification obtained will have "0" values, corresponding to unclassified areas (the areas corresponding to the mask and those outside of the Park's boundaries). Since the presence of this "class" interferes with the accuracy assessment process, it is necessary to remove it by setting 0 as the no data value using *gdal_translate*. After this, the accuracy assessment and creation of the error matrix can be carried out using the rasterized IUTI points.

This process was repeated using the Landsat scene after it had been corrected for topological effects with the Minnaert correction. After obtaining a classification map and an error matrix for both the topologically corrected and uncorrected image for each data, the results were compared.

Excellent tutorials on how to use the Semi Automatic Classification Plugin for all the steps described above can be found at http://fromgistors.blogspot.com/, so they were not described in detail here.

APPENDIX C. RESULTS

C1. NDVI and EVI time series

NDVI

ID	DESCRIPTION	VALUE	2005_06_10	2005_07_28	2005_08_29	2005_09_30	2005_10_16
11	GRASSLAND	NDVImin_mean	4907,98	6926,11	5527,43	5224,72	4340,38
		NDVImax_mean	7408,20	8144,48	7718,53	6941,70	5930,59
		NDVI_MEAN	6285,71	7645,80	6960,84	6189,71	5166,42
		NDVI σ	1005,43	489,62	622,40	578,15	747,15
21	SHRUBS	NDVImin_mean	4992,64	6286,44	5602,77	5191,25	4262,57
		NDVImax_mean	7382,15	7825,00	7910,65	7773,32	7212,14
		NDVI_MEAN	6404,20	7193,59	7036,43	6654,19	5974,61
		NDVI σ	740,50	472,83	710,90	604,98	811,39
31	BARE SOIL	NDVImin_mean	1636,56	2263,49	2011,67	1579,74	1234,36
		NDVImax_mean	4325,69	5105,89	4971,86	4825,97	4486,19
		NDVI_MEAN	2784,45	3519,73	3361,45	3084,29	2774,10
		NDVI σ	715,12	850,15	844,25	907,86	845,54
41	CONIFERS	NDVImin_mean	6866,56	7172,97	6968,60	6049,35	4790,48
		NDVImax_mean	8409,30	8325,90	8580,79	8223,16	7550,15
		NDVI_MEAN	7807,06	7878,12	7963,97	7395,34	6401,21
		NDVI σ	431,86	264,01	356,97	606,58	780,92
42	BROADLEAVED	NDVImin_mean	7140,93	7519,20	7082,67	5702,63	3896,53
		NDVImax_mean	8869,21	8713,89	8912,64	8577,71	7390,19
		NDVI_MEAN	8404,52	8323,24	8329,54	7636,35	5990,12
		NDVI σ	301,60	269,47	371,91	543,75	795,37
		NDVI_mean sum	6337,19	6912,09	6730,45	6191,98	5261,29
		NDVImin_mean sum	5108,93	6033,64	5438,63	4749,54	3704,86
		NDVImax_mean sum	7278,91	7623,03	7618,89	7268,37	6513,85

EVI

ID	DESCRIPTION	VALUE	2005_06_10	2005_07_28	2005_08_29	2005_09_30	2005_10_16
11	GRASSLAND	EVImin_mean	1427,33	2208,74	1595,55	1266,33	1068,38
		EVImax_mean	2448,07	2766,67	2483,84	2106,59	1800,66
		EVI_MEAN	1901,01	2495,34	2105,30	1713,21	1471,19
		EVI σ	437,41	298,30	478,53	381,33	334,21
21	SHRUBS	EVImin_mean	1063,85	1311,31	934,26	640,48	538,91

		EVImax_mean	1681,29	1788,10	1685,03	1423,50	1324,66
		EVI_MEAN	1349,30	1553,58	1337,86	1038,80	954,11
		EVI σ	278,30	338,62	428,88	452,14	466,16
31	**BARE SOIL**	**EVImin_mean**	511,57	750,21	536,51	381,43	343,11
		EVImax_mean	1318,43	1595,68	1514,58	1264,44	1158,56
		EVI_MEAN	889,27	1125,99	1004,85	771,05	703,96
		EVI σ	185,52	257,23	282,79	323,58	344,87
41	**CONIFERS**	**EVImin_mean**	1472,89	1529,61	1230,49	793,35	573,35
		EVImax_mean	2286,07	2052,75	1989,46	1699,42	1435,89
		EVI_MEAN	1862,64	1798,45	1636,76	1278,77	1028,13
		EVI σ	363,59	338,55	415,63	487,90	435,97
42	**BROADLEAVED**	**EVImin_mean**	1848,55	1991,51	1503,12	839,96	435,96
		EVImax_mean	2963,41	2584,74	2507,06	2196,24	1615,03
		EVI_MEAN	2500,04	2303,50	2076,64	1597,78	1046,27
		EVI σ	501,97	498,18	648,47	694,65	556,56
		EVI_mean sum	1700,45	1855,37	1632,28	1279,92	1040,73
		EVImin_mean sum	1264,84	1558,28	1159,99	784,31	591,94
		EVImax_mean sum	2139,45	2157,59	2035,99	1738,04	1466,96

C2. Classification scenarios results and Accuracy Assessment

For each classification scenario based on single date Landsat images, the results presented are: a) class extension and error matrix for the classification conducted on the SR bands without topographic correction ("original bands"); and b) class extension and error matrix for the classification conducted on the bands with Minnaert topographic correction ("topographically corrected bands").

Classes used for the classification:

Class 1: Grassland

Class 2: Shrubs and sparse trees

Class 3: Bare soil and rocks

Class 4: Forest (includes the sub-classes Conifer and Broadleaved, not separated)

IMAGE 1 – 2005/06/10

A) ORIGINAL BANDS

Spatial extent of each land cover class

Class	PixelSum	Percentage %	Area (ha)
1	48655	16,29	4378,95
2	73365	24,56	6602,85
3	24017	8,04	2161,53
4	152728	51,12	13745,52

Error Matrix

	Reference (IUTI 2008)				
Classification	**1**	**2**	**3**	**4**	**Total**
1	**85**	28	2	54	**169**
2	18	**103**	23	94	**238**
3	30	23	**32**	4	**89**
4	7	29	3	**522**	**561**
Total	**140**	**183**	**60**	**674**	**1057**

Overall accuracy [%] = 70.20		
Class 1 producer accuracy [%] = 60.71	**user accuracy [%] = 50.30**	**Kappa hat = 0.43**
Class 2 producer accuracy [%] = 56.28	user accuracy [%] = 43.28	Kappa hat = 0.31
Class 3 producer accuracy [%] = 53.33	user accuracy [%] = 35.96	Kappa hat = 0.32
Class 4 producer accuracy [%] = 77.45	user accuracy [%] = 93.05	Kappa hat = 0.81
Kappa hat classification = 0.50		

B) TOPOGRAPHICALLY CORRECTED BANDS:

Spatial extent occupied by each land cover class

Class	PixelSum	Percentage %	Area_ha
1	46499	15,56	4184,91
2	66862	22,38	6017,58
3	26884	9,00	2419,56
4	158520	53,06	14266,8

Error Matrix

	Reference (IUTI 2008)				
Classification	**1**	**2**	**3**	**4**	**Total**
1	**88**	30	4	54	**176**
2	20	**102**	17	88	**227**
3	29	20	**35**	7	**91**
4	3	31	4	**525**	**563**
Total	**140**	**183**	**60**	**674**	**1057**

Overall accuracy [%] = 70.96		
Class 1.0 producer accuracy [%] = 62.86	**user accuracy [%] = 50.0**	**Kappa hat = 0.42**
Class 2.0 producer accuracy [%] = 55.74	user accuracy [%] = 44.93	Kappa hat = 0.33
Class 3.0 producer accuracy [%] = 58.33	user accuracy [%] = 38.46	Kappa hat = 0.35
Class 4.0 producer accuracy [%] = 77.89	user accuracy [%] = 93.25	Kappa hat = 0.81
Kappa hat classification = 0.51		

IMAGE 2 - 2005/07/28

A) ORIGINAL BANDS

Spatial extent occupied by each land cover class

Class	PixelSum	Percentage %	Area_ha
1	39405	13,19	3546,45
2	76450	25,59	6880,5
3	42020	14,06	3781,8
4	140890	47,16	12680,1

Error Matrix

	Reference (IUTI 2008)				
Classification	**1**	**2**	**3**	**4**	**Total**
1	88	15	1	30	**134**
2	10	87	20	142	**259**
3	35	47	36	25	**143**
4	7	34	3	477	**521**
Total	**140**	**183**	**60**	**674**	**1057**

Overall accuracy [%] = 65.09		
Class 1 producer accuracy [%] = 62.86	**user accuracy [%] = 65.67**	**Kappa hat = 0.60**
Class 2 producer accuracy [%] = 47.54	user accuracy [%] = 33.59	Kappa hat = 0.20
Class 3 producer accuracy [%] = 60.0	user accuracy [%] = 25.17	Kappa hat = 0.21
Class 4 producer accuracy [%] = 70.77	user accuracy [%] = 91.55	Kappa hat = 0.77
Kappa hat classification = 0.43		

B) TOPOGRAPHICALLY CORRECTED BANDS:

Spatial extent occupied by each land cover class

Class	PixelSum	Percentage %	Area_ha
1	36428	12,19	3278,52
2	62490	20,92	5624,1
3	46562	15,58	4190,58

4	153285	51,31	13795,65

Error Matrix

	Reference (IUTI 2008)				
Classification	**1**	**2**	**3**	**4**	**Total**
1	89	13	0	25	**127**
2	8	81	10	111	**210**
3	39	54	45	26	**164**
4	4	35	5	512	**556**
Total	**140**	**183**	**60**	**674**	**1057**

Overall accuracy [%] = 68.78		
Class 1.0 producer accuracy [%] = 63.57	**user accuracy [%] = 70.08**	**Kappa hat = 0.65**
Class 2.0 producer accuracy [%] = 44.26	user accuracy [%] = 38.57	Kappa hat = 0.26
Class 3.0 producer accuracy [%] = 75.0	user accuracy [%] = 27.44	Kappa hat = 0.23
Class 4.0 producer accuracy [%] = 75.96	user accuracy [%] = 92.09	Kappa hat = 0.78
Kappa hat classification = 0.48		

IMAGE 3 - 2005/08/29

A) ORIGINAL BANDS

Spatial extent occupied by each land cover class

Class	PixelSum	Percentage %	Area_ha
1	44396,00	14,86	3995,64
2	89343,00	29,91	8040,87
3	29565,00	9,90	2660,85
4	135450,00	45,34	12190,5

Error Matrix

	Reference (IUTI 2008)				
Classification	**1**	**2**	**3**	**4**	**Total**
1	**82**	24	2	43	**151**
2	25	**106**	24	182	**337**
3	31	32	**29**	9	**101**
4	2	21	5	**440**	**468**
Total	**140**	**183**	**60**	**674**	**1057**

Overall accuracy [%] = 62.16		
Class 1 producer accuracy [%] = 58.57	**user accuracy [%] = 54.30**	**Kappa hat = 0.47**
Class 2 producer accuracy [%] = 57.92	user accuracy [%] = 31.45	Kappa hat = 0.17
Class 3 producer accuracy [%] = 48.33	user accuracy [%] = 28.71	Kappa hat = 0.24
Class 4 producer accuracy [%] = 65.28	user accuracy [%] = 94.02	Kappa hat = 0.83
Kappa hat classification = 0.41		

B) TOPOGRAPHICALLY CORRECTED BANDS:

Spatial extent occupied by each land cover class

Class	PixelSum	Percentage %	Area_ha
1	43501,00	14,56	3915,09
2	86350,00	28,90	7771,5
3	34275,00	11,47	3084,75
4	134628,00	45,06	12116,52

Error Matrix

	Reference (IUTI 2008)				
Classification	**1**	**2**	**3**	**4**	**Total**
1	**85**	30	3	43	**161**
2	24	**107**	21	156	**308**
3	30	32	**34**	15	**111**
4	1	14	2	**460**	**477**
Total	**140**	**183**	**60**	**674**	**1057**

Overall accuracy [%] = 64.90		
Class 1 producer accuracy [%] = 60.71	**user accuracy [%] = 52.80**	**Kappa hat = 0.46**
Class 2 producer accuracy [%] = 58.47	user accuracy [%] = 34.74	Kappa hat = 0.21
Class 3 producer accuracy [%] = 56.67	user accuracy [%] = 30.63	Kappa hat = 0.26
Class 4 producer accuracy [%] = 68.25	user accuracy [%] = 96.44	Kappa hat = 0.90
Kappa hat classification = 0.45		

IMAGE 4 - 2005/09/30

A) ORIGINAL BANDS

Spatial extent occupied by each land cover class

Class	**PixelSum**	**Percentage %**	**Area_ha**
1	46080	15,43	4147,2
2	121428	40,67	10928,52
3	26654	8,93	2398,86
4	104433	34,97	9398,97

Error Matrix

	Reference (IUTI 2008)				
Classification	**1**	**2**	**3**	**4**	**Total**
1	**82**	28	4	41	**155**
2	21	**110**	29	271	**431**
3	31	22	**21**	12	**86**
4	6	23	6	**349**	**384**
Total	**140**	**183**	**60**	**673**	**1056**

Overall accuracy [%] = 53.22		
Class 1 producer accuracy [%] = 58.57	**user accuracy [%] = 52.90**	**Kappa hat = 0.46**
Class 2 producer accuracy [%] = 60.11	user accuracy [%] = 25.52	Kappa hat = 0.10
Class 3 producer accuracy [%] = 35.0	user accuracy [%] = 24.42	Kappa hat = 0.20
Class 4 producer accuracy [%] = 51.86	user accuracy [%] = 90.89	Kappa hat = 0.75
Kappa hat classification = 0.31		

B) TOPOGRAPHICALLY CORRECTED BANDS:

Spatial extent occupied by each land cover class

Class	PixelSum	Percentage %	Area_ha
1	61936	20,74	5574,24
2	23069	7,73	2076,21
3	29141	9,76	2622,69
4	184449	61,77230027	16600,41

Error Matrix

	Reference (IUTI 2008)				
Classification	**1**	**2**	**3**	**4**	**Total**
1	**89**	43	4	91	**227**
2	6	**16**	3	43	**68**
3	31	26	**27**	18	**102**
4	14	98	26	**521**	**659**
Total	**140**	**183**	**60**	**673**	**1056**

Overall accuracy [%] = 61.84		
Class 1.0 producer accuracy [%] = 63.57	**user accuracy [%] = 39.21**	**Kappa hat = 0.30**
Class 2.0 producer accuracy [%] = 8.74	user accuracy [%] = 23.53	Kappa hat = 0.07
Class 3.0 producer accuracy [%] = 45.0	user accuracy [%] = 26.47	Kappa hat = 0.22
Class 4.0 producer accuracy [%] = 77.41	user accuracy [%] = 79.06	Kappa hat = 0.42
Kappa hat classification = 0.32		

IMAGE 5 - 2005/10/16

A) ORIGINAL BANDS

Spatial extent occupied by each land cover class

Class	PixelSum	Percentage %	Area_ha
1	44582	14,92	4012,38
2	101725	34,05	9155,25
3	24267	8,12	2184,03
4	128158	42,90	11534,22

Error Matrix

	Reference (IUTI 2008)				
Classification	**1**	**2**	**3**	**4**	**Total**
1	**91**	24	1	45	**161**
2	10	**95**	19	245	**369**
3	26	20	**21**	8	**75**
4	13	44	19	**376**	**452**
Total	**140**	**183**	**60**	**674**	**1057**

Overall accuracy [%] = 55.16		
Class 1 producer accuracy [%] = 65.0	**user accuracy [%] = 56.52**	**Kappa hat = 0.50**
Class 2 producer accuracy [%] = 51.91	user accuracy [%] = 25.75	Kappa hat = 0.10
Class 3 producer accuracy [%] = 35.0	user accuracy [%] = 28.0	Kappa hat = 0.24
Class 4 producer accuracy [%] = 55.79	user accuracy [%] = 83.19	Kappa hat = 0.54
Kappa hat classification = 0.30		

B) TOPOGRAPHICALLY CORRECTED BANDS:

Spatial extent occupied by each land cover class

Class	PixelSum	Percentage %	Area (ha)
1	36774	12,31	3309,66
2	105822	35,42	9523,98
3	24643	8,25	2217,87
4	131493	44,02	11834,37

Error Matrix

	Reference (IUTI 2008)				
Classification	**1**	**2**	**3**	**4**	**Total**
1	**91**	15	0	27	**133**
2	14	**99**	26	252	**391**
3	25	22	**21**	13	**81**
4	10	47	13	**382**	**452**
Total	**140**	**183**	**60**	**674**	**1057**

Overall accuracy [%] = 56.10		
Class 1 producer accuracy [%] = 65.0	**user accuracy [%] = 68.42**	**Kappa hat = 0.64**
Class 2 producer accuracy [%] = 54.1	user accuracy [%] = 25.32	Kappa hat = 0.1
Class 3 producer accuracy [%] = 35.0	user accuracy [%] = 25.93	Kappa hat = 0.21
Class 4 producer accuracy [%] = 56.68	user accuracy [%] = 84.51	Kappa hat = 0.57
Kappa hat classification = 0.32		

MULTIDATE/MULTI-IMAGE CLASSIFICATION SCENARIOS

DATE 2 (JULY) + DATE 5 (OCTOBER)

(topographically corrected bands of Landsat scene)

Spatial extent occupied by each land cover class

Class	PixelSum	Percentage %	Area (ha)
1	33774	11,31	3039,66
2	61199	20,49	5507,91
3	45310	15,17	4077,9
4	158449	53,04	14260,41

Error Matrix

	Reference				
Classification	**1**	**2**	**3**	**4**	**Total**
1	**90**	14	0	14	**118**
2	8	**78**	8	99	**193**
3	38	51	**45**	28	**162**
4	4	40	7	**533**	**584**
Total	**140**	**183**	**60**	**674**	**1057**

Overall accuracy [%] = 70.5771050142		**Kappa hat classification = 0.50**
Class 1.0 producer accuracy [%] = 64.29	**user accuracy [%] = 76.27**	**Kappa hat = 0.73**
Class 2.0 producer accuracy [%] = 42.62	user accuracy [%] = 40.41	Kappa hat = 0.28
Class 3.0 producer accuracy [%] = 75.0	user accuracy [%] = 27.78	Kappa hat = 0.23
Class 4.0 producer accuracy [%] = 79.08	user accuracy [%] = 91.27	Kappa hat = 0.76

NDVI STACK CLASSIFICATION - ALL DATES

Spatial extent occupied by each land cover class

Class	PixelSum	Percentage %	Area (ha)
1	43678	14,62	3931,02
2	64375	21,55	5793,75
3	42408	14,20	3816,72
4	148286	49,64	13345,74

Error Matrix

	Reference (IUTI 2008)				
Classification	**1**	**2**	**3**	**4**	**Total**
1	**85**	32	2	46	**165**
2	8	**93**	4	112	**217**
3	40	40	**53**	14	**147**
4	7	18	1	**502**	**528**

Total	**140**	**183**	**60**	**674**	**1057**

Overall accuracy [%] = 69.35		
Class 1.0 producer accuracy [%] = 60.71	**user accuracy [%] = 51.51**	**Kappa hat = 0.44**
Class 2.0 producer accuracy [%] = 50.82	user accuracy [%] = 42.86	Kappa hat = 0.31
Class 3.0 producer accuracy [%] = 88.33	user accuracy [%] = 36.05	Kappa hat = 0.32
Class 4.0 producer accuracy [%] = 74.48	user accuracy [%] = 95.08	Kappa hat = 0.86
Kappa hat classification = 0.50		

NDVI – DATES 2 AND 5

Spatial extent occupied by each land cover class

Class	PixelSum	Percentage %	Area (ha)
1	62081	20,78	5587,29
2	49253	16,49	4432,77
3	47110	15,77	4239,90
4	140303	46,96	12627,27

Error Matrix

	Reference (IUTI 2008)				
Classification	**1**	**2**	**3**	**4**	**Total**
1	**65**	43	2	136	**246**
2	17	**69**	5	69	**160**
3	37	50	**53**	17	**157**
4	21	21	0	**452**	**494**
Total	**140**	**183**	**60**	**674**	**1057**

Overall accuracy [%] = 60.45		
Class 1.0 producer accuracy [%] = 46.43	**user accuracy [%] = 26.42**	**Kappa hat = 0.15**
Class 2.0 producer accuracy [%] = 37.70	user accuracy [%] = 43.13	Kappa hat = 0.31
Class 3.0 producer accuracy [%] = 88.33	user accuracy [%] = 33.76	Kappa hat = 0.30
Class 4.0 producer accuracy [%] = 67.06	user accuracy [%] = 91.50	Kappa hat = 0.77
Kappa hat classification = 0.38		

EVI STACK CLASSIFICATION - ALL DATES

Spatial extent occupied by each land cover class

Class	PixelSum	Percentage %	Area (ha)
1	36980	12,38	3328,20
2	35241	11,80	3171,69
3	55223	18,48	4970,07
4	171303	57,34	15417,27

Error Matrix

	Reference (IUTI 2008)				
Classification	**1**	**2**	**3**	**4**	**Total**
1	**82**	17	1	39	**139**
2	17	**50**	3	64	**134**
3	30	65	**52**	34	**181**
4	11	51	4	**537**	**603**
Total	**140**	**183**	**60**	**674**	**1057**

Overall accuracy [%] = 68.21		
Class 1 producer accuracy [%] = 58.57	**user accuracy [%] = 59.00**	**Kappa hat = 0.53**
Class 2 producer accuracy [%] = 27.32	user accuracy [%] = 37.31	Kappa hat = 0.24
Class 3 producer accuracy [%] = 86.67	user accuracy [%] = 28.73	Kappa hat = 0.24
Class 4 producer accuracy [%] = 79.67	user accuracy [%] = 89.05	Kappa hat = 0.70
Kappa hat classification = 0.46		

EVI – DATES 2 AND 5

Spatial extent occupied by each land cover class

Class	PixelSum	Percentage %	Area (ha)
1	83642	28,00	7527,78
2	50144	16,78	4512,96
3	61783	20,68	5560,47
4	103178	34,54	9286,02

Error Matrix

	Reference (IUTI 2008)				
Classification	**1**	**2**	**3**	**4**	**Total**
1	**73**	15	1	216	**305**
2	11	**56**	5	117	**189**
3	14	73	**51**	74	**212**
4	42	39	3	**267**	**351**
Total	**140**	**183**	**60**	**674**	**1057**

Overall accuracy [%] = 42.29		
Class 1 producer accuracy [%] = 52.14	**user accuracy [%] = 23.93**	**Kappa hat = 0.12**
Class 2 producer accuracy [%] = 30.6010928962	user accuracy [%] = 29.63	Kappa hat = 0.15
Class 3 producer accuracy [%] = 85.0	user accuracy [%] = 24.06	Kappa hat = 0.19
Class 4 producer accuracy [%] = 39.6142433234	user accuracy [%] = 76.07	Kappa hat = 0.34
Kappa hat classification = 0.18		

DATE 2 (JULY) + NDVI + EVI

(topographically corrected bands of Landsat scene)

Spatial extent occupied by each land cover class

Class	PixelSum	Percentage %	Area (ha)
1	33845	11,33	3046,05
2	71649	23,98	6448,41
3	45661	15,28	4109,49
4	147610	49,41	13284,9

Error Matrix

	Reference (IUTI 2008)				
Classification	**1**	**2**	**3**	**4**	**Total**
1	**88**	12	1	15	**116**
2	9	**92**	7	127	**235**
3	40	49	**51**	19	**159**
4	3	30	1	**513**	**547**
Total	**140**	**183**	**60**	**674**	**1057**

Overall accuracy [%] = 70.39		
Class 1 producer accuracy [%] = 62.86	**user accuracy [%] = 75.86**	**Kappa hat = 0.72**
Class 2 producer accuracy [%] = 50.27	user accuracy [%] = 39.15	Kappa hat = 0.26
Class 3 producer accuracy [%] = 85.0	user accuracy [%] = 32.08	Kappa hat = 0.28
Class 4 producer accuracy [%] = 76.11	user accuracy [%] = 93.78	Kappa hat = 0.83
Kappa hat classification = 0.51		

DATE 2 (JULY) + NDVI

(topographically corrected bands of Landsat scene)

Spatial extent occupied by each land cover class

Class	PixelSum	Percentage %	Area (ha)
1	36045	12,06	3244,05
2	62369	20,88	5613,21
3	47003	15,73	4230,27
4	153348	51,33	13801,32

Error Matrix

	Reference				
Classification	**1**	**2**	**3**	**4**	**Total**
1	**89**	14	1	18	**122**
2	9	**89**	6	101	**205**
3	39	50	**52**	21	**162**
4	3	30	1	**534**	**568**
Total	**140**	**183**	**60**	**674**	**1057**

Overall accuracy [%] = 72.28		
Class 1.0 producer accuracy [%] = 63,57	**user accuracy [%] = 72,95**	**Kappa hat = 0.69**
Class 2.0 producer accuracy [%] = 48.63	user accuracy [%] = 43,41	Kappa hat = 0.32
Class 3.0 producer accuracy [%] = 86,67	user accuracy [%] = 32,10	Kappa hat = 0.28
Class 4.0 producer accuracy [%] = 79.23	user accuracy [%] = 94,01	Kappa hat = 0.83
Kappa hat classification = 0.54		